

2009

# Ionic liquids: MALDI-MS matrices and gas chromatography stationary phases

Jeffrey Aaron Crank  
*Iowa State University*

Follow this and additional works at: <https://lib.dr.iastate.edu/etd>

 Part of the [Chemistry Commons](#)

## Recommended Citation

Crank, Jeffrey Aaron, "Ionic liquids: MALDI-MS matrices and gas chromatography stationary phases" (2009). *Graduate Theses and Dissertations*. 10615.  
<https://lib.dr.iastate.edu/etd/10615>

This Dissertation is brought to you for free and open access by the Iowa State University Capstones, Theses and Dissertations at Iowa State University Digital Repository. It has been accepted for inclusion in Graduate Theses and Dissertations by an authorized administrator of Iowa State University Digital Repository. For more information, please contact [digirep@iastate.edu](mailto:digirep@iastate.edu).

Ionic liquids: MALDI-MS matrices and gas chromatography stationary phases

By

Jeffrey Aaron Crank

A dissertation submitted to the graduate faculty  
in partial fulfillment of the requirements for the degree of

DOCTOR OF PHILOSOPHY

Major: Analytical Chemistry

Program of Study Committee  
Daniel W. Armstrong, Co-major Professor  
Victor Shang-Yi Lin, Co-major Professor  
Robert S. Houk  
Nicola L. Pohl  
Hans Stauffer

Iowa State University

Ames, Iowa

2009

Copyright Jeffrey Aaron Crank, 2009 All rights reserved.

This thesis is dedicated:

To Deborah Crank for her unwavering support and love during the good and bad times of my graduate career. To Wayne and Erma Crank for inspiration to succeed and to Greg and Caryl Crank for support and giving me the strength to persevere.

## Table of Contents

<b>ACKNOWLEDGMENTS</b>	v
<b>CHAPTER 1 GENERAL INTRODUCTION</b>	1
Ionic liquids	1
Ionic liquids and MALDI	2
Ionic liquids as gas chromatography stationary phases	3
References	6
 <b>CHAPTER 2 TOWARDS A SECOND GENERATION OF IONIC LIQUID MATRICES (ILM'S) FOR MALDI-MS OF PEPTIDES, PROTEINS, AND CARBOHYDRATES</b>	8
Abstract	8
Introduction	9
Experimental	11
Results and discussion	14
Conclusions	27
Acknowledgements	27
References	27
Tables	35
Figures	39
Supplemental information	44
 <b>CHAPTER 3 EFFECTIVE MS ANALYSIS OF BIODEGRADABLE POLYMERS WITH SECOND GENERATION IONIC LIQUID MALDI MATRICES</b>	51
Abstract	51
Introduction	52
Experimental	54
Results and discussion	58
Conclusions	67
References	67
Tables and figures	70

Supplemental information	85
<b>CHAPTER 4 RAPID DETERMINATION OF COMPLEX MIXTURES BY DUAL-COLUMN GAS CHROMATOGRAPHY WITH A NOVEL STATIONARY PHASE COMBINATION AND SPECTROMETRIC DETECTION</b>	<b>115</b>
Abstract	115
Introduction	116
Experimental	121
Results and discussion	125
Conclusions	134
Acknowledgements	136
References	136
Figures and Tables	141
<b>CHAPTER 5 CHARACTERIZATION AND UTILIZATION OF A NOVEL TRIFLATE IONIC LIQUID STATIONARY PHASE FOR USE IN COMPREHENSIVE TWO-DIMENSIONAL GAS CHROMATOGRAPHY</b>	<b>151</b>
Abstract	151
Introduction	152
Experimental	154
Results and discussion	157
Conclusions	164
Acknowledgements	165
References	165
Figures and tables	167
<b>CHAPTER 6 GENERAL CONCLUSIONS</b>	<b>174</b>

## ACKNOWLEDGEMENTS

Growing up in a small farming community in Illinois, it was hard to imagine that one day I would receive a PhD in chemistry. I have been very fortunate to have many people that encouraged me along the way. The first people to peak my interest in science were my high school teachers Eric Rittenhouse and Brad Stork. Mr. Rittenhouse and Stork taught me that science could be fun and I soon found that I had a knack for it. It was Mr. Rittenhouse that introduced me to science fair and research. Our project won the regional science fair and allowed me to go to both the national and international science fairs. This project exposed me to many new experiences (i.e. flying, traveling to other states, and public speaking) for which I am very grateful.

I would also like to acknowledge Dr. Armstrong for his guidance during graduate school. Dr. Armstrong has been both a teacher and mentor during graduate school. Dr. Armstrong's knowledge, straightforwardness, and approachability is a large asset to students when faced with problems. I would also like to acknowledge my current and former group members for their support.

Next I would like to acknowledge my family. Although three out of four of my grandparents will not see this thesis I know that they have helped me tremendously throughout my graduate career and life. I would also like to acknowledge my parents Greg and Caryl Crank.

Academics have never been easy for me and my parents have always been supportive. Through their support and encouragement I have been able to achieve far more than I ever thought.

Finally I would like to acknowledge the newest member of my family, my wife Debbie Crank. Throughout the ups and downs of graduate school she has always been by my side supporting me. I am immensely lucky that I have found someone who understands what it takes to get a PhD and has been supportive throughout.

## CHAPTER 1

### INTRODUCTION

#### Ionic Liquids

Ionic liquids are a class of non-molecular salts whose melting points are at or below 100 deg. Celsius. These salts are considered room temperature ionic liquids if their melting point is at or below room temperature. Ionic liquids have unique properties such as negligible vapor pressure, a wide range of viscosities, high thermal stability, and can be custom synthesized for many different applications.<sup>1-3</sup> The first ionic liquids reported were ammonium based and were called molten salts. This initial report by Walden in 1914 described the synthesis of ethylammonium nitrate.<sup>4</sup> However, this initial ionic liquid was unstable and few reports of ionic liquids were seen in the literature in the following years. Ionic liquids did not become popular until 78 years later when Wilkes reported an air and water stable imidazolium ionic liquid.<sup>5</sup> Typical ionic liquid cations reported in current literature are substituted imidazolium, ammonium, phosphonium, and pyridinium compounds.<sup>2</sup> Typical anions used are the halides ( $\text{Cl}^-$ ,  $\text{Br}^-$ ,  $\text{I}^-$ ),  $\text{PF}_6^-$ ,  $\text{BF}_4^-$ , bis(trifluoromethane)sulfonimide ( $\text{NTf}_2^-$ ), and triflate ( $\text{TfO}^-$ ).<sup>2</sup> Ionic liquids have been custom synthesized for many applications including solvents for liquid-liquid extractions,<sup>6-10</sup> stationary phases for solid phase microextraction,<sup>11</sup> <sup>12</sup> ion pairing reagents for the trace analysis of anions by electrospray ionization mass spectrometry in the positive mode,<sup>13-15</sup> MALDI-MS matrices,<sup>16-22</sup> and gas chromatography



stationary phases.<sup>23-29</sup> Herein MALDI-MS matrices and gas chromatography stationary phases are discussed.

### **Ionic liquids and MALDI**

Ionic liquids were first reported as MALDI matrices by Armstrong et al. in 2001.<sup>17</sup> In this initial report it was shown that the ionic liquid matrices (ILMs) could produce stronger analyte signals than solid matrices. It was also shown that there was far greater homogeneity of the analyte in the ILM. Solid matrices, such as sinapinic acid and  $\alpha$ -cyano-4-hydroxycinnamic acid, rely on co-crystallization of the matrix and dilute analyte to achieve ionization. This leads to searching for so called “hot spots” where the concentration of analyte in the matrix crystal is adequate to produce an analyte signal. On the other hand, ILMs form homogeneous solutions of the matrix and analyte which show better shot to shot reproducibility with no searching for “hot spots”. Subsequent publications have also shown the superior quantitative ability of the ILMs.<sup>18, 30</sup> In these publications quantitation of small molecules, proteins, and protein digests were shown.

Several studies have shown ionic liquid matrices to be useful for many different applications. One such application is tissue analysis and imaging.<sup>31</sup> Lemaire et al. successfully used ILMs to image a rat brain and showed that ILMs have better sensitivity and analyte signal intensity, show a resistance to laser ablation, and work equally well in positive and negative ion mode. Another unique application of an ILM is the screening of thin layer chromatography (TLC) plates.<sup>32</sup> In their report the authors spot the ionic liquid matrix directly on TLC plates,

which are then placed directly in the MALDI. It is shown that the ILMs can detect low molecular weight alkaloids with high sensitivity and no pretreatment of the TLC plate.

Although many new applications have been presented in the literature, such as the aforementioned examples, there have been no systematic studies investigating how varying the cation and anion of the ILMs changes the physical state and analyte signal intensity. In this thesis Chapter 2 shows the systematic variation of both the cation and anion to find an ionic liquid matrix that produces the greatest analyte S/N ratio. It is also demonstrated that these new ILMs have a greater mass detection range and can be used for a wider variety of analytes. Analytes tested include peptides, proteins, and carbohydrates.

Chapter 3 reports the characterization of sixteen biodegradable polymers with two ILMs and five solid matrices. It is shown that the ILM produces less degradation and typically allows detection of an almost Gaussian distribution of analyte peaks. This allows detection of a more accurate and precise number average molecular weight and weight average molecular weight.

### **Ionic liquids as gas chromatography stationary phases**

The earliest reports of ionic liquids, then called molten salts or liquid organic salts, used as gas chromatography stationary phases were in the late 1960's<sup>33</sup> with a few reports in the mid 1980's.<sup>34, 35</sup> These initial reports used ammonium and phosphonium salts which have narrow

liquid ranges and are not thermally stable. It was not until 1999 that a moisture and thermally stable ionic liquid stationary phase was introduced.<sup>36</sup> This report was the first to use “modern” imidazolium cations which have a wide liquid range and are moisture and thermally stable. Butylmethylimidazolium (BMIM) chloride and BMIM PF<sub>6</sub> were classified using Rohrschneider-McReynolds constants. The stationary phases were then compared to existing GC stationary phases. It was found that the ionic liquid stationary phases showed a “dual nature” retention which separated both polar and nonpolar analytes. Ionic liquid stationary phases were probed further in a subsequent report by using the Abraham solvation parameter model.<sup>37</sup>

The thermal stability of these IL stationary phases were still too low (~150°C) to be effective GC phases. The thermal stability was increased by synthesizing the NTf<sub>2</sub> analogs of methylimidazolium, butylimidazolium, benzylimidazolium, and pyrrolidinium geminal dicationic ionic liquids.<sup>38</sup> These new ionic liquid stationary phases have a high thermal stability in the range of 200-400°C. It was also shown that the polymerization of vinylimidazolium dicationic ionic liquids increase the thermal stability of these ionic liquid stationary phases.<sup>39</sup> The degree of polymerization was controlled by adding varying amounts of vinylimidazolium monocationic ionic liquids. These thermally stable ILs have been shown to be useful for many applications such as the separation of fatty acid methyl esters, polycyclic aromatic hydrocarbons, alcohols, alkanes, and mixtures of flavors and fragrances.

Ionic liquid stationary phases have also been shown to be useful in two dimensional gas chromatography (2D-GC, GCXGC) separations. 2D-GC is used for the fast separation of

complex mixtures of analytes. Typically two short columns (< 5m) are connected in series and are run at high flow rates. Requirements for columns in 2D-GC are that they have high efficiency and that the columns are orthogonal. In this application orthogonal is defined as the stationary phases having different separation mechanisms. Typical columns that are considered to be orthogonal are the polar Carbowax (polyethylene glycol) columns and non-polar polysiloxane columns. Ionic liquid columns are well suited for 2D-GC separations because they have a unique “dual nature” retention mechanism which is orthogonal to the polysiloxane. This “dual nature” retention mechanism allows for a far greater number of compounds to be separated when compared to the Carbowax columns, since the ionic liquid stationary phases can separate both polar and non-polar compounds.

Chapter 4 demonstrates the use of an ionic liquid stationary phase as the secondary column for the separation of volatile organic compounds and 13 chemical markers found in the headspace of US currency. This chapter also demonstrates the use of 2D-GC in the stop flow operation mode. Stop flow operation is used because peaks that are separated on both the primary and secondary columns in a one dimensional separation, sometimes co-elute when the columns are placed in series. In the stop flow operation mode the flow of the primary column is stopped for a short period of time while the secondary column carrier gas continues to flow. For peaks that co-elute on secondary column, the flow is stopped on the primary column after the first peak enters the secondary column. This creates a space in the chromatogram so that the previously co-eluting peaks are separated.

Chapter 5 demonstrates the separation of phosphorus-oxygen (P-O) containing compounds from a complex mixture using a triflate ionic liquid column as the secondary column in 2D-GC. These phosphorus-oxygen containing compounds are chemical warfare agent simulants. The separation of the P-O containing compounds on the triflate ionic liquid and the commercial DB-WAX (polyethylene glycol) columns are compared. It was found that the triflate IL column was much more selective for the P-O containing compounds than was the DB-WAX column.

#### References

- (1) Anderson, J. L.; Armstrong, D. W.; Wei, G. *Anal. Chem.* **2006**, *78*, 2893-2902.
- (2) Han, X.; Armstrong, D. W. *Acc. Chem. Res.* **2007**, *40*, 1079-1086.
- (3) Soukup-Hein, R.; Warnke, M. M.; Armstrong, D. W. *Annual Review of Analytical Chemistry* **2009**, *2*.
- (4) Walden, P. *Bull.Acad.Imp.Sci.St.-Petersbourg; Bulletin de l'Academie Imperiale des Sciences de St.-Petersbourg* **1914**, , 405-422.
- (5) Wilkes, J. S.; Zaworotko, M. J. *J.Chem.Soc., Chem.Commun.; Journal of the Chemical Society, Chemical Communications* **1992**, , 965-967.
- (6) Pino, V.; Anderson, J. L.; Ayala, J. H.; Gonzalez, V.; Afonso, A. M. *J. Chromatogr. A* **2008**, *1182*, 145-152.
- (7) Lohithakshan, K. V.; Aggarwal, S. K. *Radiochim.Acta; Radiochimica Acta* **2008**, *96*, 93-97.
- (8) Lo, W.; Yang, H.; Wei, G. *Green Chem.* **2003**, *5*, 639-642.
- (9) Pei, Y.; Wu, K.; Wang, J.; Fan, J. *Sep. Sci. Technol.* **2008**, *43*, 2090-2102.
- (10) Carda-Broch, S.; Berthod, A.; Armstrong, D. W. *Anal.Bioanal.Chem.; Analytical and Bioanalytical Chemistry* **2003**, *375*, 191-199.
- (11) Liu, J.; Li, N.; Jiang, G.; Liu, J.; Jonsson, J. A.; Wen, M. *J. Chromatogr. A* **2005**, *1066*, 27-32.
- (12) Yao, C.; Pino, V.; Anderson, J. L. *J. Chromatogr. A* **2009**, *1216*, 948-955.
- (13) Soukup-Hein, R. J.; Remsburg, J. W.; Dasgupta, P. K.; Armstrong, D. W. *Anal.Chem.(Washington, DC, U.S.); Analytical Chemistry (Washington, DC, United States)* **2007**, *79*, 7346-7352.
- (14) Remsburg, J. W.; Soukup-Hein, R. J.; Crank, J. A.; Breitbach, Z. S.; Payagala, T.; Armstrong, D. W. *J. Am. Soc. Mass Spectrom.* **2008**, *19*, 261-269.
- (15) Soukup-Hein, R. J.; Remsburg, J. W.; Breitbach, Z. S.; Sharma, P. S.; Payagala, T.; Wanigasekara, E.; Huang, J.; Armstrong, D. W. *Anal. Chem.* **2008**, *80*, 2612-2616.

- (16) Carda-Broch, S.; Berthod, A.; Armstrong, D. W. *Rapid Commun. Mass Spectrom.* **2003**, *17*, 553-560.
- (17) Armstrong, D. W.; Zhang, L.; He, L.; Gross, M. L. *Anal. Chem.* **2001**, *73*, 3679-3686.
- (18) Li, Y. L.; Gross, M. L. *J. Am. Soc. Mass Spectrom.* **2004**, *15*, 1833-1837.
- (19) Zabet-Moghaddam, M.; Krueger, R.; Heinzle, E.; Tholey, A. *J. Mass Spectrom.* **2004**, *39*, 1494-1505.
- (20) Li, Y. L.; Gross, M. L.; Hsu, F. *J. Am. Soc. Mass Spectrom.* **2005**, *16*, 679-682.
- (21) Catharino, R. R.; de Marques, L.; Santos, L. S.; Baptista, A. S.; Gloria, E. M.; Calori-Domingues, M. A.; Facco, E. M. P.; Eberlin, M. N. *Anal. Chem.* **2005**, *77*, 8155-8157.
- (22) Santos, L. S.; Haddad, R.; Hoeehr, N. F.; Pilli, R. A.; Eberlin, M. N. *Anal. Chem.* **2004**, *76*, 2144-2147.
- (23) Baltazar, Q. Q.; Leininger, S. K.; Anderson, J. L. *J. Chromatogr. A* **2008**, *1182*, 119-127.
- (24) Huang, K.; Han, X.; Zhang, X.; Armstrong, D. W. *Anal. Bioanal. Chem.; Analytical and Bioanalytical Chemistry* **2007**, *389*, 2265-2275.
- (25) Seeley, J. V.; Seeley, S. K.; Libby, E. K.; Breitbach, Z. S.; Armstrong, D. W. *Anal. Bioanal. Chem.; Analytical and Bioanalytical Chemistry* **2008**, *390*, 323-332.
- (26) Lambertus, G. R.; Crank, J. A.; McGuigan, M. E.; Kendler, S.; Armstrong, D. W.; Sacks, R. D. *J. Chromatogr. A* **2006**, *1135*, 230-240.
- (27) Breitbach, Z. S.; Armstrong, D. W. *Anal. Bioanal. Chem.; Analytical and Bioanalytical Chemistry* **2008**, *390*, 1605-1617.
- (28) Anderson, J. L.; Armstrong, D. W. *Anal. Chem.* **2005**, *77*, 6453-6462.
- (29) Ding, J.; Welton, T.; Armstrong, D. W. *Anal. Chem.* **2004**, *76*, 6819-6822.
- (30) Tholey, A.; Zabet-Moghaddam, M.; Heinzle, E. *Anal. Chem.* **2006**, *78*, 291-297.
- (31) Lemaire, R.; Tabet, J. C.; Ducoroy, P.; Hendra, J. B.; Salzet, M.; Fournier, I. *Anal. Chem.* **2006**, *78*, 809-819.
- (32) Santos, L. S.; Haddad, R.; Hoeehr, N. F.; Pilli, R. A.; Eberlin, M. N. *Anal. Chem.* **2004**, *76*, 2144-2147.
- (33) Gordon, J. E.; Selwyn, J. E.; Thorne, R. L. *J. Org. Chem.* **1966**, *31*, 1925-1930.
- (34) Pacholec, F.; Butler, H. T.; Poole, C. F. *Anal. Chem.* **1982**, *54*, 1938-1941.
- (35) Poole, C. F.; Butler, H. T.; Coddens, M. E.; Dhanesar, S. C.; Pacholec, F. *J. Chromatogr.* **1984**, *289*, 299-320.
- (36) Armstrong, D. W.; He, L.; Liu, Y. *Anal. Chem.* **1999**, *71*, 3873-3876.
- (37) Anderson, J. L.; Ding, J.; Welton, T.; Armstrong, D. W. *J. Am. Chem. Soc.* **2002**, *124*, 14247-14254.
- (38) Anderson, J. L.; Ding, R.; Ellern, A.; Armstrong, D. W. *J. Am. Chem. Soc.* **2005**, *127*, 593-604.
- (39) Anderson, J. L.; Armstrong, D. W. *Anal. Chem.* **2005**, *77*, 6453-6462.

## CHAPTER 2

# TOWARDS A SECOND GENERATION OF IONIC LIQUID MATRICES (ILM'S) FOR MALDI-MS OF PEPTIDES, PROTEINS, AND CARBOHYDRATES

Jeffrey A. Crank and Daniel W. Armstrong  
Chemistry and Biochemistry Department, University of Texas Arlington, Arlington TX  
76019

### Abstract

Second generation ionic liquid matrices are developed, examined, and tested. They have shown a wide mass detection range (< 1000 Da to > 270000 Da) for proteins and peptides with greater S/N ratios than solid matrices. These ionic liquid matrices also exhibit the ability to effectively ionize proteins of large mass without disrupting non-covalent interactions between monomers. Both the anionic and cationic moieties have been varied systematically to find an ionic liquid matrix with the best physical properties, analyte signal intensity, and widest mass detection range. It was determined that both the proton affinity and  $pK_a$  of the cation have a large effect on the ionic liquid matrices ability to effectively ionize the analyte. The ionic liquid matrices can be used to detect polysaccharides with fewer degradation products than solid matrices. *N,N*-diisopropylethylammonium  $\alpha$ -cyano-4-hydroxycinnamate and *N*-isopropyl-*N*-methyl-*t*-butylamine  $\alpha$ -cyano-4-hydroxycinnamate were the best matrices for proteins and peptides and that *N,N*-diisopropylethylammonium  $\alpha$ -cyano-4-hydroxycinnamate and *N,N*-diisopropylethylammonium ferulate were the best matrices for carbohydrates.

## Introduction

There has been considerable interest in the properties and applications of ionic liquids (ILs). ILs are defined as non-molecular salts that have a melting point below 100°C and are called room temperature ILs if the melting point is at or below room temperature. There have been many applications of ILs including solvents for organic synthesis and liquid-liquid extraction [1-5], gas chromatography stationary phases [6-12], matrix assisted laser desorption/ionization (MALDI) matrices [13-19], and recently as ion pairing reagents for the trace analysis of anions by electrospray ionization mass spectrometry in the positive mode [20-22].

ILs used as MALDI matrices were first reported by Armstrong et al. in 2001[14]. In this initial report, the authors showed the many advantages of using ILs as MALDI matrices such as the homogeneity of the sample in the matrix which leads to better shot to shot reproducibility, the negligible vapor pressure of the IL, and an increase in signal compared to solid matrices. It was also shown in a subsequent publication by Li and Gross [15] that the use of ionic liquid matrices (ILMs) enhanced quantitative analysis with MALDI compared to solid matrices. This improved quantification is mainly due to the homogeneity of the sample. Solid matrices such as  $\alpha$ -cyano-4-hydroxycinnamic acid (CHCA), ferulic acid (FA), and sinapinic acid (SA) rely on co-crystallization of matrix and analyte which can lead to non-homogeneity and searching for so called “hot spots”. These “hot spots” lead to poor shot to shot reproducibility. Other problems associated with solid matrices are difficult sample preparation, analyte size and/or type restrictions for different matrices [14], and harsh



conditions used for preparation of the matrix [23]. Difficulty in sample preparation is typically caused by the analyte disrupting crystallization. Specific MALDI matrices are thought to be optimal for specific types and sizes (i.e. molecular weights) of analytes. For example, CHCA is typically used for proteins and peptides below 10,000 Da, whereas SA is typically used for proteins above 10,000 Da. The type of analyte is also important with regard to the matrix selected. Matrices that work well for one class of analytes may not work for another class even though they may be in the same molecular weight range. One example of this is the use of MALDI to detect carbohydrates and small proteins. CHCA is used for small proteins and 2,5-dihydroxybenzoic acid is used for carbohydrates. Harsh matrix preparation conditions can also be a problem with high molecular weight proteins that have non-covalently coordinated subunits [23]. Typically solid matrix preparation requires 0.05-0.2 % trifluoroacetic acid. This results in an acidic matrix solution which can disrupt non-covalent interactions.

Ionic liquid matrices (ILMs) can be used to overcome many of the shortcomings of solid matrices. They are easily prepared, require no co-crystallization with the analyte, and produce homogeneous solutions of matrix and analyte, so there is no searching for “hot spots”. ILMs also can be used for detection of many different types of analytes and for broader ranges of molecular sizes. Also ILMs use no trifluoroacetic acid in the sample preparation. Thus a less acidic matrix helps to preserve the protein structural elements that require non-covalently assembled subunits. This makes detection of large intact proteins easier.

Recent publications on ILMs show many applications for previously reported matrices [24-29], but very few new matrices have been synthesized. Also, to our knowledge there have been no reports of exhaustive studies on how varying the IL's anionic and cationic moieties can affect the physical state of the ILM as well as the signal that can be achieved and/or the analyte specificity. In this study we examine over 100 cation/anion pairs and show that systematically changing the cation or anion will imbue the ILM with different desirable properties. Finally, we show how one ILM can be used for the detection of many analytes of a wide mass range (<1000 Da to > 270000 Da), with stronger signals than can be obtained with solid matrices. In essence we develop, examine, and test a second generation of ionic liquid based MALDI matrices.

## Experimental

### *Materials and Instrument*

The following reagents were purchased from Sigma-Aldrich (St Louis, MO, USA) :  $\alpha$ -cyano-4-hydroxycinnamic acid, ferulic acid, sinapinic acid, diphenic acid, 2,5-dihydroxybenzoic acid, all trans retinoic acid, butylamine, octylamine, 2-aminopentane, triethanolamine, tributylamine, triisobutylamine, N,N- diisopropylethylamine, N-isopropyl-N-methyl-tert-butylamine, (4-bromophenyl) diphenyl sulfonium bis(trifluoromethane)sulfonimide, 1,4-diaminobutane, triethylenetetramine hydrate, N-isopropyl diethylenetriamine, (4-methylthiophenyl) methyl phenyl sulfonium bis(trifluoromethane)sulfonimide,

diphenyliodinium bromide, naphthyl diphenylsulfonium bis(trifluoromethane)sulfonamide, anthraquinone-2-carboxylic acid, bradykinin, polyethylene glycol 4600, insulin, cytochrome C, bovine serum albumin (BSA), catalase, urease, dextran enzymatic synth.(MW=1500 Da) , and mannan from *Saccharomyces cerevisiae*.  $\beta$ -Cyclodextran was obtained from Advanced Separation Technologies inc.(Whippany, NJ, USA). Solvents, microcentrifuge tubes and TFA were obtained from VWR(West Chester, PA, USA ). All data was collected on a Bruker Autoflex mass spectrometer and analyzed with Bruker Flex Analysis Software.

Carbohydrates were analyzed using Bruker Polytools software. All spectra shown are the sum of 100 laser shots with at least 3 spectra taken for each analyte to confirm analyte signal intensity consistency and mass. pH measurements were taken on an Orion 410A pH meter.

#### *Matrix and Sample Preparation*

Stock solutions of analytes were prepared at the following concentrations: bradykinin 0.1 mM, dextran 0.1 mM, cyclodextrin 0.1 mM, cytochrome c 0.1 mM, insulin 0.1 mM, polyethylene glycol 4600 0.1 mM, BSA 0.05 mM, catalase 0.05 mM, urease 0.05 mM. Mannan was prepared as a 1 mg/ml solution due to the fact that no molecular weight information could be obtained from the manufacturer.

Solid matrices were prepared according to the following procedure. A solution of water/acetonitrile (50/50, v/v) with 0.1% TFA was added to microcentrifuge tubes containing the solid matrices SA, FA, and CHCA. The solutions were then vortexed to make saturated solutions of the matrices. The matrices were then mixed with the analyte in a ratio of 10:1

(matrix/analyte, v/v) and vortexed to ensure complete mixing. Then, one  $\mu\text{L}$  of the matrix/analyte solution was spotted on the MALDI plate and allowed to dry. 2,5-Dihydroxybenzoic acid (DHB) matrix solution was prepared by the following procedure. DHB was added to a solution of water/acetonitrile (50/50, v/v) with 0.1% TFA to make a 20mg/ml solution. The DHB solution was then mixed with the analyte in a ratio from 10:1 (matrix/analyte, v/v) to 20:1 to find the optimal conditions for each analyte. The matrix/analyte solution was then vortexed to ensure complete mixing. Then, one  $\mu\text{L}$  of the matrix/analyte solution was spotted on the MALDI plate and allowed to dry. The apparent pH of the SA matrix solution was obtained by direct measurement of the hydro-organic solution with a pH meter.

ILMs were prepared as previously reported [13, 14]. In short, one molar equivalent of solid matrix was dissolved in methanol. Then, one molar equivalent of base was added to the methanol solution which was stirred for 30 min to ensure complete reaction. The solvent was then removed by rotary evaporator and the resulting ILM was placed under vacuum overnight to ensure dryness. NMR was used to confirm the ILMs structure. Next, the ILM was added to a microcentrifuge tube and ethanol was added to make a saturated solution. Note: most of the ILMs are either solids or glasses (supercooled liquids) when spotted on the MALDI plate. Lastly, the ILM solution was mixed with the analyte solution in a ratio of 10:1 (matrix/analyte v/v) and vortexed to ensure complete mixing. The mixture was then spotted on the MALDI plate and the ethanol was allowed to evaporate. For matrices with two cations, the same procedure was followed with the exception that two molar equivalents of base were added to the acid instead of one. Typically, methanol/matrix solutions are

yellow, and when one equivalent of base is added, the solution changes to an orange color. When two equivalents of base are added the solution turns red. Color change varies by matrix with the most pronounced change seen with SA. This color change is due to the ionization of the carboxylic acid and then the phenolic group of the matrix. The pH of the ILM matrix IMTBA CHCA was obtained by preparing a 0.1M solution of the matrix in water and measuring with a pH meter. The stability of dicationic ILMs under vacuum is similar that of monocationic ILMs. After the dicationic ILMs were placed under vacuum overnight, it was seen by NMR that 2 equivalents of base were still present (see SI 4).

## Results and discussion

In this study 114 matrices were tested and 105 new ionic liquids were prepared. Most of these ILMs produce signal for at least one or more of the analytes tested with a S/N above 3. Some ILMs produced much more intense signals with S/N ratios greater than any of the solid matrices. All ILs used are listed in Table 1. Six of the 105 ILMs prepared showed increased analyte S/N ratios compared to solid matrices. These ILMs are: N-isopropyl-N-methyl-N-tert-butylammonium  $\alpha$ -cyano-4-hydroxycinnamate [IMTBA CHCA], N,N-diisopropylethylammonium  $\alpha$ -cyano-4-hydroxycinnamate [DEA CHCA], *di*(2-aminopentane)  $\alpha$ -cyano-4-hydroxycinnamate [*di*(AP) CHCA], N-isopropyl-N-methyl-N-tert-butylammonium ferulate [IMTBA F], diisopropylethylammonium ferulate [DEA F], and *di*(2-amino pentane) ferulate [*di*(AP) F]. In addition to producing higher S/N ratios, use of

these ILMs also resulted in an increased mass detection range when compared to solid matrices.

Figure 1 shows a comparison of the IMTBA CHCA ionic liquid matrix with the solid matrices CHCA and SA over a wide mass range with the same laser power and analyte concentration. The laser power was decreased for spectra D and K because the intensity was too great for the ILM in spectra C and J, resulting in poor resolution. Spectra A-D in Figure 1 show the detection of bradykinin (MW=1,060 Da) with the mass plus proton peak denoted as  $[M + H]^+$ . In these four spectra it can be seen that both the CHCA (Figure 1A) and IMTBA CHCA (Figure 1C) perform well. The resolution is poor in spectrum A and C due to high laser intensity and is vastly improved to unit mass resolution with lower laser power, as can be seen in spectrum D (spectrum with reduced laser power for CHCA also achieves unit mass resolution with similar analyte signal intensity but is not shown).

Spectra E-G (Fig. 1) show the detection of cytochrome C (MW=12,000 Da) with the same  $[M + H]^+$  notation. In this case, IMTBA CHCA far out performs both CHCA and SA. Since CHCA is used for proteins <10,000 Da it did not detect cytochrome C well. However, the addition of one equivalent of base to form IMTBA CHCA can increase the S/N for cytochrome C by 19 times. The IMTBA CHCA matrix also produces a 2.6 times increase in S/N as compared to the SA matrix.

Spectra H-K (see Fig. 1) show the detection of BSA (MW=66,000 Da). Spectrum H shows that CHCA can be used for high molecular weight analytes, but the mass resolution is

typically poor. Also, many peaks are seen that can not be identified and are assumed to be fragments of the intact protein. Spectrum I shows a clean spectrum obtained using the SA matrix. In this spectrum, peaks for  $[M + 3H]^{3+}$ ,  $[M + 2H]^{2+}$ ,  $[2M + 3H]^{3+}$ ,  $[M + H]^+$ ,  $[4M + 3H]^{3+}$ ,  $[3M + 2H]^{2+}$ ,  $[2M + H]^+$ , and  $[3M + H]^+$  were observed and identified by mass [30-32]. Multiply charged peaks and singly charged peaks for n-mers of large proteins are expected and have been reported previously [30-32]. These reports show the detection of large proteins with solid matrices. However, problems such as different matrices and solvent systems for each protein are needed and difficulty in detecting large non-covalently assembled subunits arise. ILMs use the same sample preparation for every protein tested and detect non-covalently assembled subunits easily. Spectrum J shows peaks for  $[M + H]^+$ ,  $[M + 2H]^{2+}$ ,  $[2M + H]^+$ , and  $[3M + H]^+$ . A  $[4M + H]^+$  peak can also be seen in spectrum J, which is not seen when SA is used as a matrix. However, there are some peaks that are assumed to be fragments of the protein that could not be identified at this high laser intensity. Spectrum K shows the IMTBA CHCA ILM with a 6% laser power decrease. In this case the spectrum is much cleaner. Peaks that were identified in spectrum K are  $[M + 3H]^{3+}$ ,  $[M + 2H]^{2+}$ ,  $[M + H]^+$ ,  $[3M + 2H]^{2+}$ ,  $[2M + H]^+$ , and  $[3M + H]^+$ . It should be noted that n-mers of BSA are artifacts of the MALDI process and are not observed *in vivo*.

Spectra L-N (see Fig. 1) show the detection of urease which is a hexamer with subunits that are 90,000 Da each. The CHCA (spectrum L, Figure 1) does not show any peaks for urease. Spectrum M (using sinapinic acid) has two discernable peaks that are above a S/N of 3, corresponding to  $[M + H]^+$  and  $[M + 2H]^{2+}$ . The  $[M + 3H]^{3+}$  peak can also be seen but the S/N ratio is less than 2. It is believed that the trifluoroacetic acid used in the sample

preparation of the SA disrupts the non-covalent interactions between the urease subunits and therefore only the subunits are detected[32]. This can be explained by the fact that urease has an optimal activity pH of ~7.2 and will denature at low pHs(~2) [33]. The SA/TFA solution has a pH of ~2 while the ionic liquid matrix has a pH of 7.8 (measured as outlined in the Experimental section). The low pH for the SA solution will affect the assembly of the monomers and most likely denature the protein [30,33]. Spectrum N shows that the ionic liquid matrix IMTBA CHCA far out performs SA and CHCA with the S/N of the  $[M + H]^+$  peak 1.7 times that of the SA mass plus proton peak. Other peaks that were identified include  $[M + 3H]^{3+}$ ,  $[M + 2H]^{2+}$ ,  $[3M + 2H]^{2+}$ ,  $[2M + H]^+$ , and  $[3M + H]^+$ . However, it is noted that the peaks for  $[M + 3H]^{3+}$  and  $[3M + 2H]^{2+}$  have a S/N ratio of ~2.  $[4M + H]^+$  and  $[5M + H]^+$  are not seen in this spectrum and  $[6M + H]^+$  is beyond the detection ability of the instrument. Similar results were seen with the detection of catalase which is a tetramer with a monomer mass of 60,000 Da. Both CHCA and SA showed only a small monomer peak with S/N ratios of 2 and 3 respectively. On the other hand, IMTBA CHCA shows  $[M + H]^+$ ,  $[2M + H]^+$ ,  $[4M + 2H]^{2+}$ ,  $[5M + 3H]^{2+}$ ,  $[3M + H]^+$ , and  $[4M + H]^+$  peaks, with all peak intensities greater than or equal to a S/N ratio of 3 (Figure 2). Other analytes of interest that were tested are polyethylene glycol 4600, insulin (MW=5,700 Da), and  $\beta$ -cyclodextran (MW=1,135 Da). These analytes were detected using ILMs and show higher signal intensities than solid matrices (data not shown).



### *Physical properties of ILMs*

The physical states of these ILMs vary between that of solids, waxes, glasses, or liquids. Most of the ILMs synthesized exist as supercooled liquids when spotted on the MALDI plate. It was observed that the ferulate ILMs are more likely to be super cooled liquids than CHCA or sinapinate based ILMs.

The effect of the cation on the ILM physical state was studied by varying the alkyl chain length, symmetry and size of the amines. Butylamine, octylamine, and decylamine were paired with CHCA, FA, and SA to see if there is an effect of carbon chain length on physical state. It was found that there is a little or no difference in the physical state of the ILM when changing carbon chain length from 4 to 10 carbons. Unsymmetrical amines such as N-isopropyl-N-methyl-N-tert-butylamine and N,N-diisopropylethylamine were used as ILM cations to determine if the lack of symmetry would decrease the melting point of the ILM. It was found that the unsymmetric cations only decreased the melting points of the ILMs by 1-2 deg C. However, unsymmetric sterically hindered amines did produce an increase in analyte signal as will be discussed below. One tertiary amine that did lower the melting point of ILMs was triethanolamine. Pairing of triethanolamine with any solid matrix resulted in a room temperature ILM. However, no triethanolamine (TEA) ILM showed any analyte signal. This phenomenon is discussed in the cation effect on signal intensity section. ILMs with two different cations were also synthesized in an attempt to lower melting temperatures. Mixed cation ILMs showed a slight decrease (1-2°C) in melting temperature but did not show any major advantages over ILMs with two identical cations. Also, it is interesting to note

that if TEA is added as a second cation to any ILM that works well, subsequently no analyte signal can be detected.

### *Anion effects on signal intensity*

Previously it was assumed that the effect of the ILM anion on analyte signal and detection might be somewhat analogous to that observed for solid matrices. A CHCA ILM should be better for small analytes (< 10,000 Da) and a sinapinate ILM should be preferable for large analytes (> 10,000 Da). However, Figure 3 shows BSA (66,000 Da) has higher signal intensity using a CHCA-ILM than with a SA-ILM. The molecular weight limitations of solid MALDI matrices do not apply to the ionic liquid matrices. This will be discussed subsequently. Also, Figure 3 shows how the intensity of the BSA signal changes with the ILM: IMTBA CHCA (A), IMTBA ferulate (B), and IMTBA sinapinate (C). The S/N for the  $[M + H]^+$  peak of IMTBA CHCA is 7.1 times greater than IMTBA sinapinate, 1.6 times greater than IMTBA ferulate. As a general trend for ILM anions with protein analytes, the signal decreases in going from  $\alpha$ -cyano-4-hydroxycinnamate to ferulate to sinapinate. To elucidate why  $\alpha$ -cyano-4-hydroxycinnamate produces greater signal than ferulate and sinapinate, the proton affinities and pK<sub>a</sub>'s of the conjugate acids were examined. The proton affinities and the pK<sub>a</sub>'s of the acids CHCA, ferulic acid, and sinapinic acid have been published previously[34-37]. However, in this work there seems to be no correlation between these properties and the analyte signal produced.

In this study, many ILMs have been made with new anions, but as of yet none have surpassed the signal intensity achieved by IL analogues of CHCA, ferulic acid, and sinapinic acid. Unique anions such as anthroquinone-2-carboxylate, all *trans*-retinoate, and 1-(2-carboxyethyl)-3-(2-hydroxyethyl) imidazolium bromide have been used to make ILMs with each having their own unique drawbacks. Anthroquinone-2-carboxylic acid was paired with DEA and became a supercooled ILM. However, signals achieved with the anthroquinone were low and many extraneous peaks were observed. The retinoic acid ILM is extremely hydrophobic and solubility issues with the analytes and this ILM were observed. 1-(2-carboxyethyl)-3-(2-hydroxyethyl) imidazolium bromide was paired with IMTBA, which formed a room temperature IL. However, this ILM did not give sufficient signal for any analyte tested. The search for new anions is ongoing.

#### *Cation Effects on Signal Intensity*

The cation of ILMs has a large effect on signal intensity and physical state (solid, liquid, glass) and has been studied systematically. Typical cations used in previous studies are ethylamine, butylamine, tributylamine, and various pyridine derivatives [13,14]. These cations were chosen at random from a pool of amines. In this study both chain length and the steric bulk were varied to find optimal cations. Butylamine, octylamine, and decylamine were used to see the effect of carbon chain length on signal intensity. The intensity of the analyte peaks corresponding to these ILMs can vary drastically. Typically the signal intensity resulting from the butylamine ILs are the most intense followed by octylamine and

decylamine, although the protein peaks are still not as intense as with solid ferulic acid (see Figure SI 1, ferulic-decylamine not shown).

The effect of steric bulk of the cation on signal intensity was studied systematically. This was done by pairing a variety of substituted amines with CHCA, FA, and SA to produce ILMs. The amines tested were butylamine (BA), 2-aminopentane(AP), tributylamine (TBA), *N,N*-diisopropylethylamine (DEA), *N*-isopropyl-*N*-methyl-*tert*-butylamine (IMTBA), and triisobutylamine (TIBA) giving a wide range of sterically bulky amines. Figure SI 1 shows that matrices containing sterically hindered amines produce much higher analyte signal intensities than primary amines for all analytes tested. However, steric factors alone are not the only things that contribute to the analyte signal intensity. This can be seen in the case of the AP and TBA cations. AP is a primary amine that often gives an analyte signal intensity that is equal to or greater than TBA. TBA is a tertiary amine that does not give signal intensities that are expected for a sterically hindered amine. TBA often shows little or no analyte signal. It is not structurally evident why TBA produces poor analyte signal intensities. It appears that possible explanations for a cation's effectiveness as a matrix component involves its  $pK_a$  and proton affinity (PA). Essentially, the  $pK_a$  represents the solution phase acidity of the protonated amine and the PA represents the acidity in the gas phase of the conjugate base of the amine. When considering ILM cations that work well, a general trend is observed. Cations must have a high  $pK_a$  ( $\geq 11$ ) and PA ( $>930$  kJ/mole) as seen in Table 2. If either the PA or  $pK_a$  is low, the matrix tends to perform poorly. TBA has a  $pK_a$  of 9.9 and a PA of 998.5 kJ/mole[38]. In comparison, other tertiary amines that work well as ILM cations such as DEA, which has a  $pK_a$  of 11.4 and a PA of 994.3 kJ/mole[38].

TBA's  $pK_a$  is only slightly above that of ammonia (9.24). Other cations that do not work well as ILMs cations have similar or lower  $pK_a$ 's. One of these cations is TIBA with a proton affinity of 967.6 kJ/mole [38] and a  $pK_a$  of 9.51. TIBA is so sterically hindered that the proton transfer does not happen easily in solution with the matrix acids CHCA, FA, and SA. Typically when synthesizing TIBA ILMs, after removal of the solvent, neat TIBA will collect in the bottom of the flask after 2-3 min (see Experimental).

Other cations of interest that did not produce good results are triethanol amine (TEA), 1,4-diaminobutane, triethylenetetramine hydrate, and N-isopropyl-diethylenetriamine. It was originally thought that TEA would help with the ionization process and lower the melting point of the ILMs. All TEA ILMs were room temperature ILMs, however, no analyte signal was observed with any TEA based matrix. This phenomenon can also be explained by the  $pK_a$  and proton affinity. TEA has a  $pK_a$  of 7.8 and a proton affinity of 941 kJ/mole [39]. TEA has a moderate proton affinity but a relatively acidic  $pK_a$  when compared to other protonated amines. It was also hypothesized that 1,4-diaminobutane, triethylenetetramine, and N-isopropyl-diethylenetriamine might be good cations for ILMs because multiple anions can be paired with single molecules of di-, tri-, or tetraamines. However, there was no increase in signal for the analytes tested compared to other ILM's and the melting point was not decreased enough to make a room temperature ILM. Also, in an attempt to lower melting point and increase the analyte signal intensity for low and high molecular weight analytes, different anions were paired with a di-, tri-, or tetraamine molecules. SA, FA, and CHCA were paired with a triamine but did not show improved signal or a lower melting point (Table

1). Two FA molecules and one CHCA molecule were also paired with a triamine with similar unimpressive results. Di(1,1,3,3-tetramethyl-guanidinium)  $\alpha$ -cyano-4-hydroxycinnamate [29] was also evaluated. Di(1,1,3,3-tetramethyl-guanidinium)  $\alpha$ -cyano-4-hydroxycinnamate was showed satisfactory results with bradykinin but failed to produce adequate signal for cytochrome C and mannan (Table 1).

The effect of using multiple cations also was explored. All acids tested (SA, FA, and CHCA) have two ionizable groups (one phenolic OH and one carboxylic OH). Systematic testing of the matrices with zero (solid matrices), one, and two cations was performed. It was found that the addition of one or two cations may increase the signal intensity, but the benefits of adding cations to solid matrices must be evaluated on a case by case basis. The effects of multiple cations can be seen in Figure SI 2 for the detection of cytochrome C with CHCA (A), BA CHCA (B), and *di*(BA) CHCA (C). The addition of 1 and 2 cations increases the analyte signal. The signal is increased by a factor of 2 when one butylamine is added and by a factor of 4 when 2 butylamines are added. The non-gaussian peak shapes in this figure are due to the large laser intensity used in the spectra. A relatively large laser intensity was used in these spectra so that the analyte peak in the CHCA spectrum could be seen. All spectra are presented on the same mass and intensity scale. The presence of 2 BA molecules was verified by NMR by the disappearance of the acidic protons and the integration of the spectrum (see Supplemental Information).

However, addition of multiple equivalents of base does not necessarily guarantee the removal of the phenolic proton and an increase in signal. Figure SI 3 shows the detection of

cytochrome C with CHCA (A), IMTBA CHCA (B), and *di*(IMTBA) CHCA (C). When one cation is added the S/N increases by a factor of 24, and when the second IMTBA is added there does not appear to be further improvement in the S/N. This phenomenon can be explained by the NMR spectrum of *di*(IMTBA) CHCA. Through NMR it is seen that for the sterically hindered bases (DEA and IMTBA) do not remove the phenolic proton and only one equivalent of base is present. No further improvement in analyte signal intensity is seen because the second equivalent of base is removed when the ILM is placed under vacuum (see Experimental, and Supplemental Information). The non-gaussian peak shapes in this figure are also due to the large laser intensity used in the spectra. A relatively large laser intensity was used in these spectra so that the analyte peak in the CHCA spectrum could be seen. All spectra are presented on the same mass and intensity scale.

### *Detection of Polysaccharides*

Detection and molecular weight determination of polysaccharides is important for the characterization of natural polymers such as dextrans and mannans. Size exclusion chromatography (SEC) will give a mass range, but can sometimes over or underestimate the molecular weight due to the fact that the standards used are not structurally or chemically similar to the polymer being analyzed [40,41].

MALDI-MS of these polymers displays its own unique drawbacks. Acid content of the matrix or the solution used to integrate the sample and matrix can start to degrade the polymer. Thus some structural information can be obtained, but any useful information about

the average molecular weight of the polymer is obscured. Also, co-crystallization with the matrix is problematic since these polymers typically form viscous solutions when dissolved. When the concentration of polymer is decreased satisfactory crystallization was achieved.

ILMs are ideally suited to overcome each of the aforementioned drawbacks because no acid is added and no crystallization is needed. Figure 4 shows the detection of Dextran 1500 with A) DHB, B) DEA F, and C) DEA CHCA. DHB ILM analogs were also tested but produced spectra similar to the DHB matrix spectrum (data not shown). Figure 4A shows that adequate signal is observed with DHB. The peaks in Figure 4A differ by 162 Da corresponding to the mass differences of the glucose units. The identified peak distribution has a mass range from 365 Da to 2311 Da, which corresponds to 2 to 14 sodiated glucose units. It appears that the acid content of the DHB partially degraded the sample resulting in a distribution of  $m/z$  that almost exponentially increases toward the low mass region of the spectrum. The number average molecular weight ( $M_n$ ) and weight average molecular weight ( $M_w$ ) obtained (see Experimental) for dextran 1500 with the DHB matrix are 727 Da and 787 Da respectively. Figure 4B shows the spectrum of dextran 1500 using DEA F as a matrix. It can be clearly seen that the spectrum obtained with the ILM shows a more uniform, almost Gaussian distribution of peaks representing 2 to 14 glucose units. Spectrum 4B also shows a second smaller distribution of peaks which represents potassium adducts of the dextran. It has been noticed experimentally that ferulic ionic liquids tend to promote the formation of sodium and potassium adducts more than CHCA or siapinic ionic liquids. The  $M_n$  and  $M_w$  of the sodium adduct distribution for dextran 1500 is 1208 Da and 1305 Da respectively. The potassium adduct distribution shows a  $M_n$  of 1274 Da and a  $M_w$  of 1319 Da. The discrepancy between



the listed  $M_w$  1500 and the MALDI  $M_w$  of 1305 is assumed to be due to differences between the SEC standard polymers used and the dextran [41,42]. Figure 4C shows the spectrum of dextran 1500 using DEA CHCA as a matrix. DEA CHCA shows a smaller but still uniform distribution of sodium adduct peaks representing 3 to 9 glucose units. The distribution shows a  $M_n$  of 1063 Da and a  $M_w$  of 1085 Da. The  $M_n$  and  $M_w$  of the spectrum obtained with DEA CHCA (see Experimental) is less than that of the spectrum from DEA F because fewer high mass peaks were detected with DEA CHCA, making  $M_n$  and  $M_w$  smaller. Although we do not vouch for the accuracy of Polytools software program, it is clear that the IL matrices give a more uniform distribution of molecular weights and higher average molecular weights; most likely leading to more accurate mass determinations.

Figure 5 shows the detection of mannan from *Saccharomyces cerevisiae* with A) IMTBA CHCA, B) DEA CHCA, and C) DHB. No molecular weight information could be obtained from the manufacturer of the mannan (see Experimental). Figure 5A shows the spectrum of mannan using IMTBA CHCA as a matrix. The spectra of mannan using ionic liquid matrices show a uniform distribution. The peaks in Fig. 5A represent the sodium adducts of 5 to 20 mannose units. The  $M_n$  and  $M_w$  of the sodium adduct distribution for mannan is 2074 Da and 2256 Da respectively. Figure 5B shows the spectrum obtained for mannan with the DEA CHCA matrix. The peaks represent the sodium adducts of 5 to 24 mannan units with the  $M_n$  and  $M_w$  equal to 2183 Da and 2431 Da respectively. Figure 5C shows that when DHB is used as a matrix, no polymer signal can be seen. CHCA was also tested for the detection of mannan with similar negative results (data not shown).

## Conclusions

A new generation of ILMs have shown themselves to be exceptional MALDI matrices. These ILMs have a practical mass working range from less than 1000 Da to greater than 270,000 Da for peptides and proteins. They also exhibit the ability to detect many different types of analytes. It also can be seen that the ILMs do not disrupt the quaternary structure of proteins allowing for the detection of intact proteins or N-mers of proteins.

Tertiary cations used in these ILMs have been shown to be dependent on  $pK_a$  and proton affinity with the minimum requirements being  $\geq 11$  and  $\geq 930\text{kJ/mole}$  respectively. It was also shown that these ILMs can be used to detect analytes such as polysaccharides with fewer degradation products. It was found that the DEA CHCA and IMTBA CHCA worked best for proteins and peptides and that DEA CHCA and DEA F worked best for carbohydrates. The search for new anions, cations, and unique analytes is ongoing and will be presented in subsequent publications.

## Acknowledgments

The authors would like to thank that Robert A. Welch foundation for its support.

## References

1. Pino, V.; Anderson, J. L.; Ayala, J. H.; Gonzalez, V.; Afonso, A. M. The Ionic Liquid 1-Hexadecyl-3-Methylimidazolium Bromide as Novel Extracting System for Polycyclic

Aromatic Hydrocarbons Contained in Sediments using Focused Microwave-Assisted Extraction. *J. Chromatogr. A.* **2008**, *1182*, 145-152.

2. Lohithakshan, K. V.; Aggarwal, S. K. Solvent Extraction Studies of Pu(IV) with CMPO in 1-Octyl 3-Methyl Imidazolium Hexa Fluorophosphate (C8mimPF6) Room Temperature Ionic Liquid (RTIL). *Radiochim.Acta.* **2008**, *96*, 93-97.

3. Lo, W.; Yang, H.; Wei, G. One-Pot Desulfurization of Light Oils by Chemical Oxidation and Solvent Extraction with Room Temperature Ionic Liquids. *Green Chem.* **2003**, *5*, 639-642.

4. Pei, Y.; Wu, K.; Wang, J.; Fan, J. Recovery of Furfural from Aqueous Solution by Ionic Liquid Based Liquid-Liquid Extraction. *Sep. Sci. Technol.* **2008**, *43*, 2090-2102.

5. Carda-Broch, S.; Berthod, A.; Armstrong, D. W. Solvent Properties of the 1-Butyl-3-Methylimidazolium Hexafluorophosphate Ionic Liquid. *Anal.Bioanal.Chem* **2003**, *375*, 191-199.

6. Baltazar, Q. Q.; Leininger, S. K.; Anderson, J. L. Binary Ionic Liquid Mixtures as Gas Chromatography Stationary Phases for Improving the Separation Selectivity of Alcohols and Aromatic Compounds. *J. Chromatogr. A.* **2008**, *1182*, 119-127.

7. Huang, K.; Han, X.; Zhang, X.; Armstrong, D. W. PEG-Linked Geminal Dicationic Ionic Liquids as Selective, High-Stability Gas Chromatographic Stationary Phases.

*Anal.Bioanal.Chem.* **2007**, *389*, 2265-2275.

8. Seeley, J. V.; Seeley, S. K.; Libby, E. K.; Breitbach, Z. S.; Armstrong, D. W.

Comprehensive Two-Dimensional Gas Chromatography using a High-Temperature Phosphonium Ionic Liquid Column. *Anal.Bioanal.Chem.* **2008**, *390*, 323-332.

9. Breitbach, Z. S.; Armstrong, D. W. Characterization of Phosphonium Ionic Liquids through a Linear Solvation Energy Relationship and their use as GLC Stationary Phases.

*Anal.Bioanal.Chem.* **2008**, *390*, 1605-1617.

10. Lambertus, G. R.; Crank, J. A.; McGuigan, M. E.; Kandler, S.; Armstrong, D. W.; Sacks, R. D. Rapid Determination of Complex Mixtures by Dual-Column Gas Chromatography with a Novel Stationary Phase Combination and Spectrometric Detection. *J. Chromatogr. A.*

**2006**, *1135*, 230-240.

11. Anderson, J. L.; Armstrong, D. W. Immobilized Ionic Liquids as High-selectivity/high-temperature/high-Stability Gas Chromatography Stationary Phases. *Anal. Chem.* **2005**, *77*,

6453-6462.

12. Ding, J.; Welton, T.; Armstrong, D. W. Chiral Ionic Liquids as Stationary Phases in Gas Chromatography. *Anal. Chem.* **2004**, *76*, 6819-6822.
13. Carda-Broch, S.; Berthod, A.; Armstrong, D. W. Ionic Matrices for Matrix-Assisted Laser desorption/ionization Time-of-Flight Detection of DNA Oligomers. *Rapid Commun. Mass Spectrom.* **2003**, *17*, 553-560.
14. Armstrong, D. W.; Zhang, L.; He, L.; Gross, M. L. Ionic Liquids as Matrixes for Matrix-Assisted Laser desorption/ionization Mass Spectrometry. *Anal. Chem.* **2001**, *73*, 3679-3686.
15. Li, Y. L.; Gross, M. L. Ionic-Liquid Matrices for Quantitative Analysis by MALDI-TOF Mass Spectrometry. *J. Am. Soc. Mass Spectrom.* **2004**, *15*, 1833-1837.
16. Zabet-Moghaddam, M.; Krueger, R.; Heinzle, E.; Tholey, A. Matrix-Assisted Laser desorption/ionization Mass Spectrometry for the Characterization of Ionic Liquids and the Analysis of Amino Acids, Peptides and Proteins in Ionic Liquids. *J. Mass Spectrom.* **2004**, *39*, 1494-1505.
17. Li, Y. L.; Gross, M. L.; Hsu, F. Ionic-Liquid Matrices for Improved Analysis of Phospholipids by MALDI-TOF Mass Spectrometry. *J. Am. Soc. Mass Spectrom.* **2005**, *16*, 679-682.

18. Ramos, C. R.; de Azevedo, M. L.; Silva, S. L.; Baptista, A. S.; Gloria, E. M.; Calori-Domingues, M. A.; Facco Elizete, M. P.; Eberlin, M. N. Aflatoxin Screening by MALDI-TOF Mass Spectrometry. *Anal. Chem.* **2005**, *77*, 8155-8157.
19. Santos, L. S.; Haddad, R.; Hoeehr, N. F.; Pilli, R. A.; Eberlin, M. N. Fast Screening of Low Molecular Weight Compounds by Thin-Layer Chromatography and "on-Spot" MALDI-TOF Mass Spectrometry. *Anal. Chem.* **2004**, *76*, 2144-2147.
20. Soukup-Hein, R. J.; Remsburg, J. W.; Dasgupta, P. K.; Armstrong, D. W. A General, Positive Ion Mode ESI-MS Approach for the Analysis of Singly Charged Inorganic and Organic Anions using a Dicationic Reagent. *Anal. Chem.* **2007**, *79*, 7346-7352.
21. Remsburg, J. W.; Soukup-Hein, R. J.; Crank, J. A.; Breitbach, Z. S.; Payagala, T.; Armstrong, D. W. Evaluation of Dicationic Reagents for their use in Detection of Anions using Positive Ion Mode ESI-MS Via Gas Phase Ion Association. *J. Am. Soc. Mass Spectrom.* **2008**, *19*, 261-269.
22. Soukup-Hein, R. J.; Remsburg, J. W.; Breitbach, Z. S.; Sharma, P. S.; Payagala, T.; Wanigasekara, E.; Huang, J.; Armstrong, D. W. Evaluating the use of Tricationic Reagents for the Detection of Doubly Charged Anions in the Positive Mode by ESI-MS. *Anal. Chem.* **2008**, *80*, 2612-2616.

23. Downard, K. M. Softly, Softly-Detection of Protein Complexes by Matrix-Assisted Laser Desorption Ionization Mass Spectrometry. *Mass Spectrom. Protein Interact.* **2007**, 25-43.
24. Tholey, A.; Zabet-Moghaddam, M.; Heinzle, E. Quantification of Peptides for the Monitoring of Protease-Catalyzed Reactions by Matrix-Assisted Laser Desorption/Ionization Mass Spectrometry using Ionic Liquid Matrixes. *Anal. Chem.* **2006**, 78, 291-297.
25. Laremore, T. N.; Zhang, F.; Linhardt, R. J. Ionic Liquid Matrix for Direct UV-MALDI-TOF-MS Analysis of Dermatan Sulfate and Chondroitin Sulfate Oligosaccharides. *Anal. Chem.* **2007**, 79, 1604-1610.
26. Lemaire, R.; Tabet, J. C.; Ducoroy, P.; Hendra, J. B.; Salzet, M.; Fournier, I. Solid Ionic Matrixes for Direct Tissue Analysis and MALDI Imaging. *Anal. Chem.* **2006**, 78, 809-819.
27. Tholey, A.; Heinzle, E. Ionic (Liquid) Matrices for Matrix-Assisted Laser desorption/ionization Mass Spectrometry - Applications and Perspectives. *Anal. Bioanal. Chem.* **2006**, 386, 24-37.
28. Naumann, I.; Darsow, K. H.; Walter, C.; Lange, H. A.; Buchholz, R. Identification of Sulfoglycolipids from the Alga *Porphyridium Purpureum* by Matrix-Assisted Laser desorption/ionisation Quadrupole Ion Trap Time-of-Flight Mass Spectrometry. *Rapid Commun. Mass Spectrom.* **2007**, 21, 3185-3192.

29. Fukuyama, Y.; Nakaya, S.; Yamazaki, Y.; Tanaka, K. Ionic Liquid Matrixes Optimized for MALDI-MS of Sulfated/Sialylated/Neutral Oligosaccharides and Glycopeptides. *Anal. Chem.* **2008**, *80*, 2171-2179.
30. Zehl, M.; Allmaier, G. Instrumental Parameters in the MALDI-TOF Mass Spectrometric Analysis of Quaternary Protein Structures. *Anal. Chem.* **2005**, *77*, 103-110.
31. Cohen, L. R. H.; Strupat, K.; Hillenkamp, F. Analysis of Quaternary Protein Ensembles by Matrix Assisted Laser desorption/ionization Mass Spectrometry. *J. Am. Soc. Mass Spectrom.* **1997**, *8*, 1046-1052.
32. Moniatte, M.; Lesieur, C.; Vecsey-Semjen, B.; Buckley, J. T.; Pattus, F.; van der Goot, F. G.; Van Dorsselaer, A. Matrix-Assisted Laser Desorption-Ionization Time-of-Flight Mass Spectrometry in the Subunit Stoichiometry Study of High-Mass Non-Covalent Complexes. *Int.J.Mass Spectrom.Ion Processes.* **1997**, *169/170*, 179-199.
33. Bhowmick, R.; Jagannadham, M. V. Multiple Intermediate Conformations of Jack Bean Urease at Low pH: Anion-Induced Refolding. *Protein J.* **2006**, *25*, 399-410.
34. Guo, Z.; He, L. A Binary Matrix for Background Suppression in MALDI-MS of Small Molecules. *Anal.Bioanal.Chem.* **2007**, *387*, 1939-1944.



35. Mirza, S. P.; Raju, N. P.; Vairamani, M. Estimation of the Proton Affinity Values of Fifteen Matrix-Assisted Laser desorption/ionization Matrices Under Electrospray Ionization Conditions using the Kinetic Method. *J. Am. Soc. Mass Spectrom.* **2004**, *15*, 431-435.
36. Beltran, J. L.; Sanli, N.; Fonrodona, G.; Barron, D.; Ozkan, G.; Barbosa, J. Spectrophotometric, Potentiometric and Chromatographic pKa Values of Polyphenolic Acids in Water and Acetonitrile-Water Media. *Anal. Chim. Acta.* **2003**, *484*, 253-264.
37. Burton, R. D.; Watson, C. H.; Eyler, J. R.; Lang, G. L.; Powell, D. H.; Avery, M. Y. Proton Affinities of Eight Matrixes used for Matrix-Assisted Laser desorption/ionization. *Rapid Commun. Mass Spectrom.* **1997**, *11*, 443-446.
38. Hunter, E. P. L.; Lias, S. G. Evaluated Gas Phase Basicities and Proton Affinities of Molecules: An Update. *J. Phys. Chem. Ref. Data.* **1998**, *27*, 413-656.
39. da Silva, E. F.; Svendsen, H. F. Prediction of the pKa Values of Amines using Ab Initio Methods and Free-Energy Perturbations. *Ind Eng Chem Res.* **2003**, *42*, 4414-4421.
40. Simekova, M.; Berek, D. Studies on High-Performance Size-Exclusion Chromatography of Synthetic Polymers. *J. Chromatogr. A.* **2005**, *1084*, 167-172.
41. Netopilik, M.; Kratochvil, P. Polystyrene-Equivalent Molecular Weight Versus True Molecular Weight in Size-Exclusion Chromatography. *Polymer.* **2003**, *44*, 3431-3436

## Tables

Table 1) ILs used as matrices for MALDI-TOF MS. In the second column the label “solid” refers to solids or solids that are super cooled liquids. Analyte signal, yes, refers to the detection by the matrix of at least one analyte listed in the Experimental section with a  $S/N \geq 3$

Ionic Liquid name	Physical State	Previously Reported <sup>13,14,35</sup>	Analyte Signal
(4-Bromophenyl) diphenyl sulfonium NTF2	solid		no
(4-methylthiophenyl) methyl phenyl sulfonium NTF2	liquid		no
naphthyl diphenylsulfonium NTF2	solid		no
(-)-cinchonidine NTF2	solid		no
pyridinium 3-hydroxypicolinate	solid	X	yes
N-isopropyl-N-methyl-N-tert-butylammonium all-trans-retanoate	solid		no
1nonal-3-vinylimidazolium $\alpha$ -cyano-4-hydroxycinnamate	liquid		yes
Methyl 1,3,5-triethylhexahydro-1,3,5-triazine triflate	solid		no
butylmethylimidazolium 3,4-dihydroxycinnamate	liquid		no
tributyl ammonium 3,4-dimethoxycinnamate	liquid		yes
butylammonium 3,4-dihydroxycinnamate	liquid		yes
octylammonium 3,4-dihydroxycinnamate	glass		yes
decylammonium 3,4-dihydroxycinnamate	solid		yes
1-(4-hydroxypropyl)methylimidazolium iodate	liquid		no
$\alpha$ -cyano-4-hydroxycinnamic acid	solid	X	yes
1-(4-hydroxypropyl)methylimidazolium $\alpha$ -cyano-4-hydroxycinnamate	liquid		yes
1-(2-carboxyethyl)-3-(2-hydroxyethyl) imidazolium bromide 2(N-isopropyl-N-methyl-N-tert-butylamine)	liquid		no
butylmethylimidazolium $\alpha$ -cyano-4-hydroxycinnamate	liquid	X	yes
dipenyliodonium $\alpha$ -cyano-4-hydroxycinnamate	solid		no
tris-(2-hydroxyethyl)-sulfonium $\alpha$ -cyano-4-hydroxycinnamate	solid		yes
tributylammonium $\alpha$ -cyano-4-hydroxycinnamate	wax		yes
di(tributylammonium) $\alpha$ -cyano-4-hydroxycinnamate(not formed)	NA		yes
diisopropylethylammonium $\alpha$ -cyano-4-hydroxycinnamate	glass		yes
di(diisopropylethylammonium) $\alpha$ -cyano-4-hydroxycinnamate (not formed)	NA		yes
N-isopropyl-N-methyl-N-tert-butylammonium $\alpha$ -cyano-4-hydroxycinnamate	glass		yes
di(N-isopropyl-N-methyl-N-tert-butylammonium) $\alpha$ -cyano-4-hydroxycinnamate (not formed)	NA		yes
butylammonium $\alpha$ -cyano-4-hydroxycinnamate	solid	X	yes
di(butylammonium) $\alpha$ -cyano-4-hydroxycinnamate	glass		yes
octylammonium $\alpha$ -cyano-4-hydroxycinnamate	solid		yes
di(octylammonium) $\alpha$ -cyano-4-hydroxycinnamate	glass		yes
decylammonium $\alpha$ -cyano-4-hydroxycinnamate	solid		yes
2-amino pentane $\alpha$ -cyano-4-hydroxycinnamate	solid		yes
di(2-aminopentane) $\alpha$ -cyano-4-hydroxycinnamate	solid		yes
di(1,1,3,3-tetramethyl-guanidinium) $\alpha$ -cyano-4-hydroxycinnamate	solid	X	yes
ferulic acid	solid	X	yes
butylammonium ferulate	glass		yes
di(butylammonium) ferulate	solid		yes

Table 1 cont.			
Ionic Liquid name	Physical State	Previously Reported <sup>13,14,35</sup>	Analyte Signal
octylammonium ferulate	solid		yes
<i>di</i> (octylammonium) ferulate	solid		no
decylammonium ferulate	solid		yes
tributylammonium ferulate	solid		yes
<i>di</i> (tributylammonium) ferulate(not formed)	NA		yes
diisopropylethylammonium ferulate	solid		yes
<i>di</i> (diisopropylethylammonium) ferulate(not formed)	solid		yes
diisopropylethylammonium triethanolammonium ferulate(not formed)	NA		no
(N-isopropyl-N-methyl-N-tert-butylammonium) ferulate	solid		yes
<i>di</i> (N-isopropyl-N-methyl-N-tert-butylammonium) ferulate(not formed)	NA		yes
N-isopropyl-N-methyl-N-tert-butylammonium diisopropylethylammonium ferulate(not formed)	NA		yes
2-aminopentane ferulate	solid		yes
<i>di</i> (2-aminopentane) ferulate	solid		yes
2-amino-2-phenylethanol ferulate	solid		no
1,4-diaminobutane <i>di</i> (ferulate)	solid		yes
diethylenetriammonium <i>tri</i> (ferulate)	solid		yes
triisobutylammonium <i>tri</i> (ferulate)	solid		yes
diethylenetriammonium di(ferulate) ( $\alpha$ -Cyano-4-hydroxycinnamate)	solid		yes
diethylenetriamine ferulate $\alpha$ -Cyano-4-hydroxycinnamate sinapinate	solid		yes
N-isopropyldiethylenetriammonium <i>tri</i> (ferulate)	solid		no
triethylenetetraammonium (ferulate) <sub>4</sub>	solid		yes
<i>di</i> (triethanolammonium) ferulate(not formed)	NA		no
triethanolammonium ferulate	liquid		no
diisopropylethylammonium anthraquinone-2-carboxylate	solid		yes
sinapinic acid	solid	X	yes
tributylammonium Sinapinate	liquid	X	yes
butylammonium sinapinate	solid		yes
<i>di</i> (butylammonium) sinapinate	solid		yes
octylammonium sinapinate	solid		yes
<i>di</i> (octylammonium) sinapinate	solid		yes
tributylammonium sinapinate	wax	X	yes
<i>di</i> (tributylammonium) sinapinate(not formed)	NA		na
diisopropylethylammonium sinapinate	solid		yes
<i>di</i> (diisopropylethylammonium) sinapinate (not formed)	NA		yes
(N-isopropyl-N-methyl-N-tert-butylammonium) sinapinate	solid		yes
<i>di</i> (N-isopropyl-N-methyl-N-tert-butylammonium) sinapinate (not formed)	NA		yes
2-aminopentane sinapinate	solid		yes
<i>di</i> (2-aminopentane) sinapinate	solid		yes
7-hydroxycoumarinyl-4-acetic acid	solid		yes
diisopropylethylammonium 7-hydroxycoumarinyl-4-acetate	solid		no
N-isopropyl-N-methyl-N-tert-butylammonium 7-hydroxycoumarinyl-4-acetate	solid		no
aurintricarboxylic acid	solid		no
diisopropylethylammonium aurintricarboxylate	solid		no
N-isopropyl-N-methyl-N-tert-butylammonium aurintricarboxylate	solid		no

Table 1 cont.			
Ionic Liquid name	Physical State	Previously Reported <sup>13,14,35</sup>	Analyte Signal
2,3-benzofurandicarboxylic acid	solid		no
diisopropylethylammonium 2,3-benzofurandicarboxylate	solid		no
N-isopropyl-N-methyl-N-tert-butylammonium 2,3-benzofurandicarboxylate	solid		no
3,6-dihydroxyflavone	solid		no
diisopropylethylammonium 3,6-dihydroxyflavone	solid		no
N-isopropyl-N-methyl-N-tert-butylammonium 3,6-dihydroxyflavone	solid		no
9-hydroxy-9-fluorene-carboxylic acid	solid		no
diisopropylethylammonium 9-hydroxy-9-fluorene-carboxylate	solid		no
N-isopropyl-N-methyl-N-tert-butylammonium 9-hydroxy-9-fluorene-carboxylate	solid		no
2-(4-hydroxyphenylazo)benzoic acid	solid		yes
diisopropylethylammonium 2-(4-hydroxyphenylazo)benzoate	solid		yes
N-isopropyl-N-methyl-N-tert-butylammonium 2-(4-hydroxyphenylazo)benzoate	solid		yes
mellitic acid	solid		no
diisopropylethylammonium mellitate	solid		no
N-isopropyl-N-methyl-N-tert-butylammonium mellitate	solid		no
2,3-naphthalenedicarboxylic acid	solid		no
diisopropylethylammonium 2,3-naphthalenedicarboxylate	solid		no
N-isopropyl-N-methyl-N-tert-butylammonium 2,3-naphthalenedicarboxylate	solid		no
diisopropylethylammonium curcumin	solid		no
piperidinium $\alpha$ -cyano-4-hydroxycinnamate	glass		yes
2,2,6,6-tetramethylpiperidine $\alpha$ -cyano-4-hydroxycinnamate	solid		yes
2,2,6,6-tetramethyl-4-piperidone $\alpha$ -cyano-4-hydroxycinnamate	solid		yes
2,2,6,6-tetramethylpiperidinol $\alpha$ -cyano-4-hydroxycinnamate	solid		yes
2,2,5,5-tetramethyl-3-pyrroline-3-carboxamide $\alpha$ -cyano-4-hydroxycinnamate	solid		yes
hexamethyldisilazane $\alpha$ -cyano-4-hydroxycinnamate	solid		no
quinuclidinium $\alpha$ -cyano-4-hydroxycinnamate	solid		yes
dicyclohexylammonium $\alpha$ -cyano-4-hydroxycinnamate	solid		yes
2,5-dihydroxybenzoic acid	solid	X	yes
N-isopropyl-N-methyl-N-tert-butylammonium 2,5-dihydroxybenzoate	solid		yes
diisopropylethylammonium 2,5-dihydroxybenzoate	solid		yes
rutin	solid		yes
diisopropylethylammonium rutin	solid		yes

Table 2) ILM ammonium properties arranged by increasing  $pK_a$ . In the proton affinity (PA) and gas phase basicity (GB) columns NA represents not available. In the performance Vs. solid matrix column “X” represents ILM cations that did not pair well with the solid matrices or showed no analyte signal, “-“ represents ILM cations that show signal but less than the solid matrix, “+” represents ILM cations that performed as well or marginally better than the solids, and “++” represents ILMs that out perform the solid matrices.

Amine name	$pK_a$	PA <sup>38</sup> (kJ/mole)	GB (kJ/mole)	Performance Vs. Solid Matrix
triethanolamine	7.8	941	NA	<b>X</b>
triisobutylamine	9.5	967.6	998.5	<b>X</b>
tributylamine	9.9	998.5	967.6	-
butylamine	10.6	921.5	886.6	-
2-amino butane	10.7	929.9	895.7	<b>+</b>
<i>N</i> -isopropyl- <i>N</i> -methyl- <i>t</i> -butylamine	10.9	NA	NA	<b>++</b>
<i>N,N</i> -diisopropylethylamine	11.4	994.3	963.5	<b>++</b>

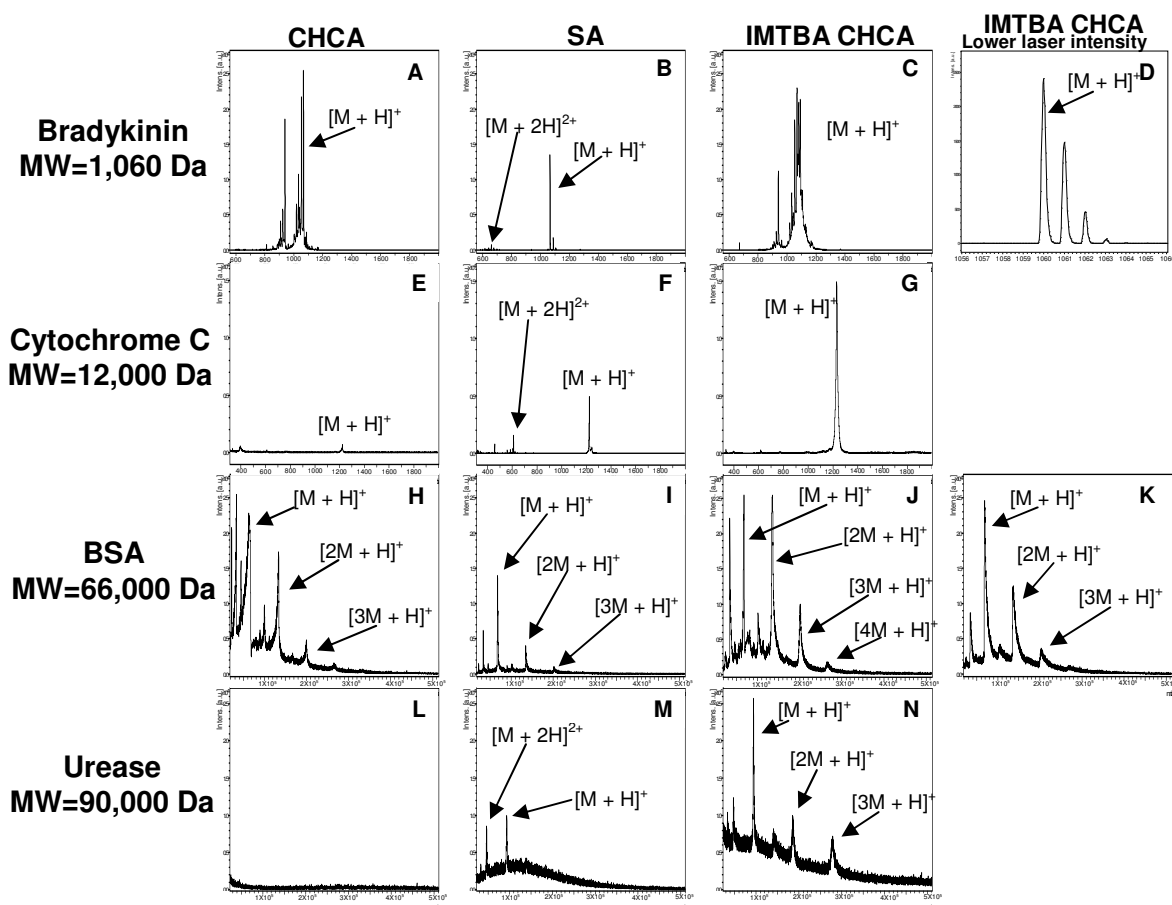


Figure 1) Comparison of solid matrices and an ILM (columns) with four different analytes (rows). CHCA, SA, and IMTBA CHCA are compared using the same laser power and analyte concentration. Analytes shown are bradykinin (MW=1,060 Da), cytochrome C (MW=12,000 Da), BSA (MW=66,000 Da), and urease (monomer MW=90,000 Da). Peaks are labeled in the  $[M + H]^+$  notation. Spectra D and K show bradykinin and BSA respectively, at lower laser powers to show that good resolution is achieved. Spectrum N shows a  $[3M + H]^+$  peak with a mass of 270,000 Da.

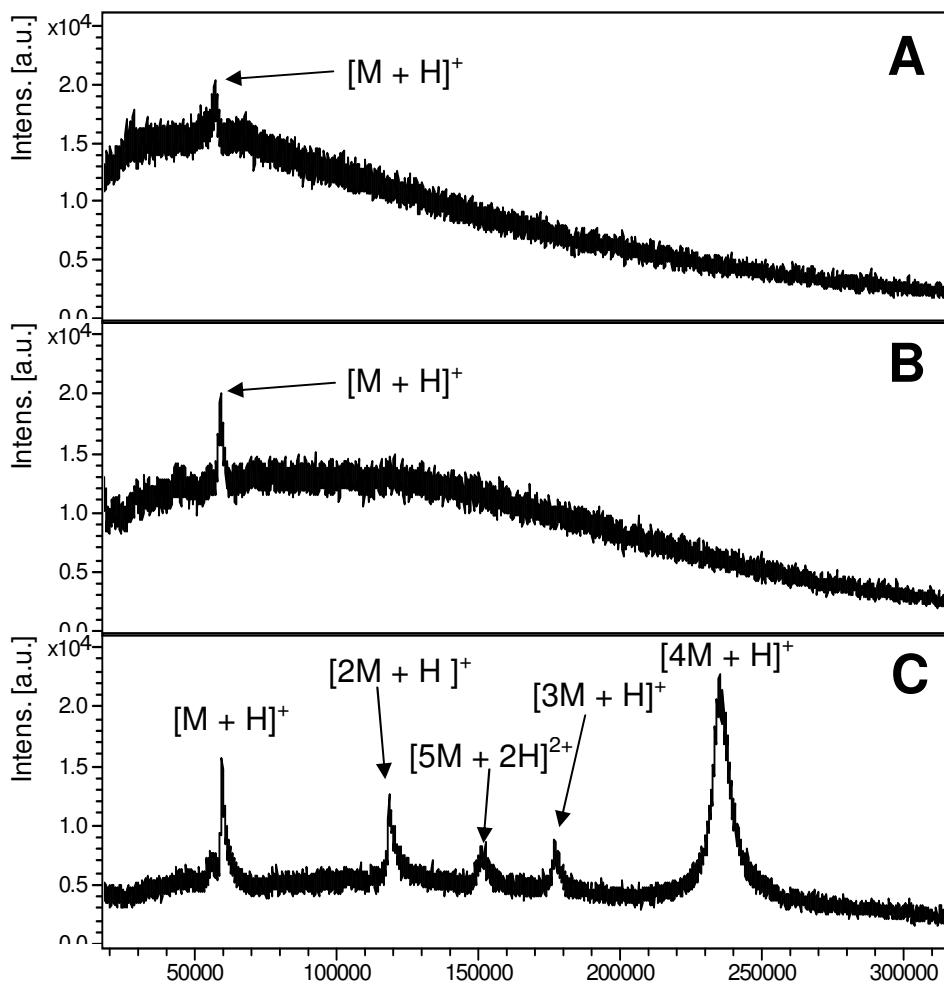


Figure 2) Detection of catalase (monomer MW=60,000 Da) with: (A) CHCA, (B) SA, and (C) IMTBA CHCA. Peaks are labeled with  $[M + H]^+$  notation. The tetramer peak (MW=240,000 Da) is labeled  $[4M + H]^+$ .

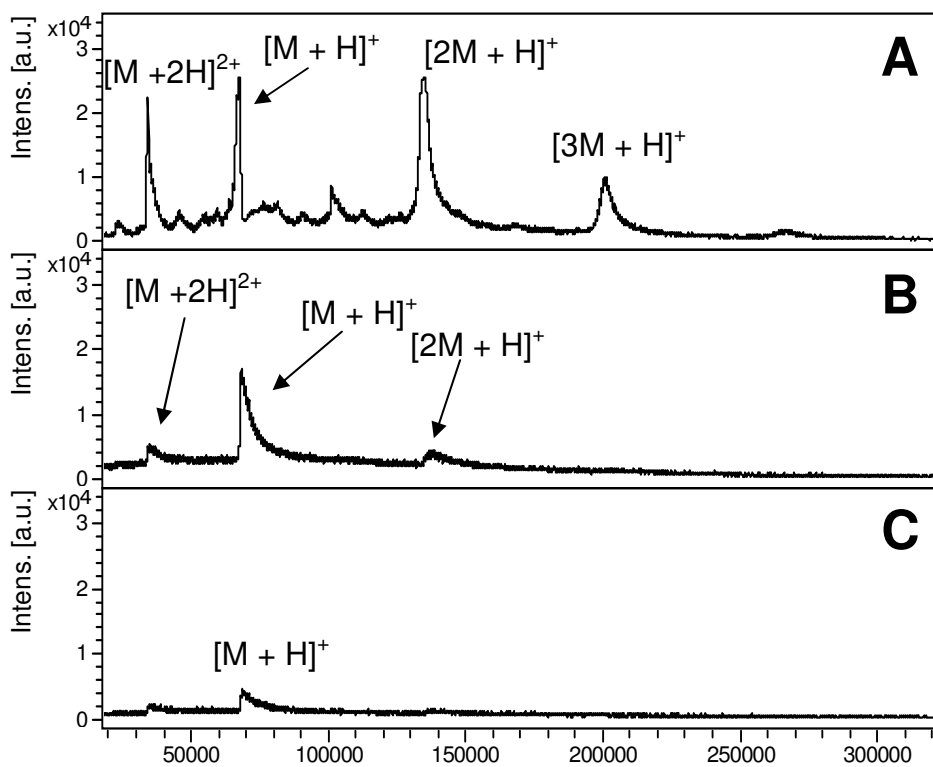


Figure 3) Effect of the anion on signal intensity with the matrices (A) IMTBA CHCA, (B) IMTBA ferulate, and (C) IMTBA sinapinate at the same laser power and analyte (BSA) concentration. Peaks are labeled with  $[M + H]^+$  notation.



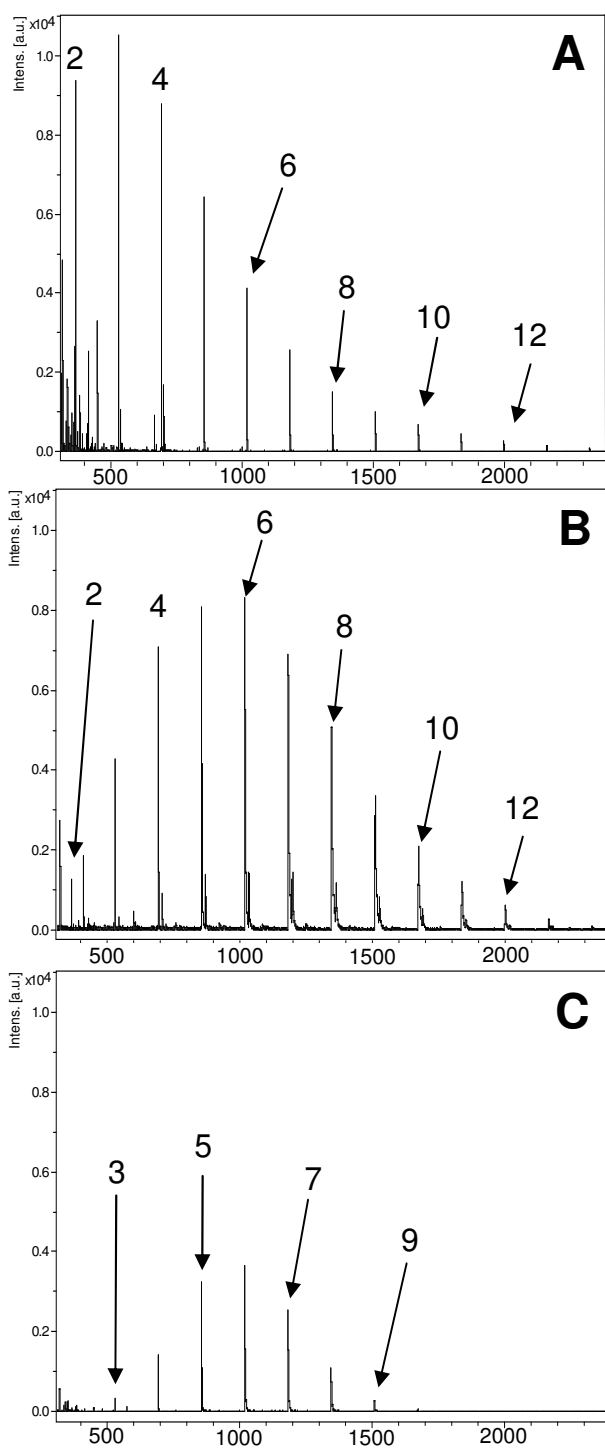


Figure 4) Spectra of dextransynth ( $M_w=1500$  Da) using (A) DHB, (B) DEA F, and (C) DEA CHCA. Peak numbers represent the number of sodiated glucose units.

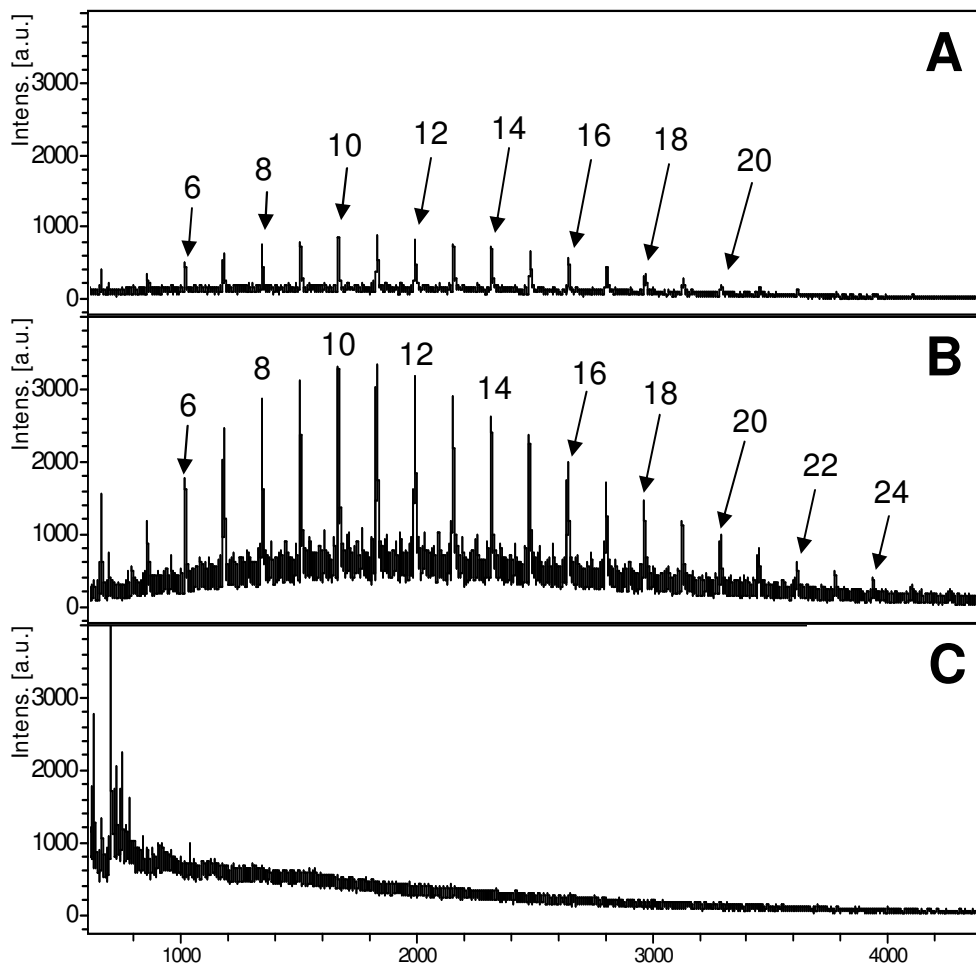
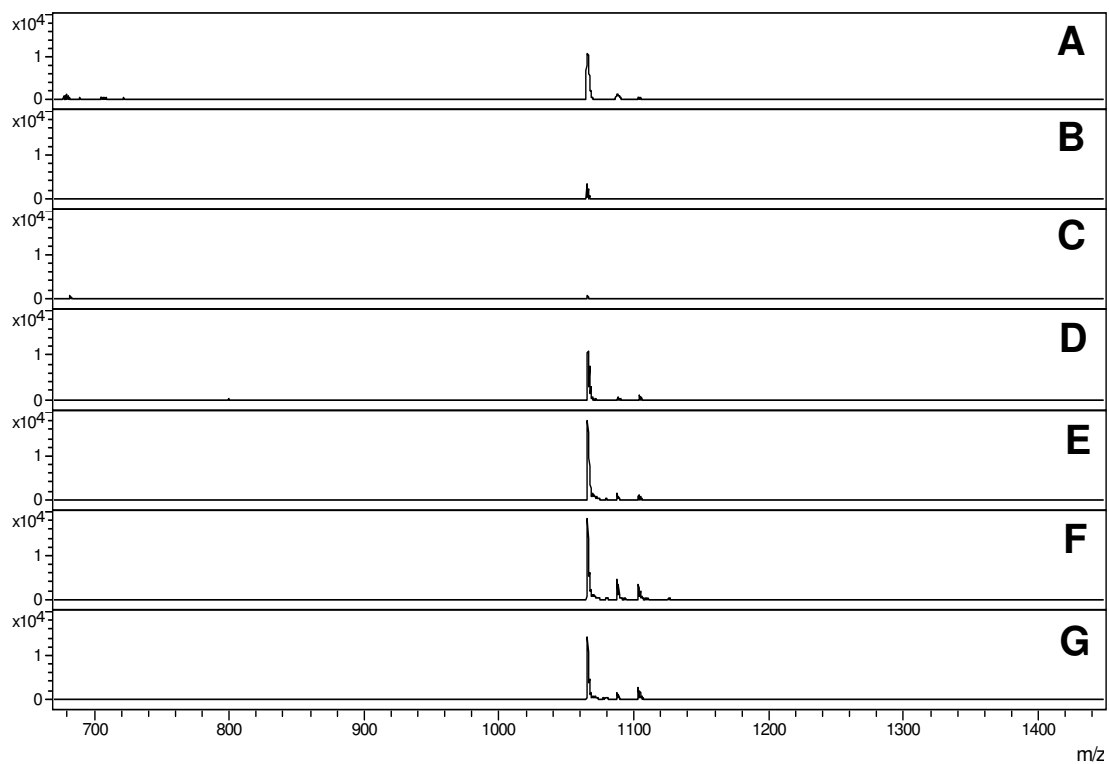


Figure 5) Spectra of mannan from *Saccharomyces cerevisiae* using (A) IMTBA CHCA, (B) DEA CHCA, and (C) DHB. Peak numbers represent the number of sodiated mannose units.

## Supplemental information



SI 1) Effect of the cation on signal intensity of the MALDI mass spectra of bradykinin with (A) Ferulic acid, (B) butylammonium ferulate, (C) octylammonium ferulate, (D) 2-aminopentane ferulate, (E) tributylammonium ferulate, (F) N,N- diisopropylethylammonium ferulate, and (G) N-isopropyl-N-methyl-N-tert-butylammonium ferulate at the same laser power and analyte concentration.

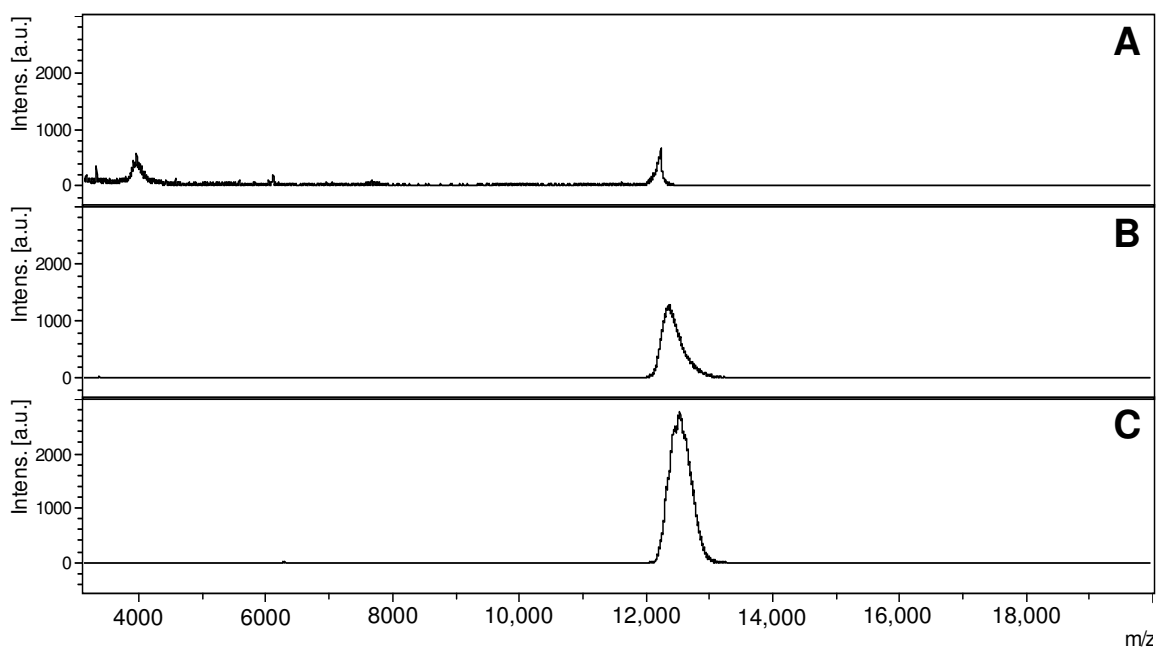


Figure SI 2) Effect of multiple cations on the signal intensity of the MALDI mass spectra of cytochrome C with (A) CHCA, (B) butylammonium CHCA, and (C) *di*(butylammonium) CHCA shown with same laser power and analyte concentration.

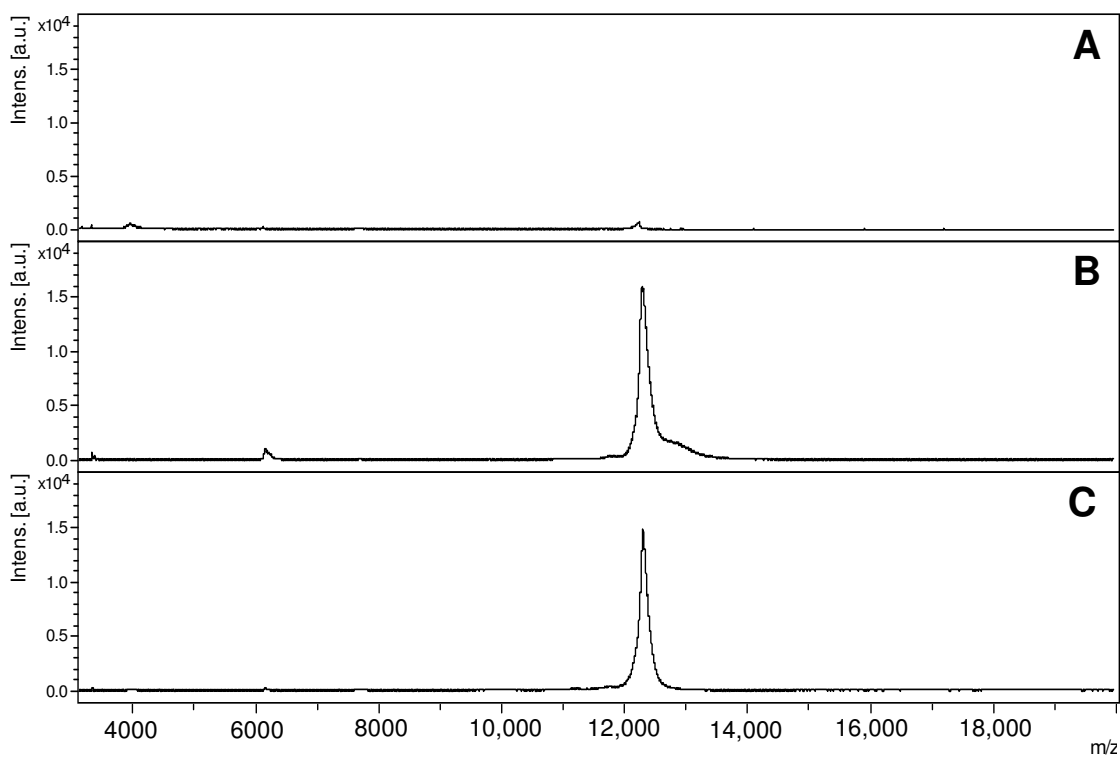
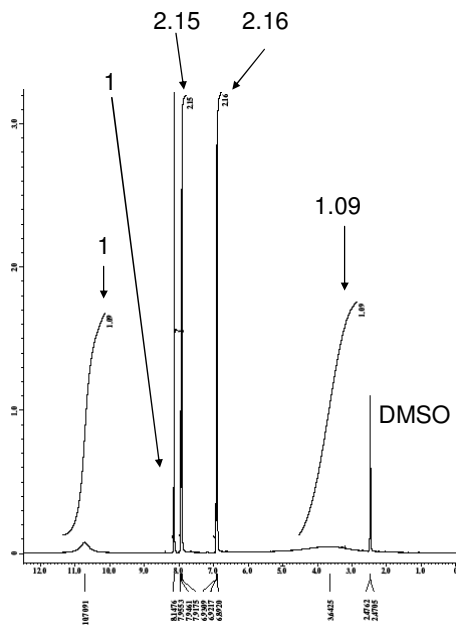
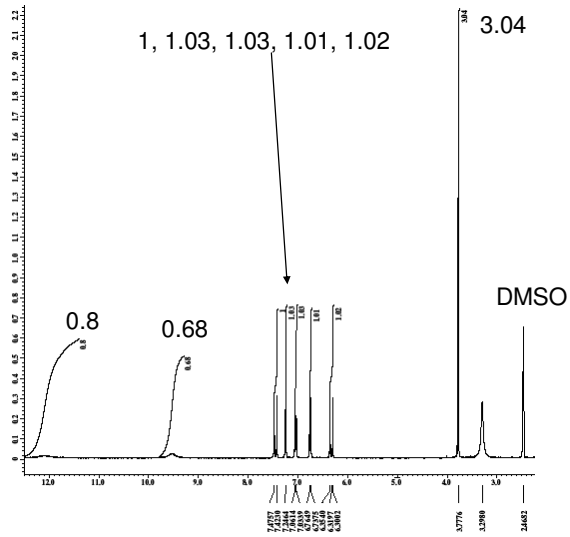


Figure SI 3) Effect of multiple cations on the signal intensity of the MALDI mass spectra of cytochrome C with (A) CHCA, (B) IMTBA CHCA, and *di*(IMTBA) CHCA shown with same laser power and analyte concentration.

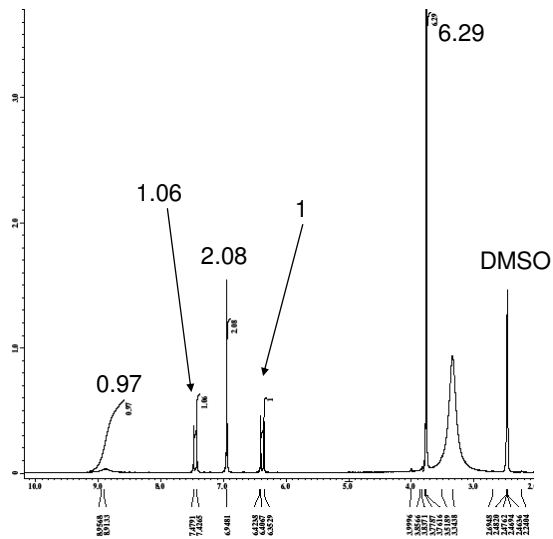
## A) CHCA



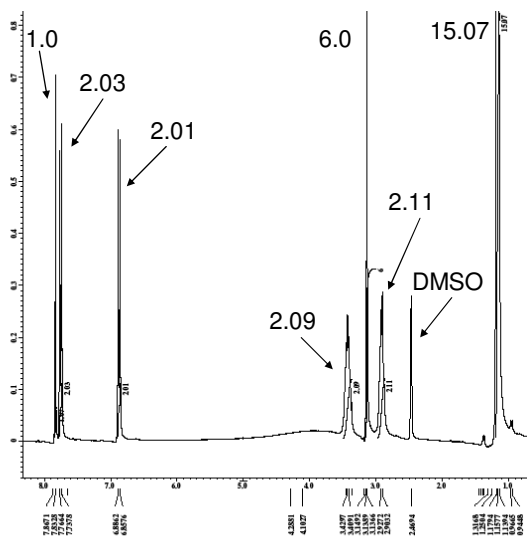
## B) Ferulic Acid



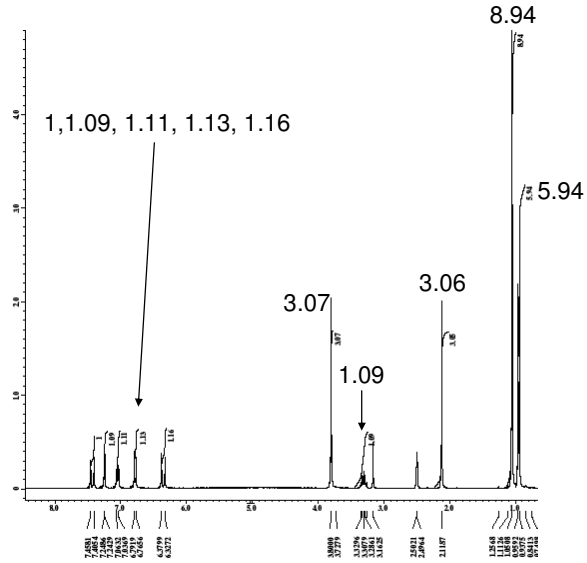
## C) Sinapinic acid



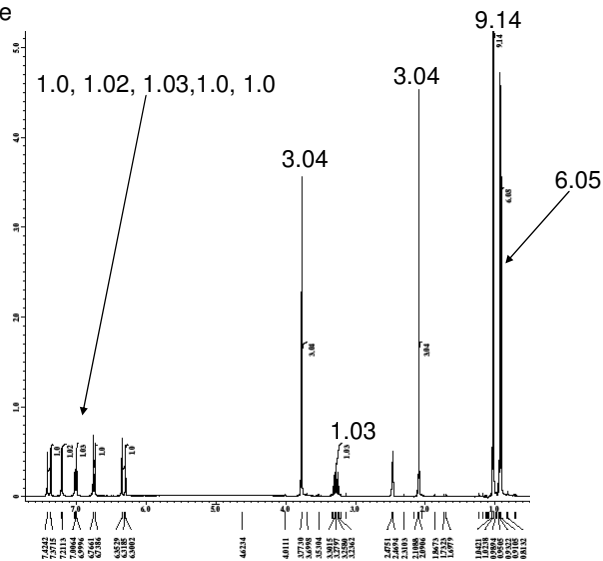
## D) di(DEA) CHCA



E) DEA ferulate

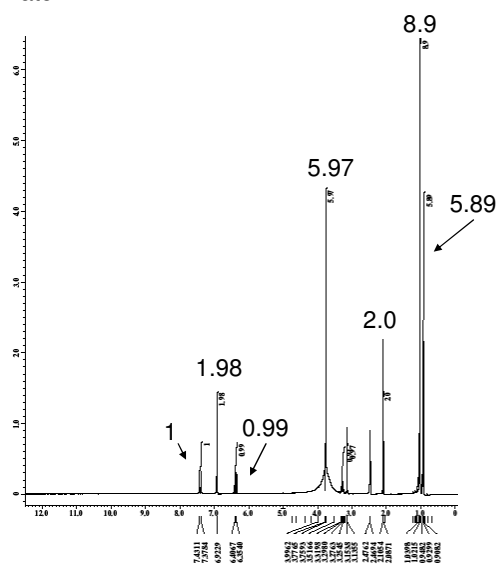


F) di(DEA) ferulate





G) di(IMTBA) sinapinate



H) di(BA) sinapinate

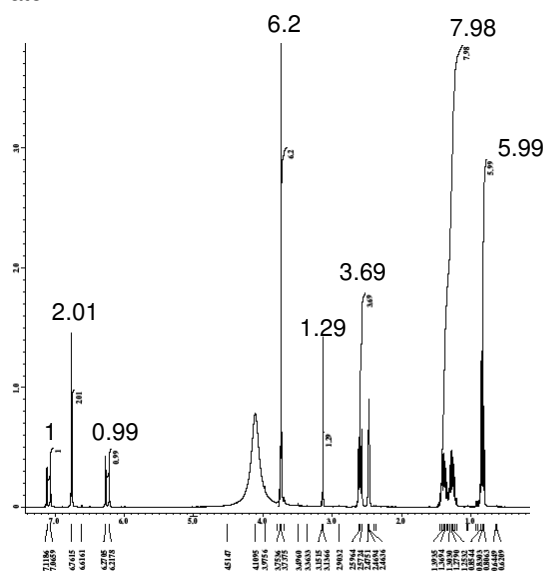


Figure SI 4) Example NMR of A) CHCA, B) ferulic acid, C) sinapinic acid, D) di(DEA) CHCA, E) DEA ferulate, F) di(DEA) ferulate, G) di(IMTBA) sinapinate, and H) di(BA) sinapinate.

## CHAPTER 3

### EFFECTIVE MS ANALYSIS OF BIODEGRADABLE POLYMERS WITH SECOND GENERATION IONIC LIQUID MALDI MATRICES

Jeffrey A. Crank<sup>1</sup>, Kimber L. Rundlett<sup>2</sup>, and Daniel W. Armstrong<sup>1</sup>

1) Chemistry and Biochemistry Department, University of Texas Arlington, Arlington TX  
76019

2) Pfizer Inc., Groton CN 06340

#### Abstract

A second generation ionic liquid matrix (ILM) *N,N*-diisopropylethylammonium  $\alpha$ -cyano-4-hydroxycinnamate (DEA CHCA) was developed for the characterization of sixteen biodegradable polymers. It is compared to five solid matrices typically used for characterization of these polymers and one other new ILM. It is shown that use of the ILM, DEA CHCA, results in a much softer ionization process and usually greater sensitivity than that found for solid matrices which typically produce spectra showing extensive polymer degradation. The symmetric distribution of analyte peaks obtained with the ionic liquid matrix allows for a more sensitive and more accurate determination of both the number average molecular weights and the weight average molecular weights. It is shown that the use of ILM (DEA CHCA) produces more precise and accurate data when evaluating the number average and weight average molecular weights of labile polymers.

Reproduced with the permission of Analytical Chemistry, submitted for publication

## Introduction

Ionic liquids have become increasingly important in many different areas of chemical analysis. Although initially used as novel solvents in organic synthesis, ionic liquids are becoming indispensable in extractions,<sup>1-7</sup> gas chromatography stationary phases,<sup>8-14</sup> matrix assisted laser desorption/ionization (MALDI) matrices,<sup>15-21</sup> and ion pairing reagents for the trace analysis of anions by electrospray ionization mass spectrometry in the positive mode.<sup>22-24</sup> An ionic liquid is defined as a non-molecular salt whose melting point is at or below 100 degrees Celsius and is considered a room temperature ionic liquid if the melting point is at or below ambient temperature. The first report on ionic liquids as MALDI matrices was in 2001 by Armstrong et al.<sup>16</sup> It was shown that ionic liquid matrices (ILMs) have an increase in signal and better shot to shot reproducibility when compared to the traditional solid matrices. In 2004 Li and Gross demonstrated that ILMs show enhanced quantitative analysis when compared to the traditional solid matrices<sup>17</sup>. This enhanced quantitative ability is attributed to the homogeneity of the analyte and the matrix.

Biodegradable polymers are important to the medical field for drug delivery and for the manufacture of dissolvable sutures.<sup>25-28</sup> The chemical industry also is interested in their synthesis and properties as they are considered as more “eco-friendly” polymers.<sup>29</sup> However, characterization of these polymers often is difficult. Size exclusion chromatography (SEC) will give a mass range, but usually over or underestimates the molecular weight due to the fact that the standards used are not structurally similar to the unknown polymer.<sup>30-32</sup> MALDI-MS of biodegradable polymers has been studied extensively.<sup>33-44</sup> However,

MALDI-MS of these polymers displays its own unique problems. Any acid content of the matrix or the solution used to integrate the sample and matrix will start to degrade the polymer.<sup>45, 46</sup> This degradation typically leads to spectra with peaks increasing in intensity as the mass decreases, forming a “wedge shape” toward the low mass region of the spectrum. Thus some structural information can be obtained, but any useful information about the average molecular weight of the polymer is limited. Another problem with MALDI-MS of biodegradable polymers is that cationization agents such as sodium trifluoroacetate, LiCl, NaCl, and KCl can significantly change the weight average molecular weight. It was reported by Chen et. al. that changing the cation from Li to Cs shifted the weight average molecular weight by as much as 15% from the calculated weight average molecular weight.<sup>47</sup> This shift in molecular weight was shown to be due to the affinity of the cation for the polymer of interest.

ILMs are ideally suited to overcome all of these problems. ILMs use no trifluoroacetic acid and have a pH of 7.8 (when in water as a 0.1M solution) whereas traditional matrices with trifluoroacetic acid have a pH of 1-2.<sup>48</sup> The ILMs also use no cationization agent so that the weight average molecular weight should not be skewed. This study demonstrates the wide applicability of a recently developed second generation ILM by effectively characterizing 16 biodegradable polymers of varying chemistries and sizes. The ILMs are also compared to five traditional solid matrices typically used to detect biodegradable polymers.

## Experimental

### *Materials and Instrument*

The following reagents were purchased from Sigma-Aldrich (St Louis, MO, USA) :  $\alpha$ -cyano-4-hydroxycinnamic acid, *trans*-3-indoleacrylic acid, 2,5-dihydroxybenzoic acid, 2-(4-hydroxyphenylazo)benzoic acid, *trans*-2-[3-(4-*tert*-butylphenyl)-2-methyl-2-propenylidene]malononitrile, sodium trifluoroacetate, *N,N*-diisopropylethylamine, polycaprolactone, polycaprolactone diol ( $M_n=530$  Da) polycaprolactone diol ( $M_n=1,250$  Da), polycaprolactone diol ( $M_n=2,000$  Da), poly(DL-lactide- *co*-glycolide) ( $M_w=5,000-15,000$  Da), poly[(lactide-*co*-ethylene glycol)-*co*-ethyloxyphosphate], poly[1,4-bis(hydroxyethyl)terephthalate-alt-ethyloxyphosphate], poly[1,4-bis(hydroxyethyl)terephthalate-alt-ethyloxyphosphate]-*co*-1,4-bis(hydroxyethyl)terephthalate-*co*-terephthalate, polycaprolactone triol ( $M_n=300$  Da), polycaprolactone triol ( $M_n=900$  Da), poly(1,4-butylene adipate-*co*-polycaprolactam), poly(ethylene glycol) ( $M_n=4,140-5,060$  Da : Average  $M_n=4,431$  Da), poly(ethylene glycol)-block-poly(propylene glycol)-block-poly(ethylene glycol) ( $M_n=1,100$  Da), poly(ethylene glycol)-block-poly(propylene glycol)-block-poly(ethylene glycol) ( $M_n=2800$  Da),  $\alpha,\omega$ -bis{2-[(3-carboxy-1-oxopropyl)amino]ethyl}polyethylene glycol ( $M_n=3000$  Da), polycaprolactone-block-polytetrahydrofuran-block-polycaprolactone ( $M_n=2000$  Da : polydispersity=1.3). Solvents, microcentrifuge tubes and trifluoroacetic acid were obtained from VWR(West Chester, PA, USA). All data was collected on a Bruker Autoflex mass spectrometer and analyzed with Bruker Flex Analysis software. All spectra shown are the sum of 100 laser shots.

### *Matrix and Sample Preparation*

Polymer samples were dissolved in solvent at a concentration of 1mg/ml. This was done because the molecular weights of some polymers tested are not known, so accurate molar solutions could not be made. Also the molecular weights that are known from SEC may not be accurate.

The matrices utilized in this study were selected from over 100 newly synthesized ILs. They are:  $\alpha$ -cyano-4-hydroxycinnamic acid (CHCA), *trans*-3-indoleacrylic acid (3-IAA), 2,5-dihydroxybenzoic acid (DHB), 2-(4-hydroxyphenylazo)benzoic acid (HABA), and *trans*-2-[3-(4-*tert*-butylphenyl)-2-methyl-2-propenylidene]malononitrile (DCTB), *N,N*-diisopropylethylammonium  $\alpha$ -cyano-4-hydroxycinnamate (DEA CHCA), and *N,N*-diisopropylethylammonium indoleacrylate (DEA IAA). The solid matrices CHCA, 3-IAA, DHB, HABA and DCTB were selected from the literature as the most common matrices used for the detection of biodegradable polymers.<sup>33, 35-44</sup> However, other solid matrices have been used for the detection of biodegradable polymers with MALDI-MS so this list should not be considered comprehensive. The ILM DEA CHCA was chosen because in previous studies it had shown promise as a matrix for detection of carbohydrates.<sup>48</sup> The matrix DEA 3-IAA was synthesized specifically for the detection of polymers but it did not show any clear advantage over the solid matrices. Each polymer was tested with all 7 matrices (see Experimental) but due to lack of space only selected spectra will be shown in each figure. All 7 spectra for each polymer are shown in Figure SII in the Supplemental Information.

Ionic liquid matrices (ILMs) were synthesized as previously reported.<sup>16, 48</sup> In short one molar equivalent of solid matrix (e.g., CHCA) is dissolved in methanol. Next one molar equivalent of base (e.g., *N,N*-diisopropylethylamine) is added to the methanol solution and stirred for 30 min to ensure complete reaction. A rotary evaporator is then used to remove methanol. The resulting ionic liquid was then placed under vacuum overnight to ensure dryness. The ionic liquid was then placed in a microcentrifuge tube and ethanol was added to decrease the viscosity. The ILM solution and the polymer analyte solution were then mixed at ratios varying from 1:1 to 1:20 (v/v : analyte/matrix) to find the optimal analyte to matrix ratio. The optimal analyte/matrix ratio was approximately 1:10. One  $\mu\text{L}$  of analyte matrix solution was then spotted on the MALDI plate and the solvent was allowed to evaporate.

Solid matrices were prepared according to procedures adapted from literature.<sup>26, 35, 37, 40, 44</sup>  $\alpha$ -cyano-4-hydroxycinnamic acid (CHCA) matrix solution was prepared by first making a solution of water/acetonitrile (50/50, v/v) with 0.1% trifluoroacetic acid. Then CHCA and one mL of the solution were placed in a microcentrifuge tube and vortexed to produce a saturated solution. 2,5-dihydroxybenzoic acid (DHB) matrix solution was prepared by dissolving DHB in acetonitrile at a concentration of 40mg/mL. 2-(4-Hydroxyphenylazo)benzoic acid (HABA) matrix solution was prepared by dissolving HABA in 1 mL of tetrahydrofuran at a concentration of 20mg/ml with 1% (w/v) sodium trifluoroacetate. Trans-2-[3-(4-tert-Butylphenyl)-2-methyl-2-propenylidene]malononitrile (DCTB) matrix solution was prepared by dissolving DCTB in tetrahydrofuran at a concentration of 40mg/mL with 1% (w/v) sodium trifluoroacetate. *Trans*-3-indoleacrylic acid

(IAA) matrix solution was prepared by dissolving IAA in tetrahydrofuran at a concentration of 40mg/ml. The matrix solution and the polymer analyte solution were then mixed at ratios varying from 1:1 to 1:20 (v/v) to find the optimal analyte to matrix ratio. One  $\mu\text{L}$  of analyte matrix solution was then spotted on the MALDI plate and the solvent was allowed to evaporate.

#### *Determination of $M_n$ , $M_w$ , and $pd$*

All spectra were integrated manually in Bruker's Flex Analysis program. All peaks with S/N ratios below 3 were rejected. The number-average molecular weight ( $M_n$ ) was calculated using equation 1:<sup>49</sup>

$$M_n = \frac{\sum m_i N_i}{\sum N_i} \quad (1)$$

where  $m_i$  is the mass at peak  $i$ , and  $N_i$  is the area of peak  $i$ . Weight average molecular weight ( $M_w$ ) was calculated using equation 2:

$$M_w = \frac{\sum m_i^2 N_i}{\sum m_i N_i} \quad (2)$$

where  $m_i$  is the mass at peak  $i$ , and  $N_i$  is the area of peak  $i$ . Polydispersity was calculated by dividing  $M_w$  by  $M_n$  as seen in equation 3.

$$pd = \frac{M_w}{M_n} \quad (3)$$



## Results and discussion

It is known that most polar, biodegradable polymers are difficult to characterize accurately by MALDI-MS as well as by other common methods.<sup>49</sup> In this study 16 different biodegradable polymers were effectively evaluated with 7 matrices (5 solids and 2 ILMs). A complete list of the polymers examined is shown in Table 1. Also listed in Table 1 is the polymer number, catalog number, lot number, the reported mass of the polymer (if available), the method of determination of the polymer mass (if available), and the industrial use of the polymer (if available). The polymers vary in both their functionalities and molecular weights, thereby showing the applicability of the ILMs. Also studied are a series of polymers of identical functionality, but different average molecular weights. All polymer structures are shown in Table 2.

Structures of the matrices used are listed in Table 3. Matrices CHCA, DHB, IAA, and HABA have carboxylic acid groups which typically cause some degradation in the biodegradable polymers. Matrices DCTB and HABA form free radicals when irradiated by the laser. These free radicals can also cause polymer degradation. DEA CHCA, on the other hand has an almost neutral pH and does not form free radicals. As will be shown, this produces less degradation when using DEA CHCA.

### *Molecular Weight Determination*

Number average molecular weight and weight average molecular weight calculations for biodegradable polymers can be difficult when using MALDI-TOF MS.<sup>49</sup> This is because

there is usually significant degradation of the polymer which biases the calculation towards low mass. However, when more Gaussian  $m/z$  distributions with minimal degradation are observed, then more accurate  $M_n$  and  $M_w$  values often can be obtained. This can be seen in Figure 1 with the MALDI-MS of polycaprolactone (polymer 8). Figure 1A shows the detection of polymer 8 with the ionic liquid matrix DEA CHCA. When using DEA CHCA as a matrix an almost Gaussian distribution of  $m/z$  peaks are seen with little degradation. The  $M_n$  and  $M_w$  were found to be 4250 Da and 4732 Da respectively. These values vary dramatically from the  $M_n$  and  $M_w$  reported by the manufacturer (see Table 1) determined by gel permeation chromatography (GPC). The  $M_n$  and  $M_w$  found by MALDI are 57% and 66% less than that of GPC. This discrepancy between direct and indirect methods of molecular weight determination is common and discrepancies have been reported to be up to 94%.<sup>49</sup> The two main reasons for these differences in  $M_n$  and  $M_w$  are: a) the calibration standards used in the secondary size exclusion chromatography or rheological method, and b) the polydispersity (pd) of the polymer. Typical calibration standards, such as linear polystyrene, are not directly comparable to the polymer being analyzed, particularly for more polar polymers and branched polymers. Differences in functional groups, the amount of branching and the solvation radius of the standards versus the analyte can cause over- or under-estimation of the analyte's  $M_n$  and  $M_w$ . It has also been shown that polymers with large polydispersities ( $> 1.2$ ) will also show large molecular weight differences when direct (MALDI) and indirect (GPC) methods are compared.<sup>49</sup> The polydispersity calculated from GPC data was found to be 1.4. This relatively large polydispersity value also may lead to large discrepancies between MALDI and GPC since the use of solid matrices typically results in the underestimation of the  $M_n$  and  $M_w$  for polymers with large polydispersities.

However, it has also been shown that these differences can be minimized by using new matrices.<sup>35</sup> This is certainly the case with the ILM used to generate Fig. 1A. In addition, given the lack of proper calibration standards for polycaprolactone (polymer 8), the inaccuracy of the GPC data is not surprising. When traditional solid matrices are used (Fig. 1 B-C) the differences in the  $M_n$  and  $M_w$  values calculated with MALDI versus GPC are even larger. Figure 1B shows the spectrum obtained with the best performing solid matrix HABA. Two distributions are observed, one of which is a degradation distribution. The  $M_n$  and  $M_w$  were calculated for all peaks and for just the higher molecular weight distribution (Table 4). It was found that the higher molecular weight distribution had slightly lower  $M_n$  (4162 Da) and  $M_w$  (4758 Da) values than was obtained by the optimal ILM. When all peaks are taken into account the  $M_n$  and  $M_w$  are significantly reduced (Table 4). Figure 1C shows the detection of polymer 8 with DHB. The  $M_n$  and  $M_w$  were found to be 1764 Da and 1959 Da respectively. The solid matrix DCTB (1D) performed more poorly than all other matrices and only produced a small degradation distribution with  $M_n$  and  $M_w$  of 784 Da and 814 Da respectively. The  $M_n$ ,  $M_w$ , and polydispersity values for all 16 polymers with all 7 matrices are listed in Table 4. In every case the DEA CHCA ionic liquid matrix produced the best results in terms of: a) most symmetrical distributions of homologues, b) highest average molecular weight average, c) least degradation, d) narrowest polydispersities, e) often the greatest sensitivity, and f) most reproducible results. All spectra are given in the Supplemental Information.

The  $M_n$  and  $M_w$  also can be affected by the instrumental parameters. It was found by Mineo et al. that grid voltage and delayed extraction times can have a large effect on the observed

molecular weight distribution.<sup>50</sup> This was observed for many of the polymers in this study, especially when using solid molecular matrices. A typical example of this is shown for poly(ethylene glycol)-block-poly(propylene glycol)-block-poly(ethylene glycol) (polymer 12,  $M_n=1,100$  Da) in Table 4. It was found that a grid voltage of 19 kV was best and the delayed extraction time was best at either 90 ns or 300 ns for different matrices. The extraction delay time had the least effect on the spectra produced when using ILMs. The delayed extraction time was changed from 90 ns to 300 ns causing the  $M_n$  and  $M_w$  to decrease by 3% and 1% respectively when using DEA CHCA. Generally polymers detected with DEA CHCA showed very little change when the delayed extraction time was changed. The solid matrices on the other hand showed a much stronger observed molecular weight dependence on the delayed extraction time. When the delayed extraction time was increased from 90ns to 300ns, the observed  $M_n$  and  $M_w$  for CHCA increased 23.5% and 15% respectively. DCTB and DHB showed similar increases of 11% and 20% for  $M_n$  and 7.5% and 17% for  $M_w$ . 3-IAA, HABA, and DEA IAA showed no analyte signal for 90 ns extraction time and therefore only the 300 ns  $M_n$  and  $M_w$  are listed. All other polymers listed in Table 4 show the maximum  $M_n$  and  $M_w$  values obtained with either 90 ns or 300 ns extraction times.

Most polymers detected with the ILM showed almost Gaussian  $m/z$  peak distributions. However, a few polymers showed either asymmetric distributions or no distributions which can bias the  $M_n$  and  $M_w$  values toward lower mass values. This phenomenon is observed in polymers 9, 14, 15, and 16. Polymers 9 and 16 show asymmetric spectra whereas spectra 14 and 15 show groups of peaks that increase in intensity at low mass. Figure 2 shows the

detection of poly(1,4-butylene adipate-co-polycaprolactam) (polymer 9) with DEA CHCA (A), CHCA (B), DHB (C), and 3-IAA (D). Polymers 14, 15, and 16 are shown in the Supplemental Information (SI1). Figure 2A shows that although the ILM is able to detect polymer 9, the distribution is not quite as symmetric as found for most other polymers and the  $S/N$  ratio is poorer at higher mass. However, it is still far superior to all other matrices. The  $M_n$  and  $M_w$  are calculated to be 1829 Da and 2014 Da respectively. Distributions observed in Figure 2A are multiple overlapping distributions of the 1,4-butylene adipate (200 Da) and caprolactam (114 Da) monomers of polymer 9. Because multiple overlapping distributions are observed, all peaks were used to determine  $M_n$  and  $M_w$ . Since no molecular weight information is available from the manufacturer it is unclear how the asymmetric nature of this spectrum effects the  $M_n$  and  $M_w$  calculations. However, it is clear that the ILM DEA CHCA does give a more substantive molecular weight information than the other matrices tested. Figure 2B shows the detection of polymer 9 with CHCA. This spectrum shows a small distribution that is 850 Da less than the  $M_n$  found with DEA CHCA ( the  $M_n$  and  $M_w$  were found to be 978 Da and 1061 Da respectively). Figure 2C shows that when DHB is used in the detection of polymer 9 a small distribution similar to that in 2B is seen (  $M_n$  and  $M_w$  are 748 Da and 799 Da respectively). When 3-IAA (Fig. 2D) is used as matrix only degradation products can be seen. The  $M_n$  and  $M_w$  were found to be 1032 Da and 1228 Da when 3-IAA is used as a matrix.

#### *Effect of the Matrix on Polymer Degradation*

When analyzing easily degradable polymers there are three main types of spectra that are observed. The first, and by far the rarest, is the Gaussian or almost Gaussian distribution of

peaks. This first case often represents the intact polymer with little to no degradation. The second case is a distribution of peaks that increase in intensity as they approach low mass forming a “wedge” shape. This distribution represents the presence of polymer degradation. The third is a Gaussian distribution of peaks with a second distribution of degradation peaks that increase in intensity as they approach low mass. In this third case the Gaussian distribution of  $m/z$  peaks has a slightly lower average mass, accounting for the breakdown of the polymer.

Figure 3 shows the spectra of a poly[(lactide-co-ethylene glycol)-co-ethoxyphosphate] copolymer (polymer 1, Table 1) obtained with DEA CHCA (A), CHCA (B), DHB (C), and HABA. Figure 3A shows that when the ionic liquid matrix DEA CHCA is used, two almost Gaussian peak distributions are observed. The major, i.e. larger, distribution represents the intact polymer with a mass difference between adjacent peaks of 72 Da. Each variation of 72 Da represents the difference of a lactide monomer in the polymer (see Table 2 structure). The second smaller distribution, which is 44 Da less than the major distribution, represents the loss of the ethoxy group from the phosphate group of the polymer. The  $M_n$  and  $M_w$  for the major distribution was found to be 2171 Da and 2227 Da with the minor distributions  $M_n$  and  $M_w$  found to be 1964 Da and 2012 Da respectively. All  $M_n$  and  $M_w$  values are listed in Table 3. Figure 3B show the mass spectrum of polymer 1 with the solid matrix CHCA. It shows significant degradation and no Gaussian distribution of peaks. This degradation may be due, in part, to the low pH of the matrix solution.<sup>45</sup> The most intense peaks correspond to the intact ethoxyphosphate polymer with a 72 Da difference between the peaks. Many other degradation products are present but the only other distribution that could be identified is the

loss of the ethoxy group of the ethoxyphosphate group. Since no clear Gaussian distribution is seen, all peaks were used to determine  $M_n$  and  $M_w$ , which was found to be 1115 Da and 1253 Da respectively. Figure 3C shows that when DHB is used as the matrix for the detection of polymer 1 there is a significant amount of degradation. The most intense peaks, which plateau as mass decreases, represent the polymer with intact ethoxyphosphate groups. Another wedge shaped distribution is also present which represents the loss of an ethoxy group and some other unidentified distributions. The  $M_n$  and  $M_w$  were found to be 1454 Da and 1700 Da respectively. Figure 3D shows the detection of polymer 1 with the HABA matrix. The HABA produced the worst results of all matrices tested for polymer 1. There is a small distribution of peaks that increase in intensity as mass decreases. There are also many unidentified peaks at low mass. The  $M_n$  and  $M_w$  were found to be 1053 Da and 1255 Da respectively. It should be noted that the DHB produced the most intense analyte signals and that the ILM produced the least intense signals for polymer 1. However, the ILM showed the least polymer degradation and the highest  $M_n$  and  $M_w$  values. No  $M_n$  or  $M_w$  information could be obtained from the supplier (see Experimental and Table 1) and the ILM is assumed to have the most accurate  $M_n$  and  $M_w$  since it showed the least degradation. Even when the degradation distribution is not included in the  $M_n$  and  $M_w$  calculation, as in the case of 3-IAA (Table 3), the  $M_n$  and  $M_w$  are significantly lower than when the ILM is used. The lack of degradation of polymer 1 in the ILM is likely due, in part, to the lack of acidic species in this matrix.

*Polymers of Differing Length and Branching*

In order to examine whether or not the results shown in the previous examples are consistent over a broader range of  $M_n$ 's, a series of chemically similar polymers with varying  $M_n$ 's were tested. Polymers 3-5 (Fig. 4) which are polycaprolactone diol polymers of three different  $M_n$ 's ( $M_n=530$ , 1250, and 2000 Da) were examined. The  $M_n$ 's for polycaprolactone diol polymers have been estimated by the supplier. It was found that the molecular weight averages of the low mass polymers were severely underestimated. The  $M_n$  for polymer 3 was found to be 2010 Da which is 379% greater than the reported  $M_n$ . Even matrices such as DHB and DCTB that produced substantial polymer degradation showed significantly higher  $M_n$ 's than that reported by the supplier. However, as the size of the polymer increases the difference between the  $M_n$  found by MALDI with the ILM and the reported  $M_n$  begins to decrease. The  $M_n$  for polymers 4 and 5 were found to be 2641 Da and 2922 Da which are 211% and 146% more than the reported  $M_n$ . Although the error in the stated  $M_w$  is less than that for the smaller polymers in this series, it was still underestimated by almost 1000 Da.

Branched polymers also were examined to show that the indirect determination of  $M_n$  and  $M_w$  (i.e. theoretical values) for branched polymers were severely underestimated by the manufacturers. Figure 5 shows the MALDI mass spectra of polymers 6 (Fig. 5A) and 7 (Fig. 5B) which are polycaprolactone triols with  $M_n$ 's reported as 300 Da and 900 Da respectively. With the ionic liquid MALDI matrix it was found that the  $M_n$  and  $M_w$  for polymer 6 is 593 Da and 628 Da respectively. Analogous higher average molecular weights were found for



polymer 7 with the  $M_n$  and  $M_w$  found to be 1930 Da and 2081 Da. This corresponds to  $M_n$ 's that are 198% and 214% underestimated by the manufactures indirect methods.

#### *Precision and Accuracy of $M_n$ Determination by MALDI*

To measure the precision of the molecular weights obtained with the ILM, multiple spectra of same polymer were taken and were averaged. Three spectra of polymer 6 were taken and averaged. It was found that polymer 6 has an average  $M_n$  of  $593 \pm 3$  Da and a  $M_w$  of  $629 \pm 10$  Da. Similarly, 4 spectra of polymer 7 were taken and averaged. The  $M_n$  was found to be  $1930 \pm 16$  Da and the  $M_w$  was found to be  $2081 \pm 24$  Da. This data shows that the  $M_n$  and  $M_w$  are highly reproducible with high precision when using the ILM DEA CHCA.

The accuracy was determined by analyzing a polymer that has  $M_n$  and  $M_w$  values determined by many different methods. PEG is well characterized with accurate GPC standards available from many manufacturers. PEG is also well suited for MALDI analysis since it is easily ionized and shows almost Gaussian distributions with most matrices. Figure 6 shows the detection of polymer 10 (reported  $M_n= 4431$  Da) with DEA CHCA (A), CHCA (B), DHB (C), and DCTB (D).  $M_n$ 's of spectra A-D were calculated to be 4731 Da, 4597 Da, 4244 Da, and 4552 Da respectively. It was found that the  $M_n$  of all matrices tested were within 1.5% to 6% of the reported  $M_n$  for polymer 10 which demonstrates that  $M_n$  from MALDI and the reported  $M_n$  are in good agreement for well characterized polymers.

## Conclusions

The second generation ionic liquid matrix, DEA CHCA, has been shown to be well suited for the MALDI-MS analysis of biodegradable polymers. This ILM produced the least degradation, near Gaussian peak distributions, and often provided greater analyte signals than the best solid matrices. It has also been shown to produce precise and accurate number average molecular weights and weight average molecular weights. Variance between spectra was found to be low. When the  $M_n$  found by MALDI-MS was compared to a well characterized polymer, the values were found to be in good agreement (within 6%).

## References

- (1) Pino, V.; Anderson, J. L.; Ayala, J. H.; Gonzalez, V.; Afonso, A. M. *J. Chromatogr. A* **2008**, *1182*, 145-152.
- (2) Lohithakshan, K. V.; Aggarwal, S. K. *Radiochim. Acta* **2008**, *96*, 93-97.
- (3) Lo, W.; Yang, H.; Wei, G. *Green Chem.* **2003**, *5*, 639-642.
- (4) Carda-Broch, S.; Berthod, A.; Armstrong, D. W. *Anal. Bioanal. Chem* **2003**, *375*, 191-199.
- (5) Zhao, F.; Meng, Y.; Anderson, J. L. *J. Chromatogr. A* **2008**, *1208*, 1-9.
- (6) Liu, J.; Li, N.; Jiang, G.; Liu, J.; Jonsson, J. A.; Wen, M. *J. Chromatogr. A* **2005**, *1066*, 27-32.
- (7) Yao, C.; Pino, V.; Anderson, J. L. *J. Chromatogr. A* **2009**, *1216*, 948-955.
- (8) Baltazar, Q. Q.; Leininger, S. K.; Anderson, J. L. *J. Chromatogr. A* **2008**, *1182*, 119-127.
- (9) Huang, K.; Han, X.; Zhang, X.; Armstrong, D. W. *Anal. Bioanal. Chem.* **2007**, *389*, 2265-2275.
- (10) Seeley, J. V.; Seeley, S. K.; Libby, E. K.; Breitbach, Z. S.; Armstrong, D. W. *Anal. Bioanal. Chem.* **2008**, *390*, 323-332.
- (11) Lambertus, G. R.; Crank, J. A.; McGuigan, M. E.; Kendler, S.; Armstrong, D. W.; Sacks, R. D. *J. Chromatogr. A* **2006**, *1135*, 230-240.
- (12) Breitbach, Z. S.; Armstrong, D. W. *Anal. Bioanal. Chem.* **2008**, *390*, 1605-1617.
- (13) Anderson, J. L.; Armstrong, D. W. *Anal. Chem.* **2005**, *77*, 6453-6462.
- (14) Ding, J.; Welton, T.; Armstrong, D. W. *Anal. Chem.* **2004**, *76*, 6819-6822.
- (15) Carda-Broch, S.; Berthod, A.; Armstrong, D. W. *Rapid Commun. Mass Spectrom.* **2003**, *17*, 553-560.
- (16) Armstrong, D. W.; Zhang, L.; He, L.; Gross, M. L. *Anal. Chem.* **2001**, *73*, 3679-3686.
- (17) Li, Y. L.; Gross, M. L. *J. Am. Soc. Mass Spectrom.* **2004**, *15*, 1833-1837.

- (18) Zabet-Moghaddam, M.; Krueger, R.; Heinzle, E.; Tholey, A. *J. Mass Spectrom.* **2004**, *39*, 1494-1505.
- (19) Li, Y. L.; Gross, M. L.; Hsu, F. *J. Am. Soc. Mass Spectrom.* **2005**, *16*, 679-682.
- (20) Catharino, R. R.; de Marques, L.; Santos, L. S.; Baptista, A. S.; Gloria, E. M.; Calori-Domingues, M. A.; Facco, E. M. P.; Eberlin, M. N. *Anal. Chem.* **2005**, *77*, 8155-8157.
- (21) Santos, L. S.; Haddad, R.; Hoechr, N. F.; Pilli, R. A.; Eberlin, M. N. *Anal. Chem.* **2004**, *76*, 2144-2147.
- (22) Soukup-Hein, R. J.; Remsburg, J. W.; Dasgupta, P. K.; Armstrong, D. W. *Anal. Chem.* **2007**, *79*, 7346-7352.
- (23) Remsburg, J. W.; Soukup-Hein, R. J.; Crank, J. A.; Breitbach, Z. S.; Payagala, T.; Armstrong, D. W. *J. Am. Soc. Mass Spectrom.* **2008**, *19*, 261-269.
- (24) Soukup-Hein, R. J.; Remsburg, J. W.; Breitbach, Z. S.; Sharma, P. S.; Payagala, T.; Wanigasekara, E.; Huang, J.; Armstrong, D. W. *Anal. Chem.* **2008**, *80*, 2612-2616.
- (25) Zhao, Z.; Wang, J.; Mao, H.; Leong, K. W. *Adv. Drug Deliv. Rev.* **2003**, *55*, 483-499.
- (26) Huang, S.; Zhuo, R. *Phosphorus, Sulfur Silicon Relat. Elem.* **2008**, *183*, 340-348.
- (27) Lee, W.; Park, J.; Jung, S.; Yang, C. W.; Kim, W.; Kim, H.; Park, J.; Park, J. *J. Controlled Release* **2005**, *105*, 77-88.
- (28) Krogman, N. R.; Weikel, A. L.; Nguyen, N. Q.; Nair, L. S.; Laurencin, C. T.; Allcock, H. R. *Macromolecules* **2008**, *41*, 7824-7828.
- (29) Siracusa, V.; Rocculi, P.; Romani, S.; Dalla Rosa, M. *Trends Food Sci. Technol.* **2008**, *19*, 634-643.
- (30) Netopilik, M.; Kratochvil, P. *Polymer* **2003**, *44*, 3431-3436.
- (31) Netopilik, M.; Podesva, J.; Lokaj, J.; Kratochvil, P. *Polym. Int.* **2008**, *57*, 1152-1158.
- (32) Simekova, M.; Berek, D. *J. Chromatogr. A* **2005**, *1084*, 167-172.
- (33) Huijser, S.; Staal, B. B. P.; Huang, J.; Duchateau, R.; Koning, C. E. *Angew. Chem., Int. Ed.* **2006**, *45*, 4104-4108.
- (34) He, M.; Chen, H. *Curr. Org. Chem.* **2007**, *11*, 909-923.
- (35) Montaudo, G.; Samperi, F.; Montaudo, M. S. *Prog. Polym. Sci.* **2006**, *31*, 277-357.
- (36) Meier, M. A. R.; Adams, N.; Schubert, U. S. *Anal. Chem.* **2007**, *79*, 863-869.
- (37) Casazza, E.; Ricco, L.; Russo, S.; Scamporrino, E. *Macromolecules* **2007**, *40*, 739-745.
- (38) Luftmann, H.; Rabani, G.; Kraft, A. *Macromolecules* **2003**, *36*, 6316-6324.
- (39) Montaudo, G.; Montaudo, M. S.; Puglisi, C.; Samperi, F. *Anal. Chem.* **1994**, *66*, 4366-4369.
- (40) Jalabert, M.; Frascini, C.; Prud'homme, R. E. *J. Polym. Sci. Part A* **2007**, *45*, 1944-1955.
- (41) Alicata, R.; Barbuzzi, T.; Giuffrida, M.; Ballistreri, A. *Rapid Commun. Mass Spectrom.* **2005**, *20*, 568-576.
- (42) Ricco, L.; Casazza, E.; Mineo, P.; Russo, S.; Scamporrino, E. *Macromolecules* **2008**, *41*, 3904-3911.
- (43) Kricheldorf, H. R.; Al Masri, M.; Schwarz, G. *Macromolecules* **2003**, *36*, 8648-8651.
- (44) Huijser, S.; Staal, B. B. P.; Huang, J.; Duchateau, R.; Koning, C. E. *Biomacromolecules* **2006**, *7*, 2465-2469.
- (45) Goepferich, A. *Biomaterials* **1996**, *17*, 103-114.
- (46) Siparsky, G. L.; Voorhees, K. J.; Miao, F. *J. Environ. Polymer Degradation* **1998**, *6*, 31-41.

- (47) Chen, H.; He, M.; Wan, X.; Yang, L.; He, H. *Rapid Commun. Mass Spectrom.* **2003**, *17*, 177-182.
- (48) Crank, J. A.; Armstrong, D. W. *JASMS Submitted*, .
- (49) Montaudo, G.; Lattimer, R. In *Mass spectrometry of polymers*; CRC Press: Boca Raton, Fla., 2002; pp 584.
- (50) Mineo, P.; Vitalini, D.; Scamporrino, E.; Bazzano, S.; Alicata, R. *Rapid Commun. Mass Spectrom.* **2005**, *19*, 2773-2779.

Table 1) List of polymers and information obtained from the manufacture. Information listed is: 1) full name of the polymer, 2) number given to the polymer for reference, 3) catalog number of the polymer, 4) lot number of the polymer, 5) reported molecular weight information in daltons ( $M_w$ = weight average molecular weight,  $M_n$ = number average molecular weight and  $M_p$ =average molecular weight), 6) the method the molecular weight was determined (if known), 7) use of the polymer (if known)

Polymer Name	Polymer #	Catalog #	Lot #	Reported $M_w$ , $M_n$ , $M_p$ (Da)	Method of Determination	Industrial Use
Poly[(lactide-co-ethylene glycol)-co-ethylolxyphosphate]	1	659606	02527HD	NA	NA	Non-Viral Gene Delivery
Poly(DL-lactide- co-glycolide)	2	531154	03807BJ	$M_w$ =5,000-15,000	GPC Polystyrene Standard	Sutures and Bioabsorbable Implantable Devices
Polycaprolactone diol	3	189405	06804CC	$M_n$ =530	Estimated by Manufacture	Drug Delivery
Polycaprolactone diol	4	189413	13711HO	$M_n$ =1250	Estimated by Manufacture	Drug Delivery
Polycaprolactone diol	5	189421	09528CE	$M_n$ =2,000	Estimated by Manufacture	Drug Delivery
Polycaprolactone triol	6	200387	01101MZ	$M_n$ =300	Estimated by Manufacture	NA
Polycaprolactone triol	7	200409	12312DD	$M_n$ =900	Estimated by Manufacture	NA
Polycaprolactone	8	440752	05006CJ	$M_n$ =10,000	GPC	Extrusion aid, Die Lubricant, Mold release Containers
Poly(1,4-butylen adipate-co-polycaprolactam)	9	468274	13812TQ	NA	NA	NA
Poly(ethylene glycol)	10	373001	11608EB	$M_n$ =4431	NA	NA
Poly(ethylene glycol)-block-poly(propylene glycol)-block-poly(ethylene glycol)	11	435430	01631MH	$M_n$ =2,800	NA	Anti-foaming Agent
Poly(ethylene glycol)-block-poly(propylene glycol)-block-poly(ethylene glycol)	12	435406	03302BN	$M_n$ =1,100	NA	Anti-foaming Agent
$\alpha$ -co-Bis(2-(3-carboxy-1-oxopropyl)amino)ethyl)poly(ethylene glycol	13	14567	1209510	$M_n$ =3000	NA	NA
Poly(1,4-bis(hydroxyethyl)terephthalate-all-ethylolxyphosphate)	14	659614	03506HD	NA	NA	NA
Poly(1,4-bis(hydroxyethyl)terephthalate-all-ethylolxyphosphate)-co-1,4-bis(hydroxyethyl)terephthalate-co-terephthalate	15	659738	02813HD	NA	NA	NA
Polycaprolactone-block-polytetrahydrofuran-block-polycaprolactone	16	526320	09415TU	$M_n$ =2,000	GPC	NA

Table 2) List of polymer structures by polymer number.

Polymer #	Polymer Structure
1	
2	
3	
4	
5	
6	
7	
8	

Table 2 Cont.	
9	
10	
11	
12	
13	
14	
15	
16	

Table 3) Matrix name, the abbreviation used for each matrix, and the structure of each matrix are listed.

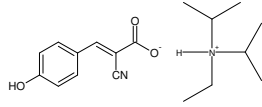
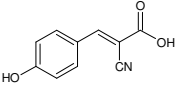
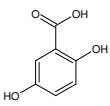
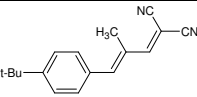
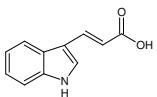
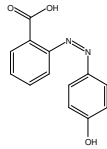
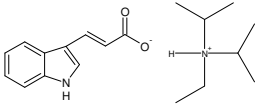
Matrix Name	Abbreviation	Structure
<i>N,N</i> -Diisopropylethylammonium $\alpha$ -cyano-4-hydroxycinnamate	DEA CHCA	
$\alpha$ -Cyano-4-hydroxycinnamic acid	CHCA	
2,5-Dihydroxybenzoic acid	DHB	
<i>trans</i> -2-[3-(4- <i>tert</i> -Butylphenyl)-2-methyl-2-propenylidene]malononitrile	DCTB	
<i>trans</i> -3-Indoleacrylic acid	IAA	
2-(4-Hydroxyphenylazo)benzoic acid	HABA	
<i>N,N</i> -Diisopropylethylammonium <i>trans</i> -3-indoleacrylate	DEA IAA	



Table 4) Polymer name, matrix used, weight average molecular weight in daltons ( $M_w$ ), number average molecular weight in Daltons ( $M_n$ ), and polydispersity (pd).

Poly[(lactide-co-ethylene glycol)-co-ethyloxyphosphate]	Matrix	$M_n$ (Da)	$M_w$ (Da)	pd
	DEA CHCA Major Distribution	2171	2228	1.03
	DEA CHCA Minor Distribution	1965	2012	1.02
	DEA IAA	1012	1137	1.12
	CHCA	1115	1253	1.12
	DCTB All	1750	1997	1.14
	DCTB Distribution	1952	2098	1.07
	DHB all	1455	1701	1.16
	DHB Distribution	1662	1836	1.1
	3-IAA Distribution	1635	1811	1.1
3-IAA all	1399	1627	1.16	
HABA	1054	1255	1.19	
Matrix	$M_n$ (Da)	$M_w$ (Da)	pd	
DEA CHCA	1928	1971	1.02	
DEA IAA	NA	NA	NA	
CHCA	874	931	1.06	
DCTB	1207	1607	1.33	
DHB	1408	1599	1.13	
3-IAA	NA	NA	NA	
HABA	NA	NA	NA	
Matrix	$M_n$ (Da)	$M_w$ (Da)	pd	
DEA CHCA	2101	2215	1.05	
DEA IAA	1181	1334	1.12	
CHCA	946	985	1.04	
DCTB	1385	1589	1.15	
DHB	1356	1545	1.14	
3-IAA	1144	1363	1.19	
HABA	968	1059	1.09	

Table 4 Cont.

Polycaprolactone diol ( $M_n=1,250$ )	Matrix	$M_n$ (Da)	$M_w$ (Da)	pd
	DEA CHCA	2641	2764	1.05
	DEA IAA	1667	1833	1.1
	CHCA	947	1019	1.07
	DCTB	1862.	2234	1.19
	DHB	1674	1952	1.17
	3-IAA	2067	2402	1.16
	HABA	1380	1670	1.21
	Matrix	$M_n$ (Da)	$M_w$ (Da)	pd
	DEA CHCA	2923	3149	1.08
	IAA DEA	1770	1913	1.08
CHCA	1053	1394	1.32	
DCTB	2628	2997	1.14	
DHB	1230	1338	1.09	
3-IAA	2946	3381	1.14	
HABA	2138	2572	1.2	
Polycaprolactone triol ( $M_n=300$ )	Matrix	$M_n$ (Da)	$M_w$ (Da)	pd
	DEA CHCA	593	629	1.06
	DEA IAA	371	403	1.09
	CHCA	431	507	1.18
	DCTB	476	507	1.07
	DHB	563	661	1.17
	3-IAA	378	400	1.06
	HABA	NA	NA	NA

Table 4 Cont.

Polycaprolactone triol (M <sub>n</sub> =900)	Matrix	M <sub>n</sub> (Da)	M <sub>w</sub> (Da)	pd
	DEA CHCA	1930	2081	1.08
	DEA IAA	1334	1520	1.14
	CHCA	778	831	1.07
	DCTB	923	1278	1.38
	DHB	1521	1767	1.16
3-IAA	1827	2011	1.1	
HABA	1330	1506	1.13	
Polycaprolactone	Matrix	M <sub>n</sub> (Da)	M <sub>w</sub> (Da)	pd
	DEA CHCA	4250	4732	1.11
	DEA IAA distribution	1906	2103	1.1
	DEA IAA ALL	1062	1436	1.35
	CHCA	1023	1110	1.09
	DCTB	784	815	1.04
	DHB all	1345	1570	1.17
	DHB Distribution	1764	1959	1.11
	3-IAA all	1783	2838	1.59
	3-IAA Distribution	2417	3515	1.45
HABA all	2447	4059	1.66	
HABA Distribution	4162	4758	1.14	
Poly(1,4-butylene adipate-co-polycaprolactam)	Matrix	M <sub>n</sub> (Da)	M <sub>w</sub> (Da)	pd
	DEA CHCA	1829	2015	1.1
	DEA IAA	1385	1700	1.23
	CHCA	979	1061	1.08
	DCTB	503	520	1.03
	DHB	748	799	1.06
3-IAA	1033	1238	1.20	
HABA	1407	1698	1.21	

Table 4 Cont.

Poly(ethylene glycol) (Average $M_n=4431$ )	Matrix	$M_n$ (Da)	$M_w$ (Da)	pd
	DEA CHCA	4731	4765	1.01
	DEA IAA	4633	4674	1.01
	CHCA	4597	4647	1.01
	DCTB	4552	4585	1.01
	DHB	4244	4389	1.03
	3-IAA	4723	4763	1.01
	HABA	4361	4439	1.02
	Matrix	$M_n$ (Da)	$M_w$ (Da)	pd
	DEA CHCA ET=90	1332	1361	1.02
	DEA CHCA ET=300	1294	1349	1.04
DEA IAA	1012	1132	1.12	
CHCA ET=90	882	1044	1.18	
CHCA ET=300	1152	1226	1.06	
DCTB ET=90	982	1052	1.07	
DCTB ET=300	1100	1138	1.03	
DHB ET=90	1004	1088	1.08	
DHB ET=300	1255	1311	1.04	
3-IAA	1188	1248	1.05	
HABA	1092	1158	1.06	
Matrix	$M_n$ (Da)	$M_w$ (Da)	pd	
DEA CHCA	3120	3163	1.01	
DEA IAA	2696	2766	1.03	
CHCA	2745	2864	1.04	
DCTB	2717	2761	1.02	
DHB	2939	3036	1.03	
3-IAA	2762	2876	1.04	
HABA	NA	NA	NA	

Table 4 Cont.

$\alpha,\omega$ -Bis[2-[(3-carboxy-1-oxopropyl)amino]ethyl]polyethylene glycol	Matrix	$M_n$ (Da)	$M_w$ (Da)	pd
	DEA CHCA	3442	3469	1.01
	DEA IAA	3301	3330	1.01
	CHCA	3399.3	3433.5	1.01
	DCTB	3315	3339	1.01
	DHB	3361	3389	1.01
	3-IAA	3313	3375	1.02
HABA	3362	3384	1.01	

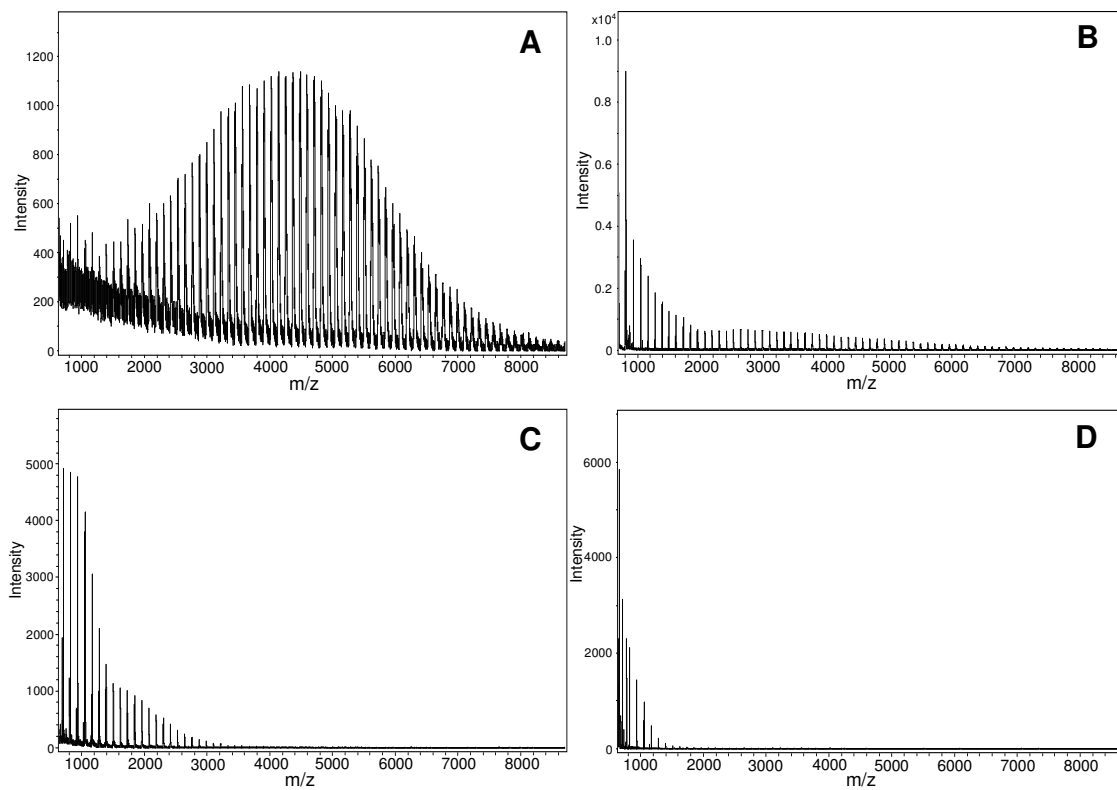


Figure 1) The detection of polycaprolactone (polymer 8) with A) DEA CHCA, B) HABA, C) DHB, and D) DCTB. The  $M_n$ 's were found to be A) 4250 Da, B) 4162 Da, C) 1764 Da, and D) 784 Da.

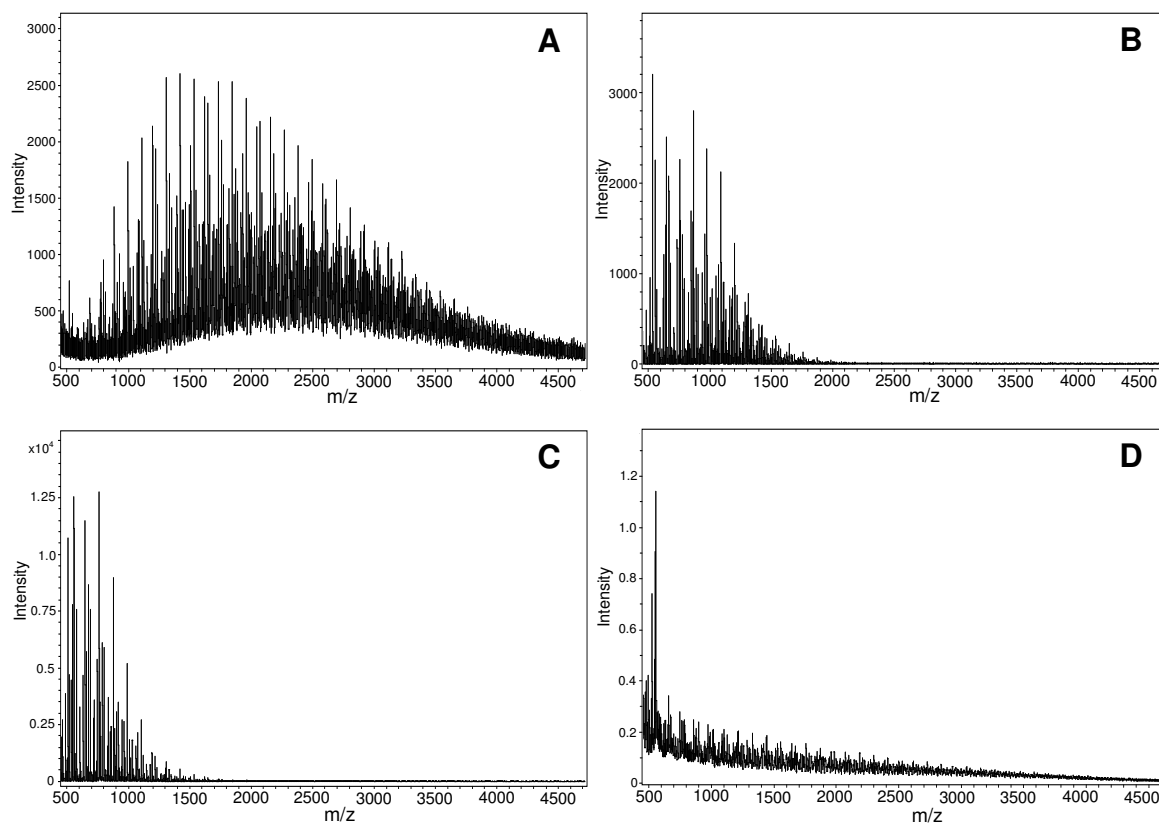


Figure 2) The detection of poly(1,4-butylene adipate-co-polycaprolactam) (polymer 9) with A) DEA CHCA, B) CHCA, C)DHB, and D) 3-IAA. Although polymer 9 is difficult to detect with all matrices, DEA CHCA out performs all matrices tested.

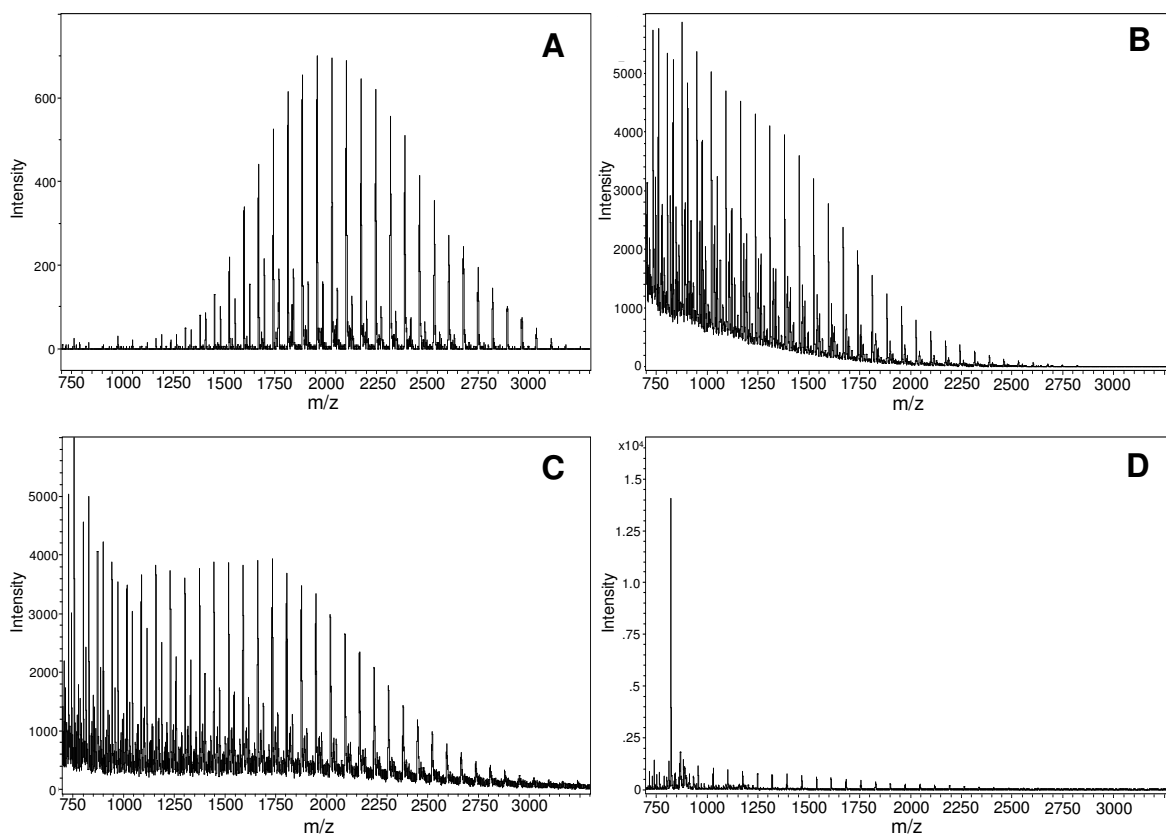


Figure 3) The detection of poly[(lactide-co-ethylene glycol)-co-ethoxyphosphate] (polymer 1) with A) DEA CHCA, B) CHCA, C)DHB, and D) HABA.



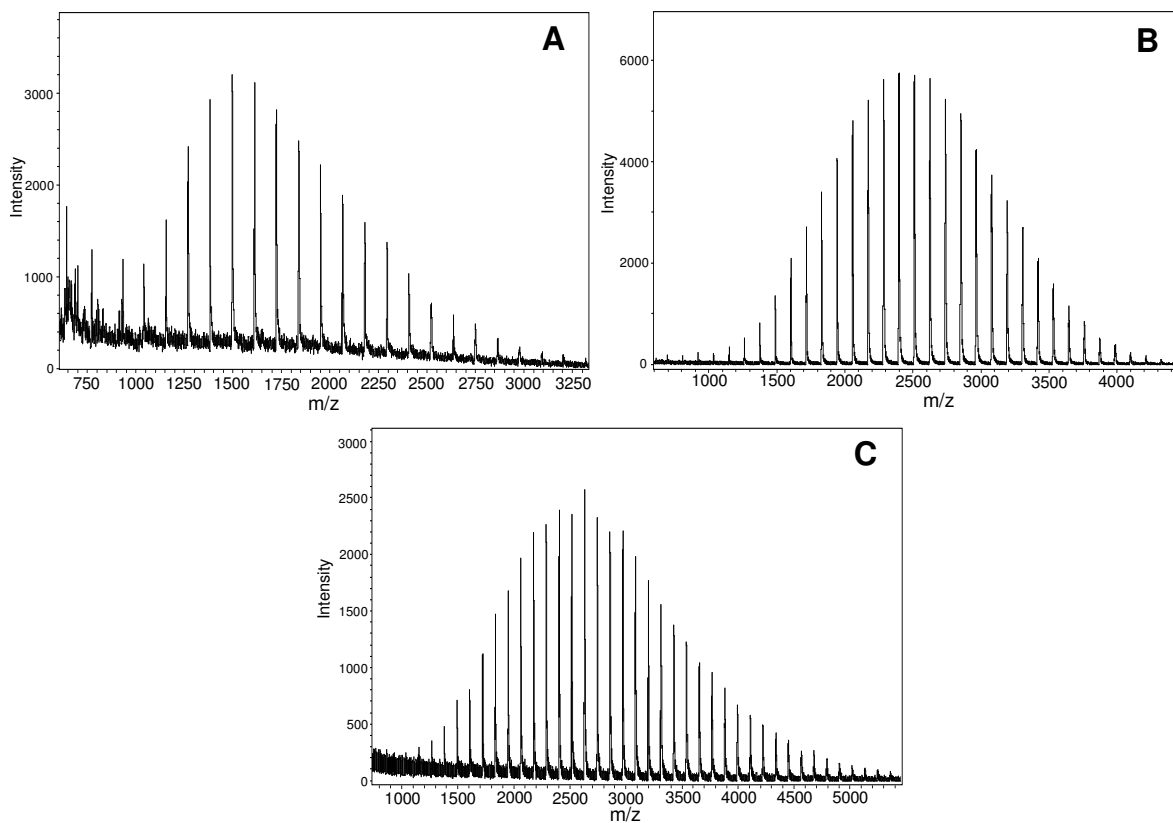


Figure 4) The detection of polycaprolactone diol polymers (3,4, and 5) with estimated number average molecular weights of A) 530 Da, B) 1250 Da, and C) 2000 Da using the ionic liquid matrix DEA CHCA . The number average molecular weights by MALDI-MS were found to be A) 2010 Da, B) 2641 Da, and C) 2922 Da.

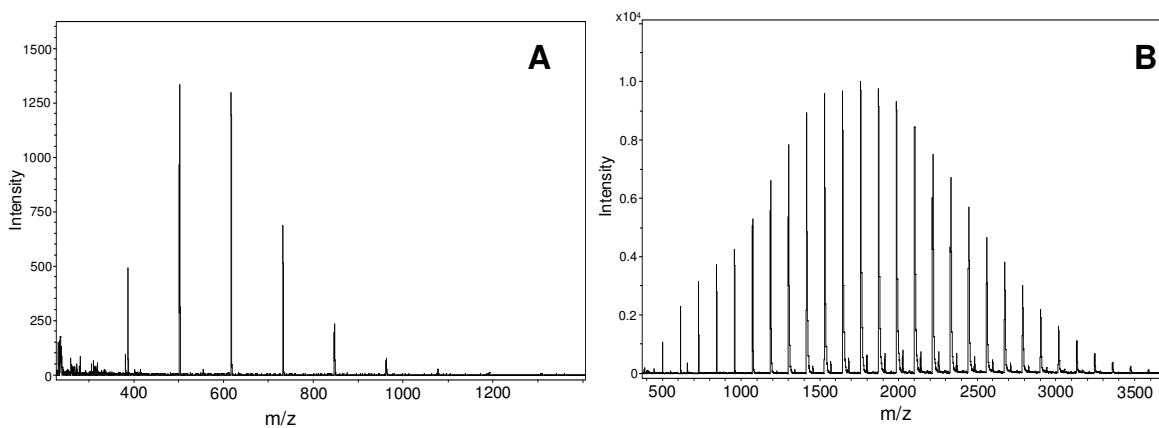


Figure 5) The detection of branched polycaprolactone triol polymers with estimated number average molecular weights of A) 300 and B) 900 using the ionic liquid matrix DEA CHCA . The number average molecular weights by MALDI-MS were found to be A)  $593 \pm 3$  Da and B)  $1930 \pm 16$  Da.

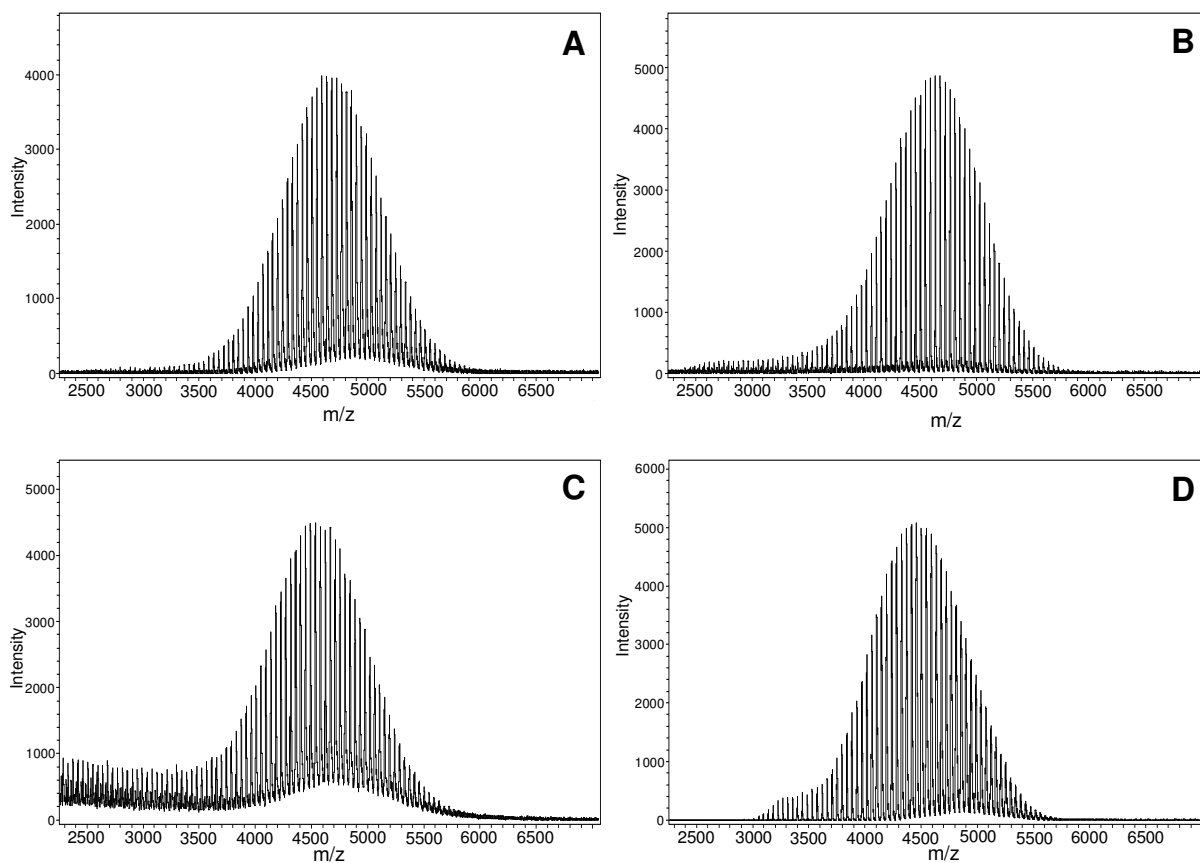
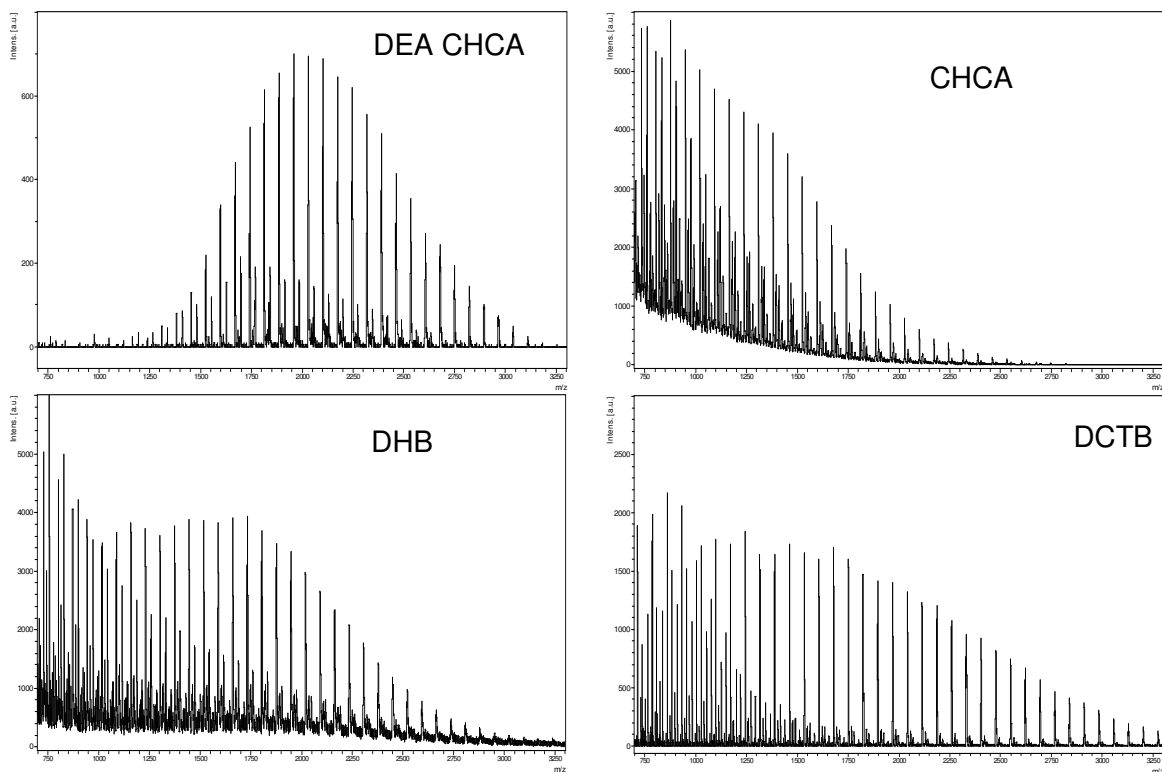


Figure 6) The detection of polyethylene glycol with A) DEA CHCA, B) CHCA, C) DHB, and D) DCTB. All matrices are within 1.5% to 6% of the reported value ( $M_n=4331$ ).

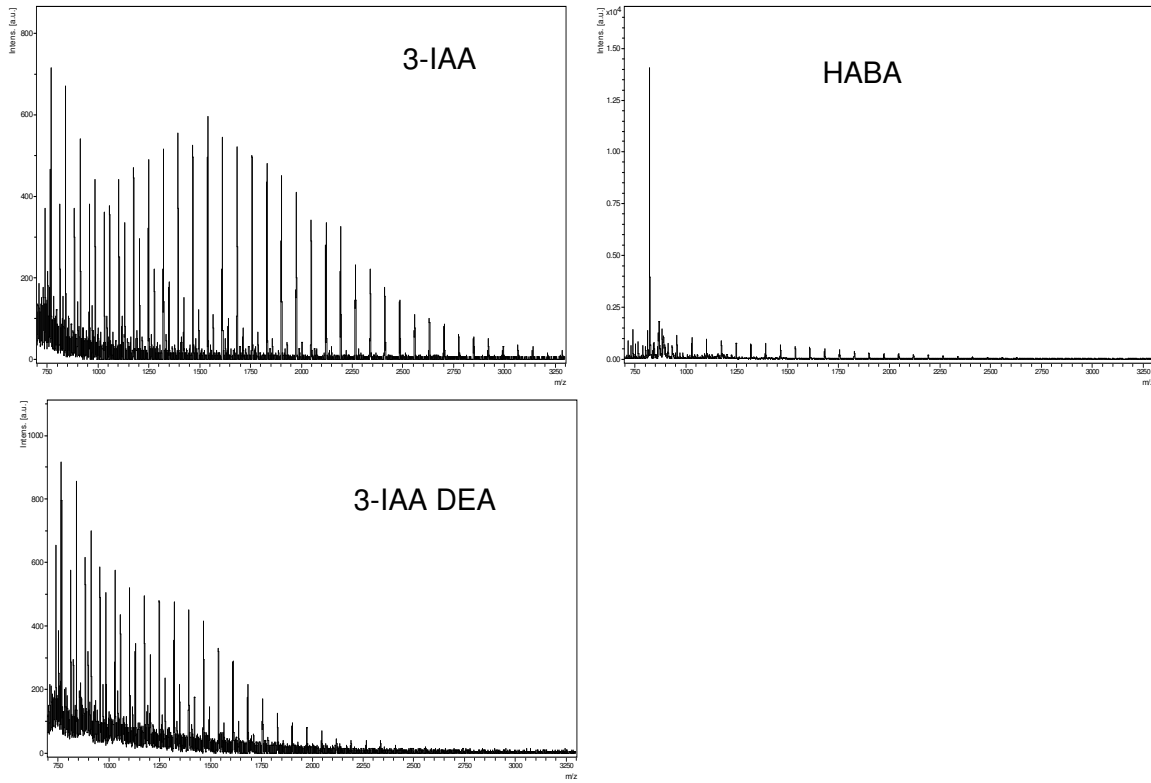
**Supplemental Information**

SI1) Spectra from all polymers listed by number with all 7 matrices.

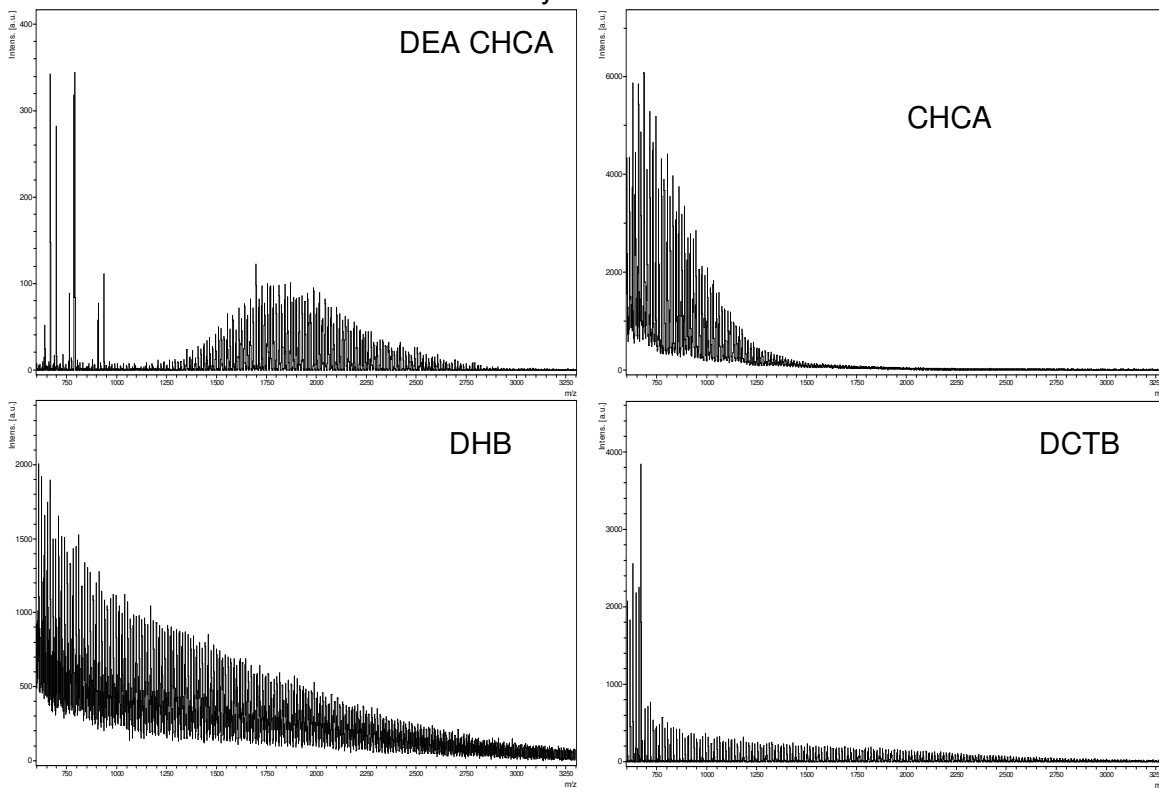
Polymer 1



Polymer 1

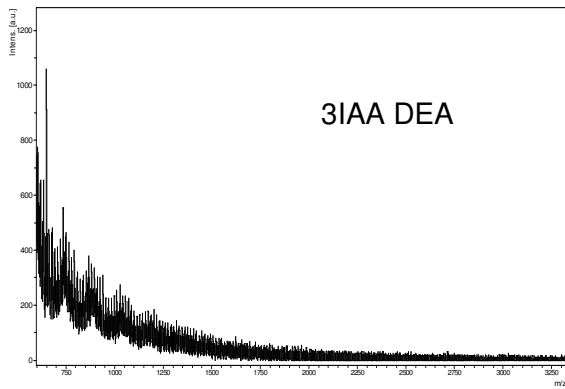
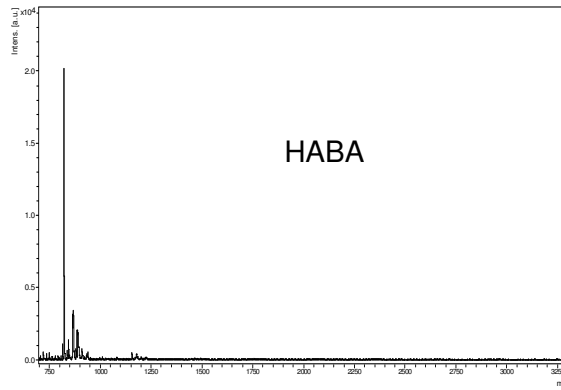


## Polymer 2

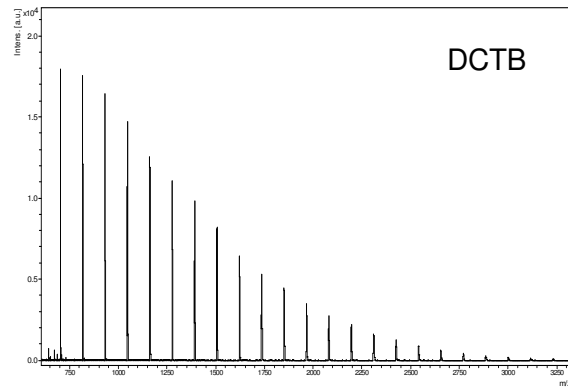
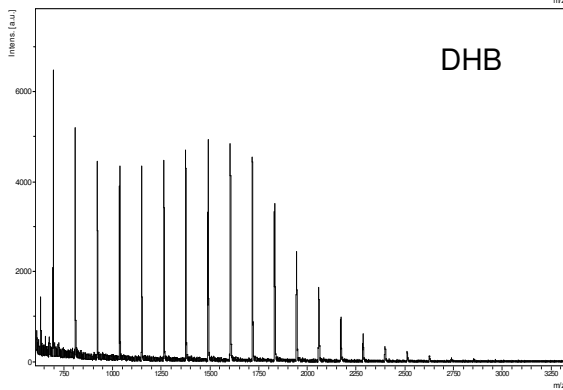
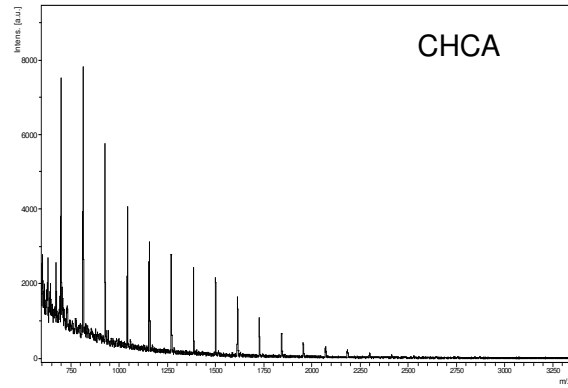
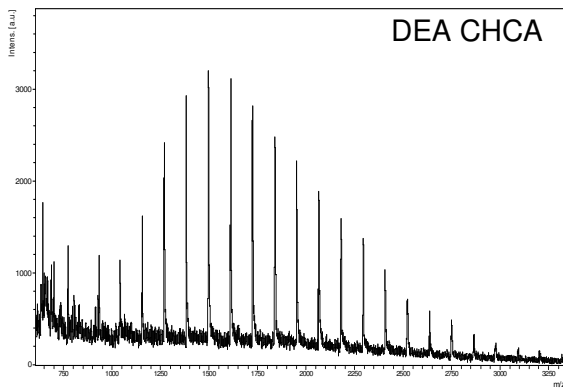


Polymer 2

IAA no analyte signal

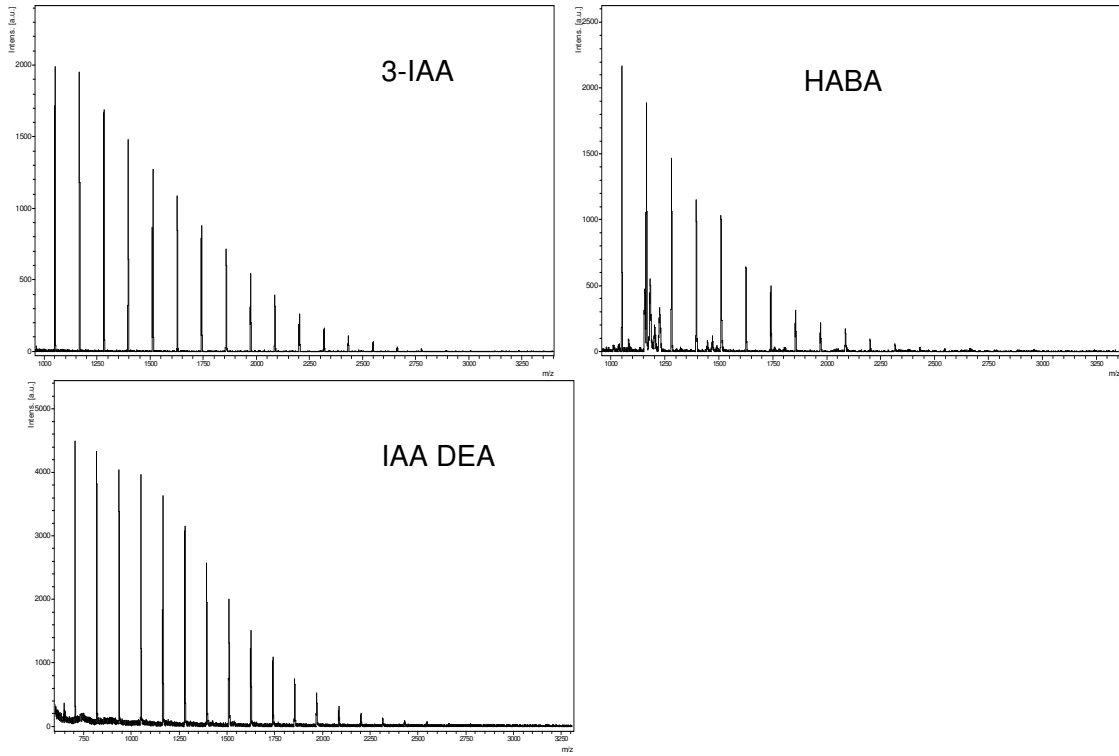


Polymer 3

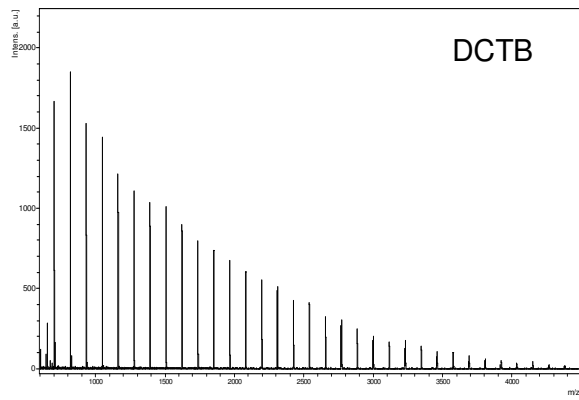
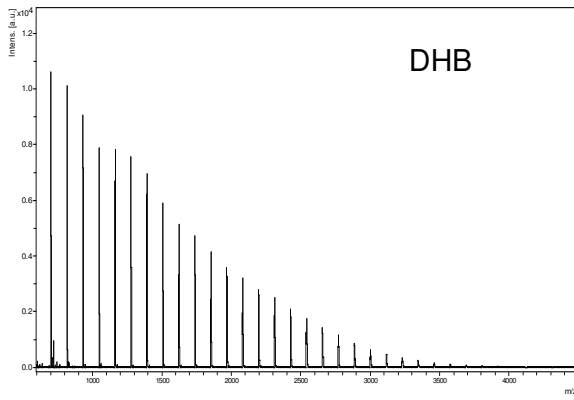
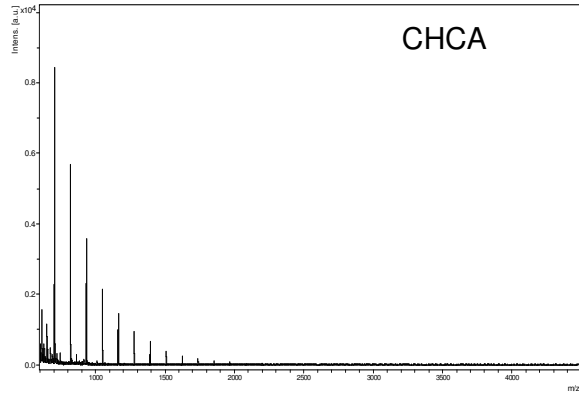
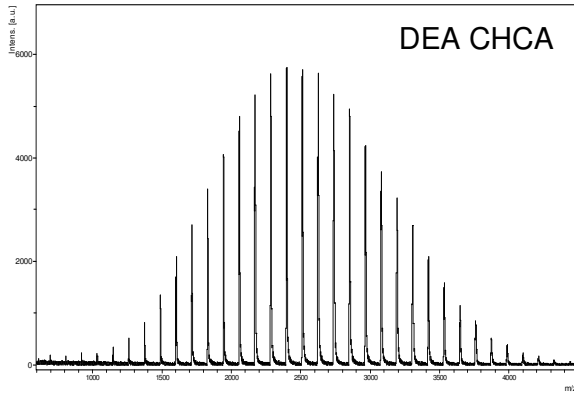




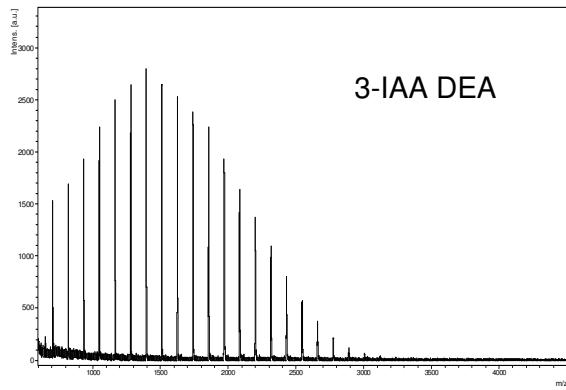
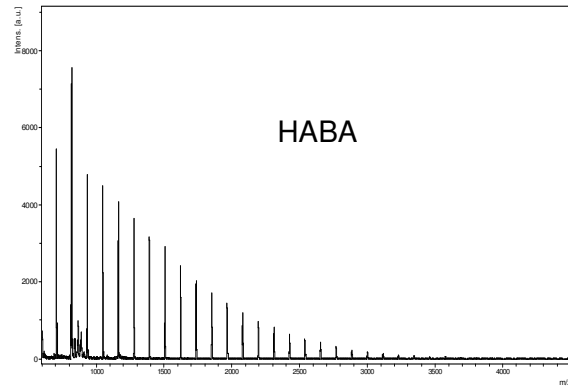
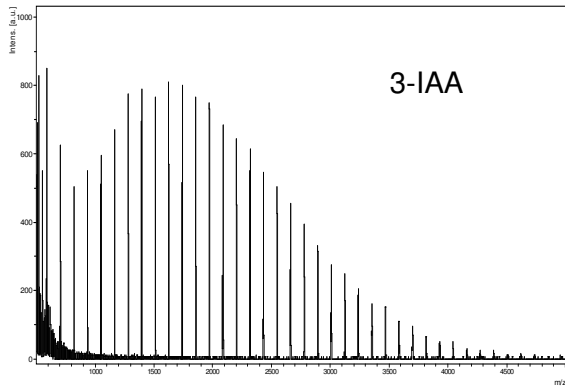
Polymer 3



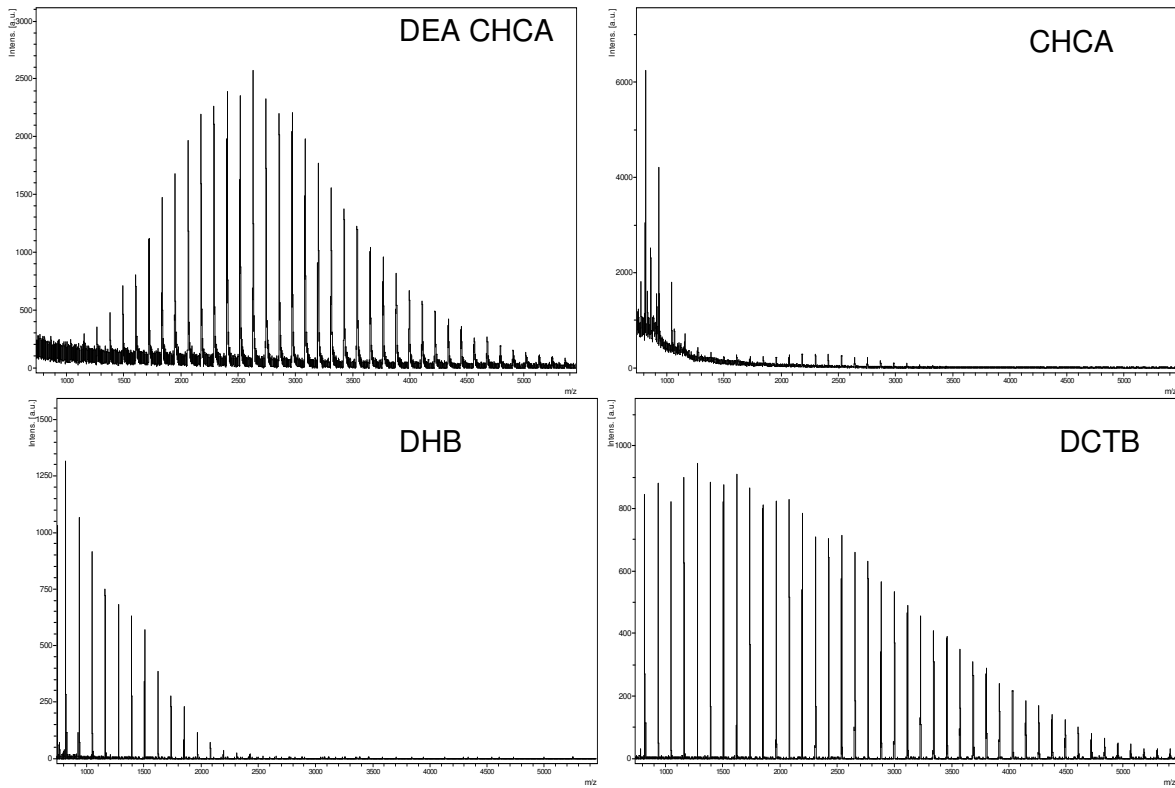
Polyme 4



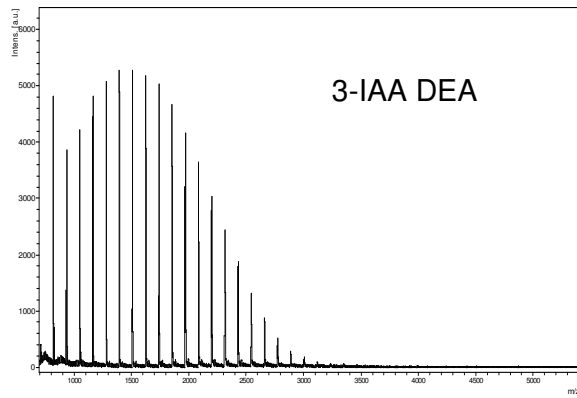
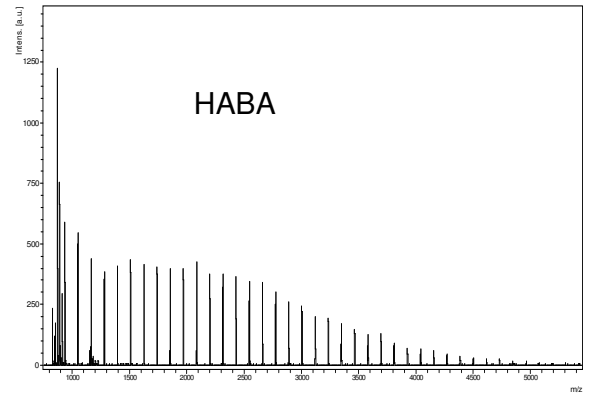
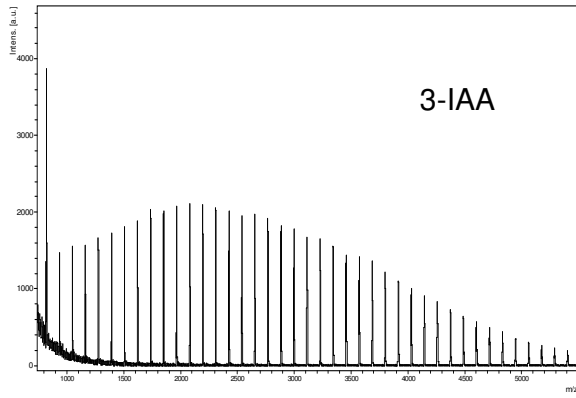
Polymer 4



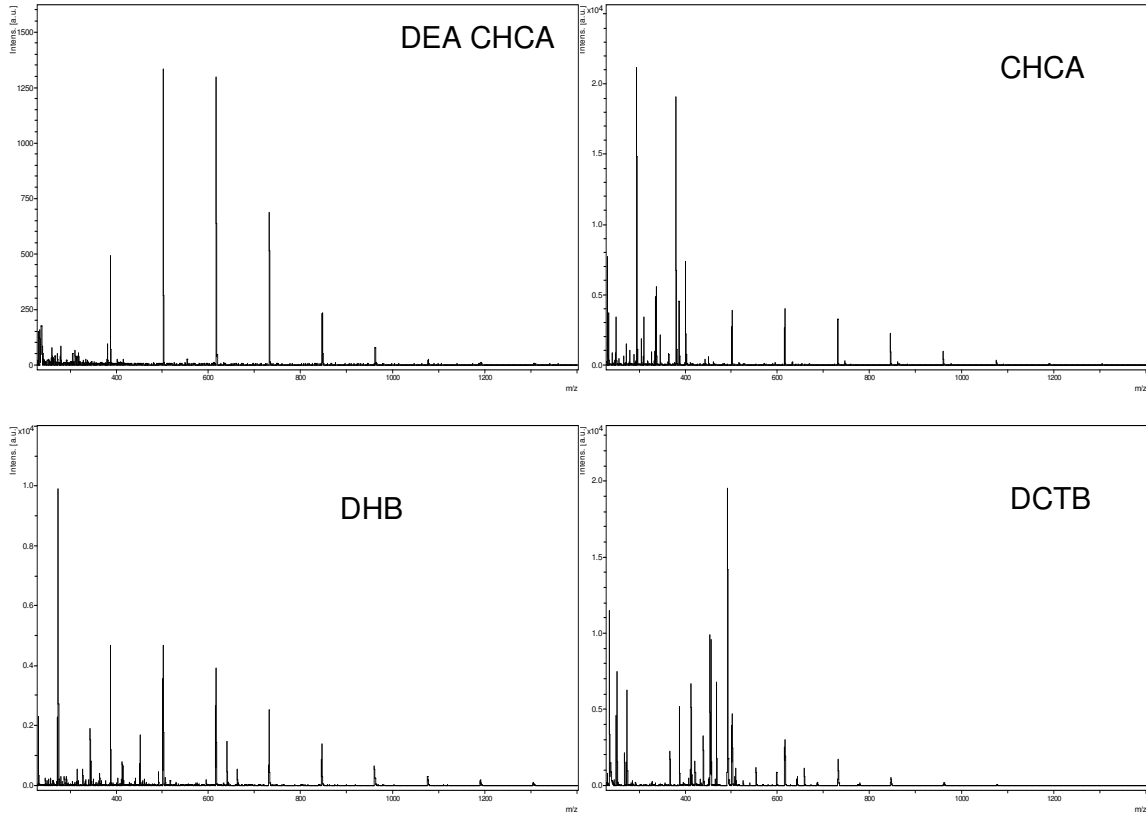
Polymer 5



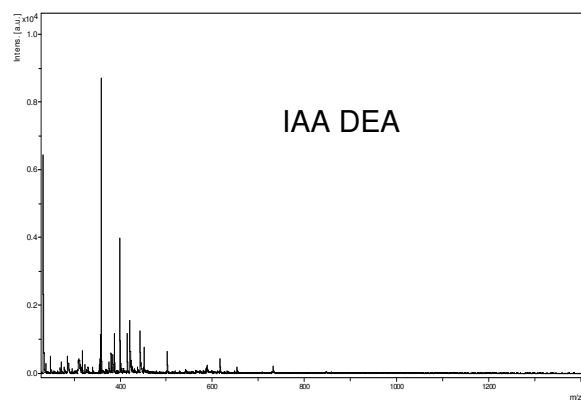
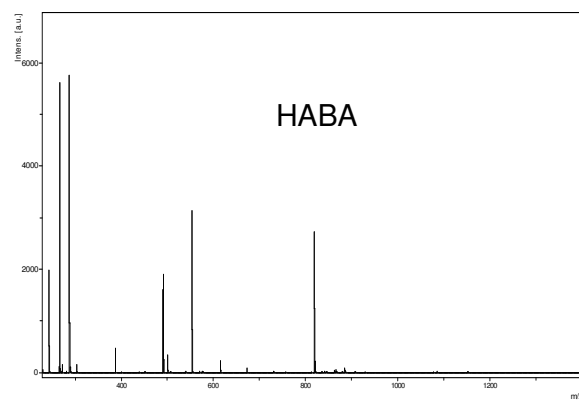
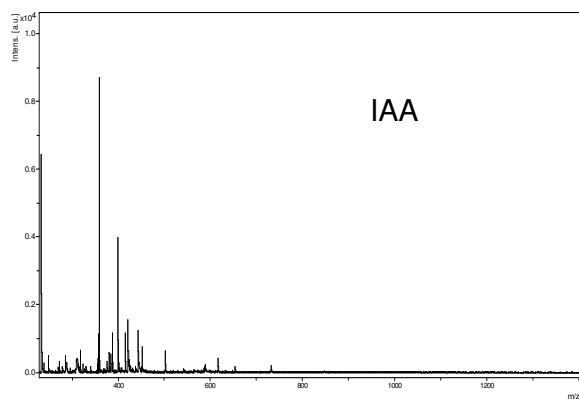
Polymer 5



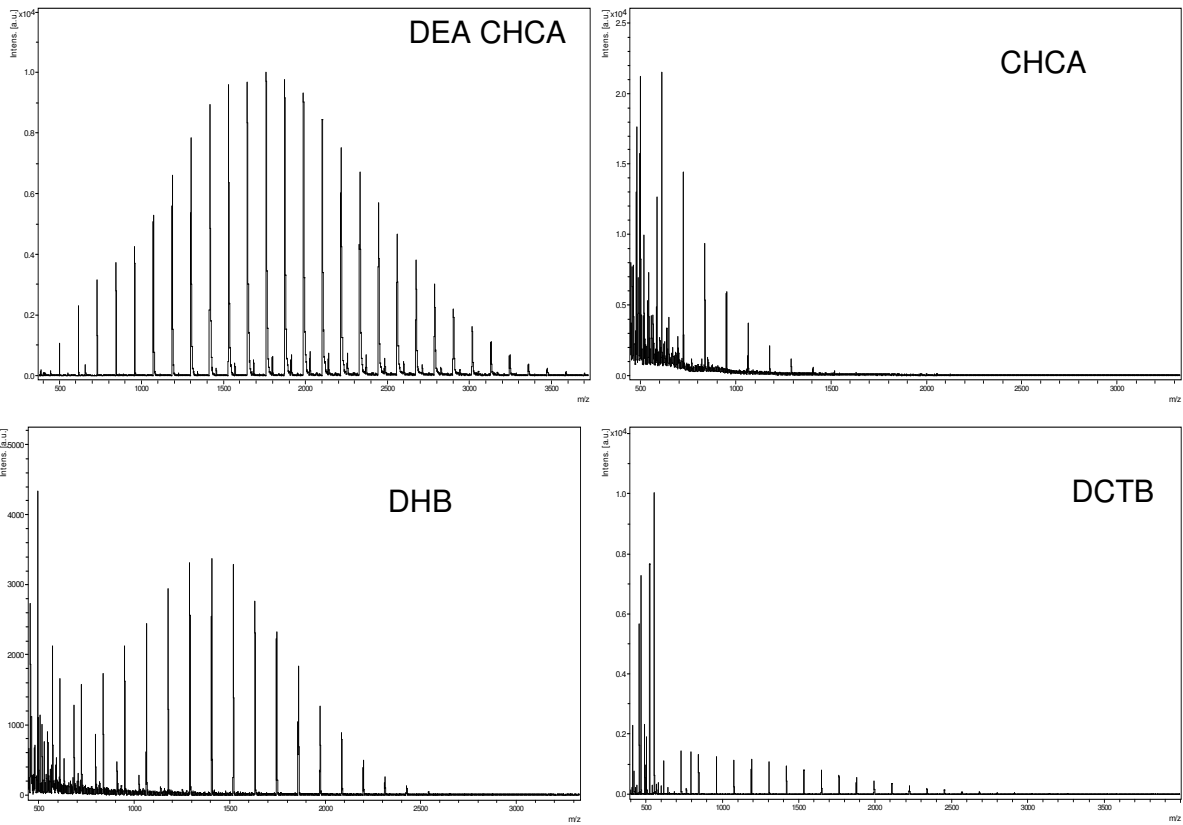
Polymer 6



## Polymer 6

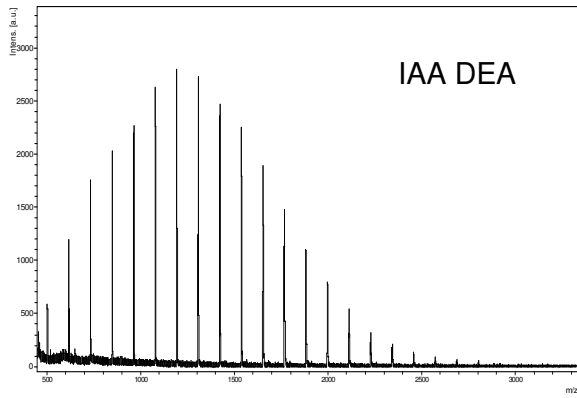
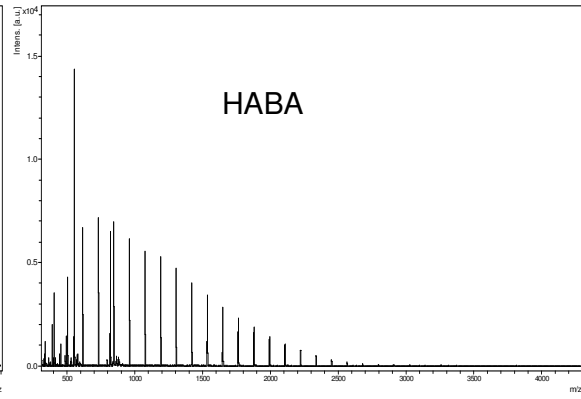
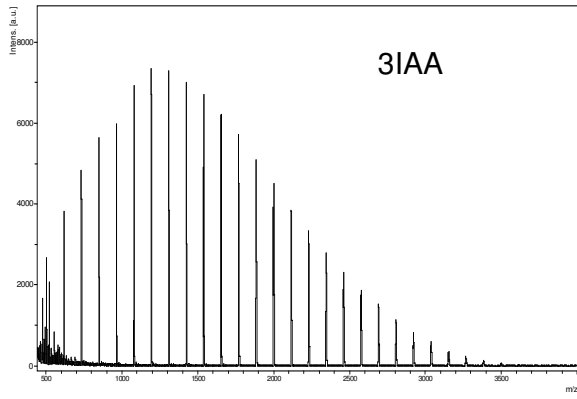


## Polymer 7

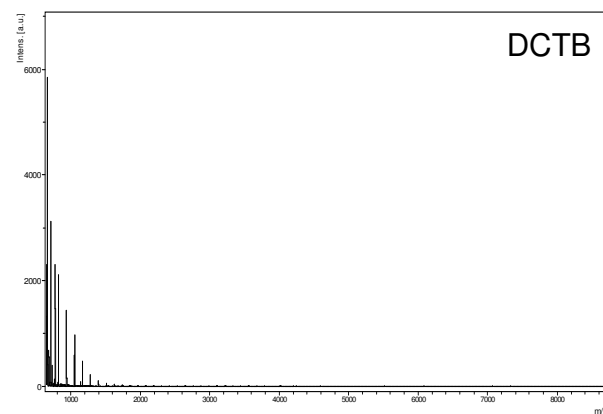
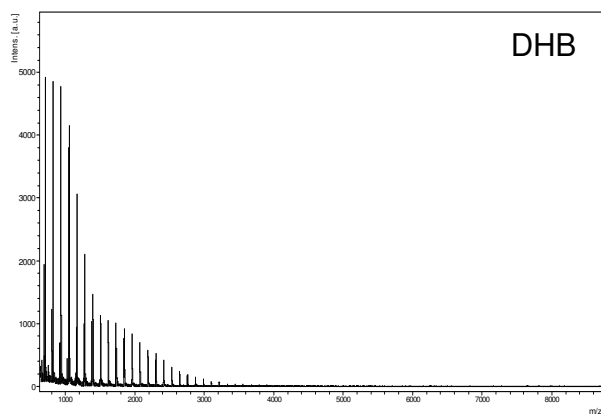
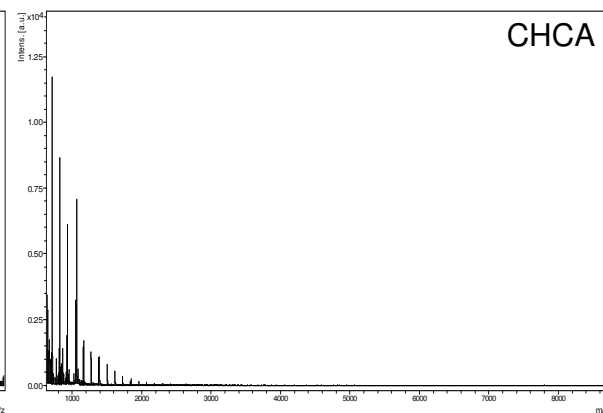
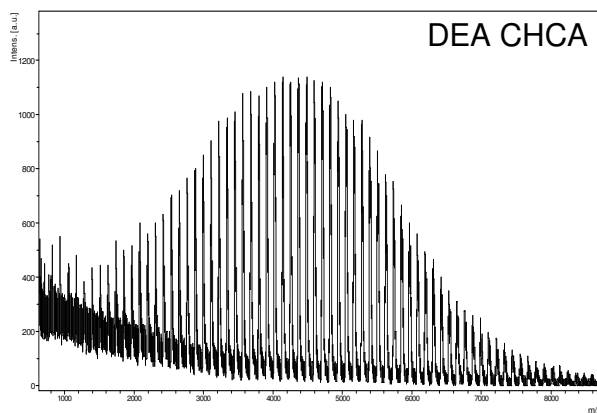




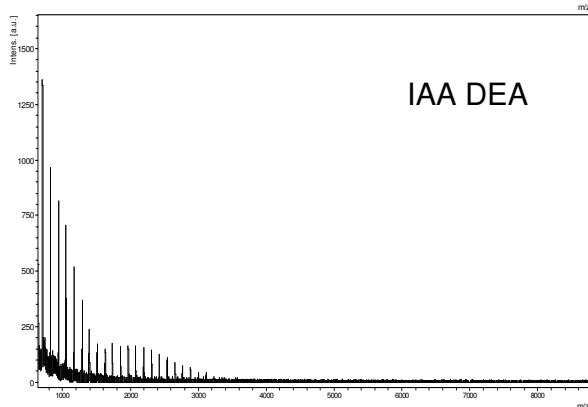
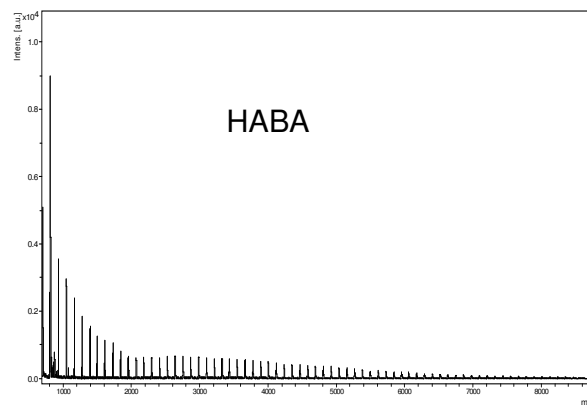
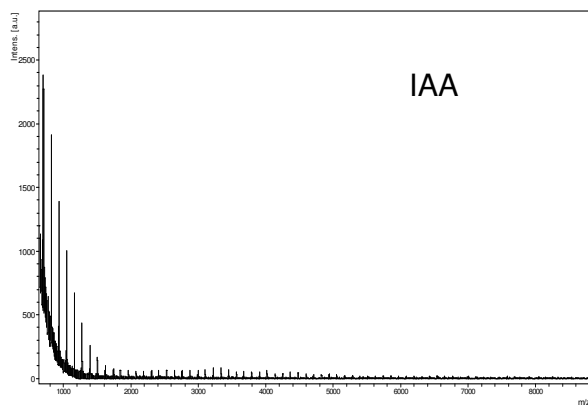
Polymer 7



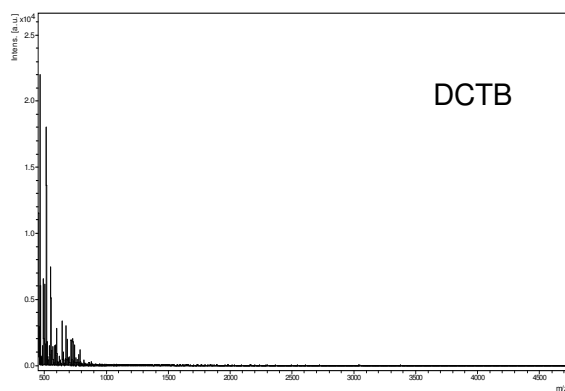
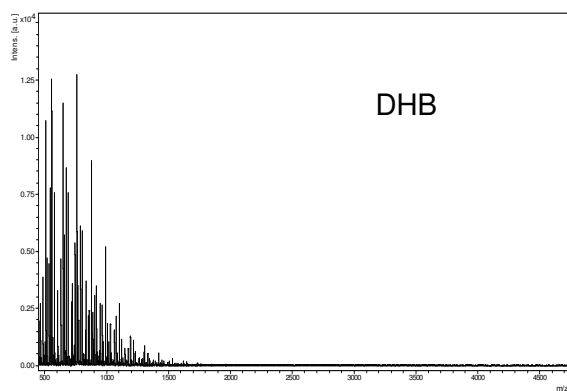
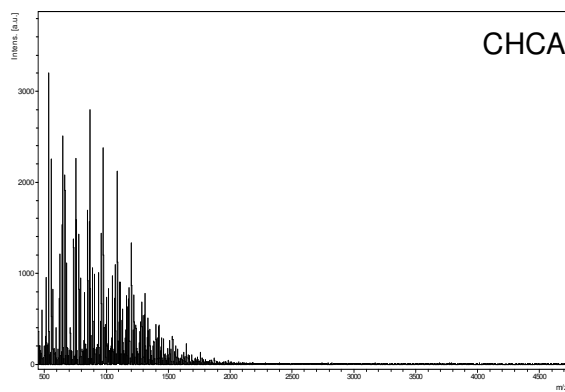
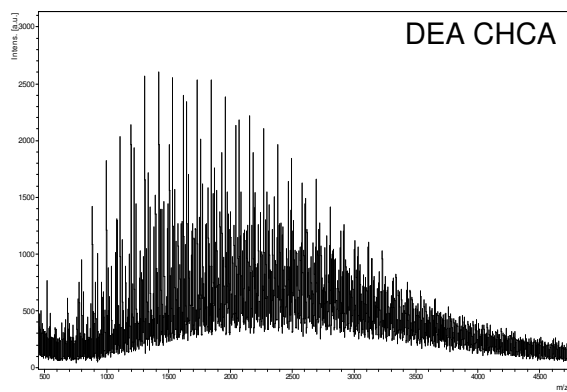
## Polymer 8



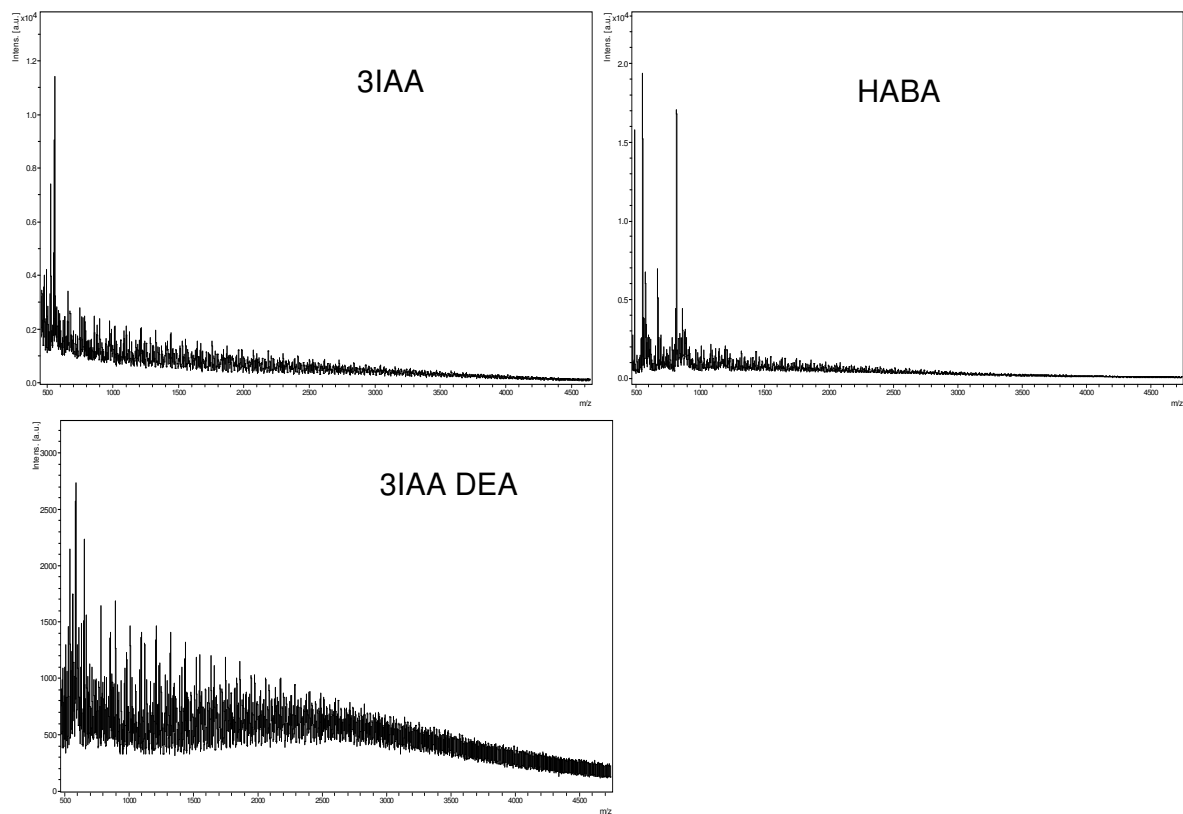
## Polymer 8



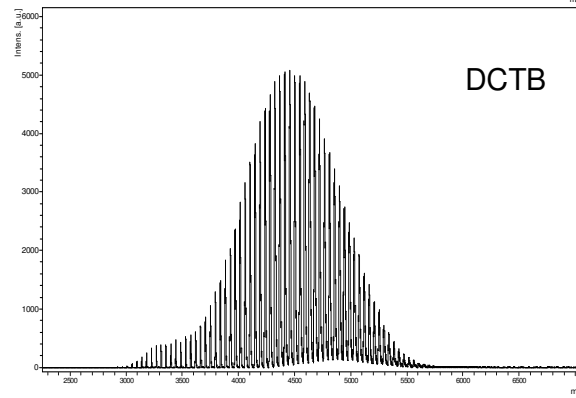
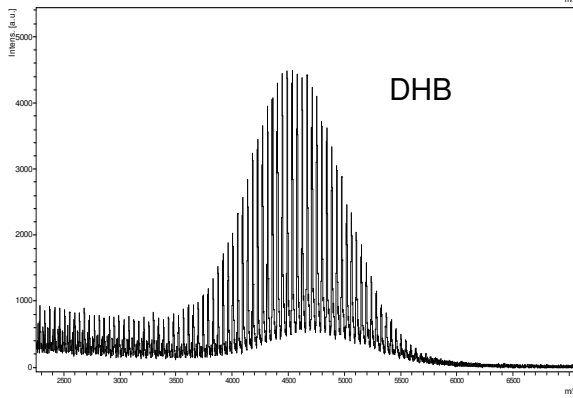
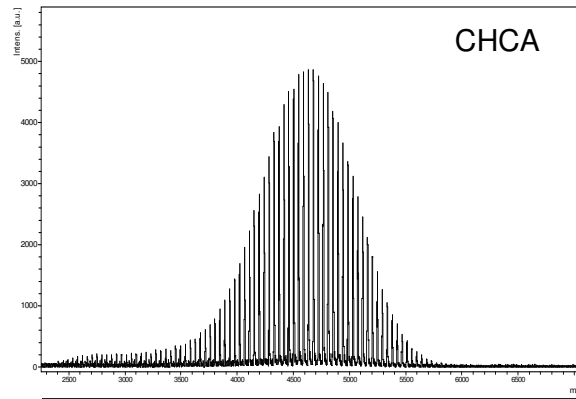
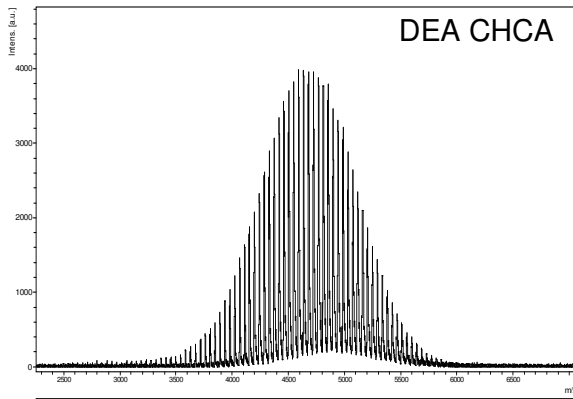
## Polymer 9



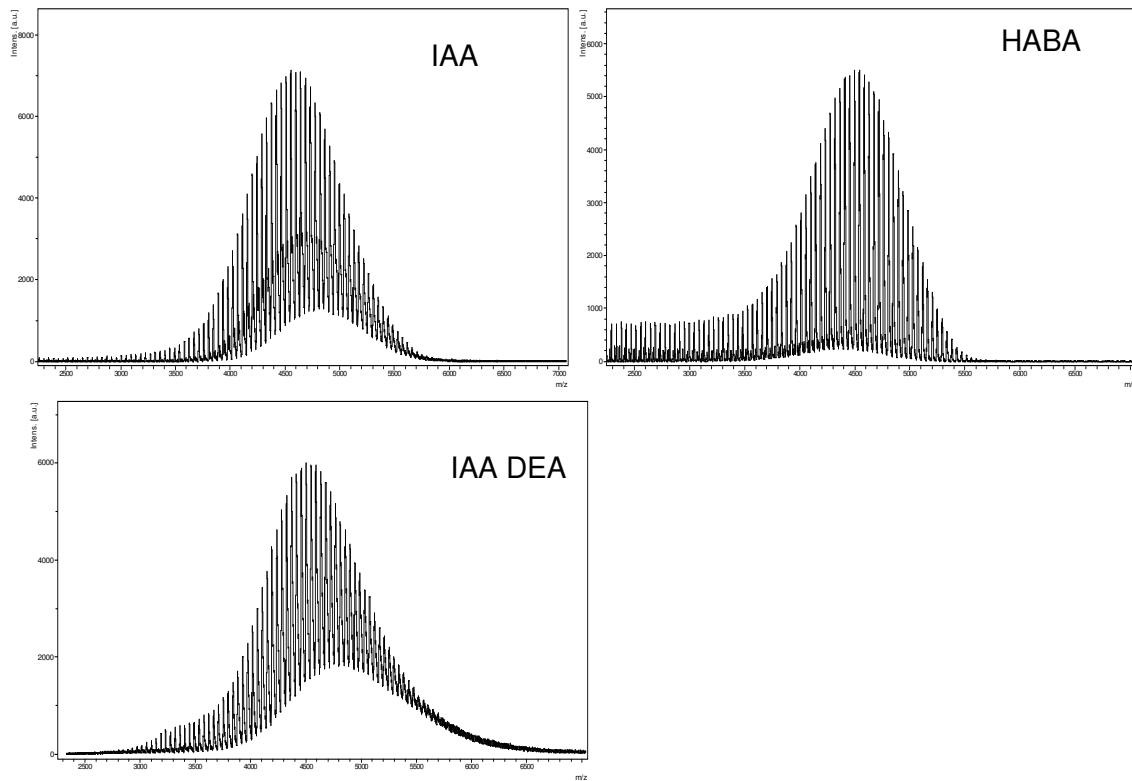
## Polymer 9



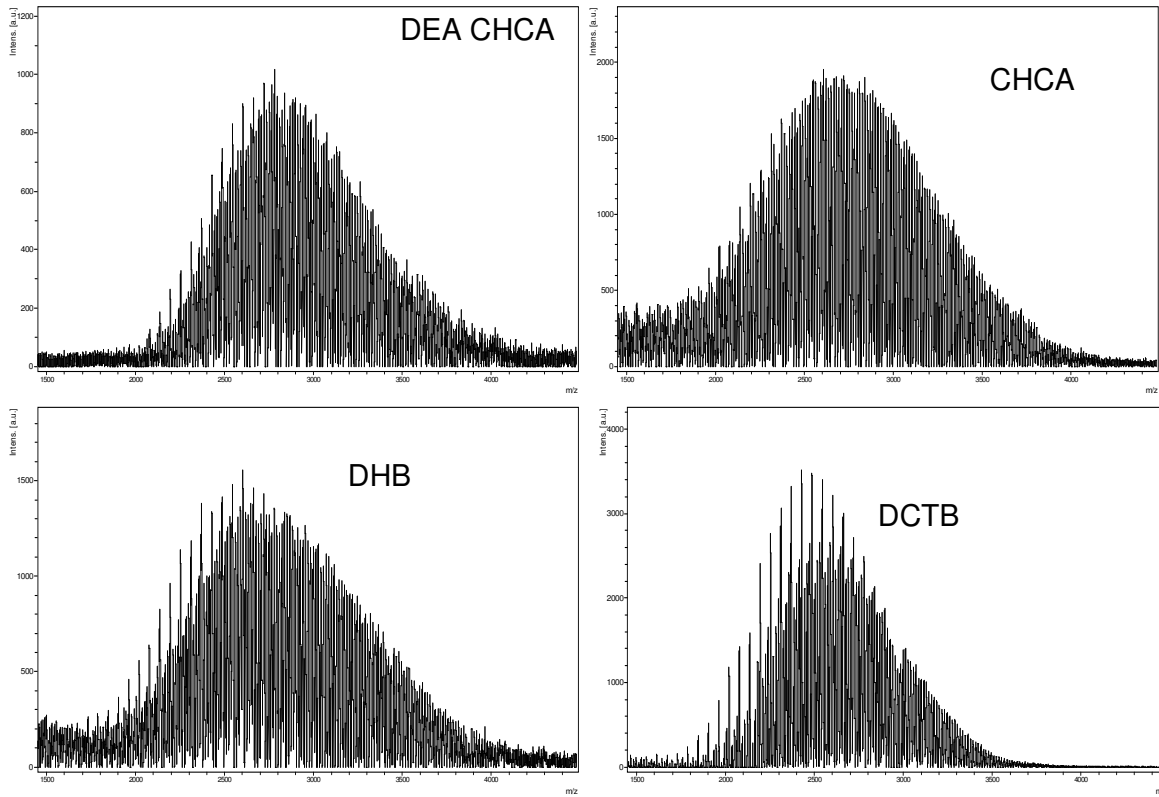
## Polymer 10



## Polymer 10

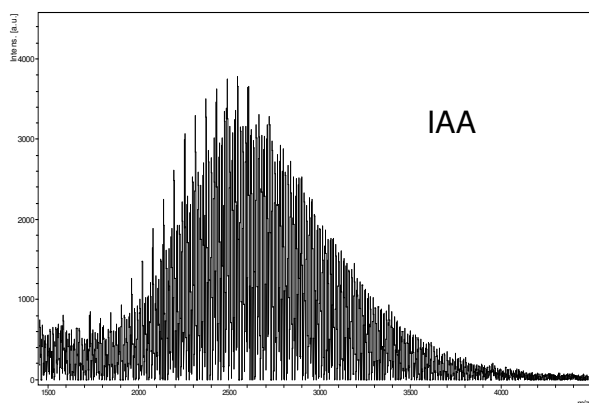


## Polymer 11

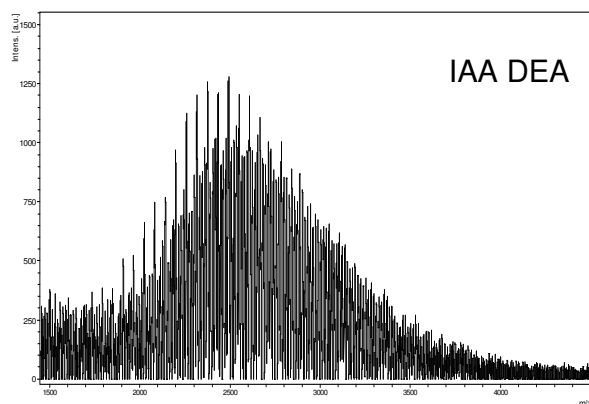




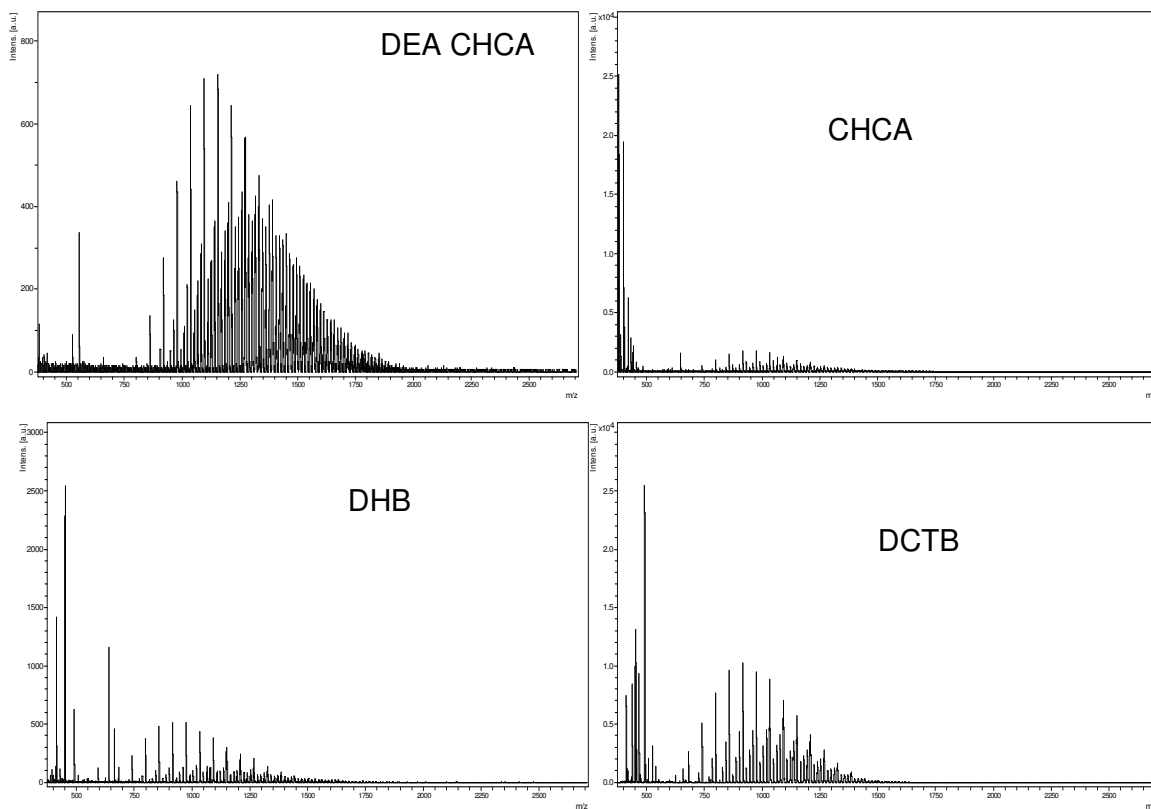
Polymer 11



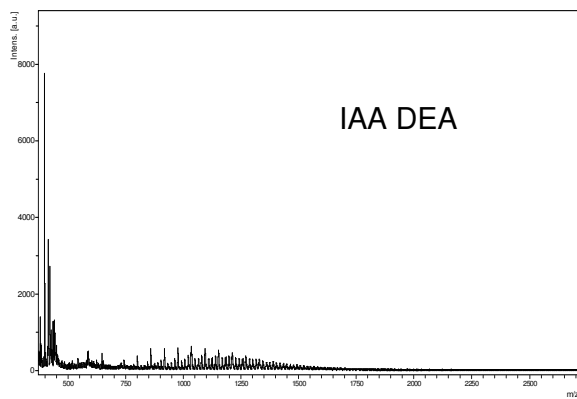
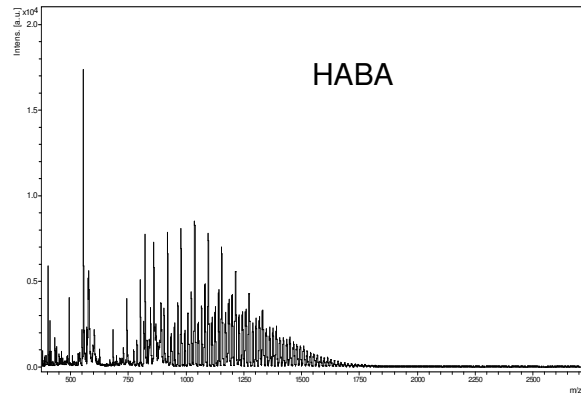
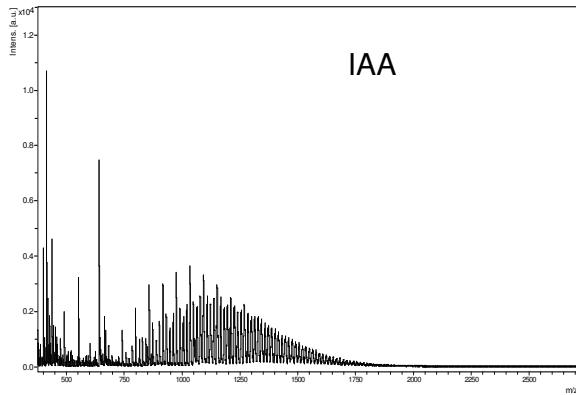
No signal for HABA



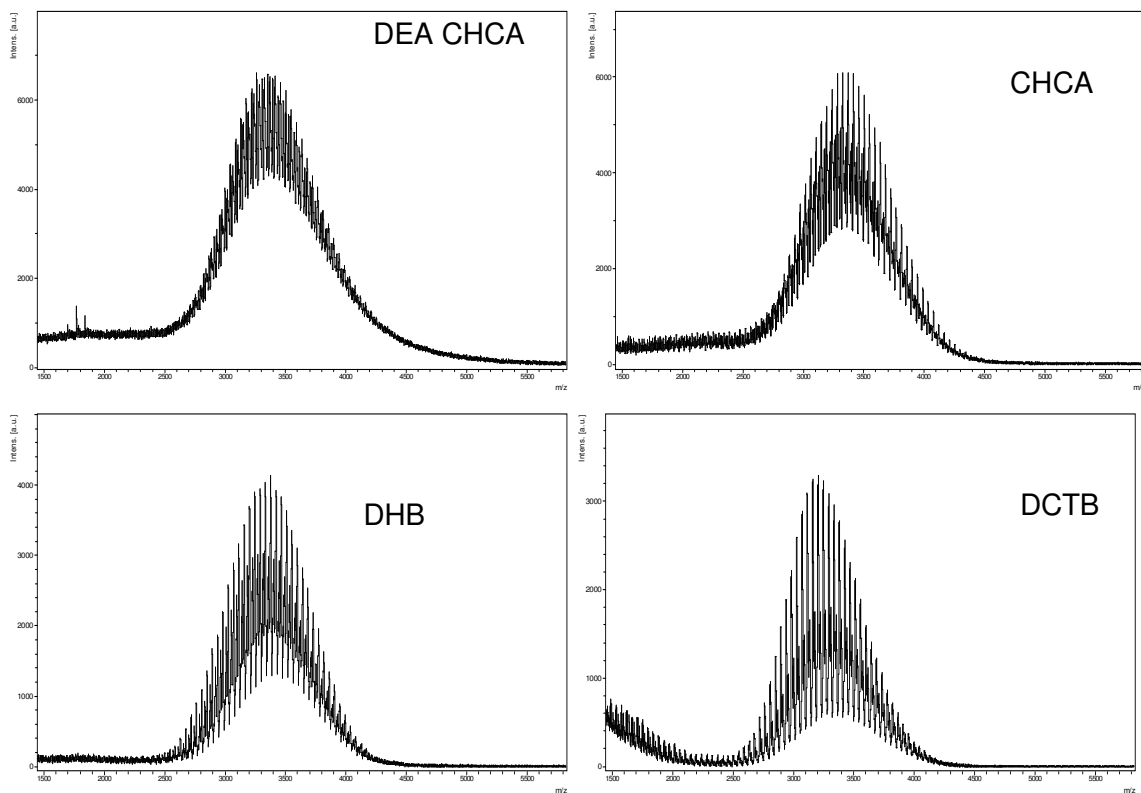
## Polymer 12



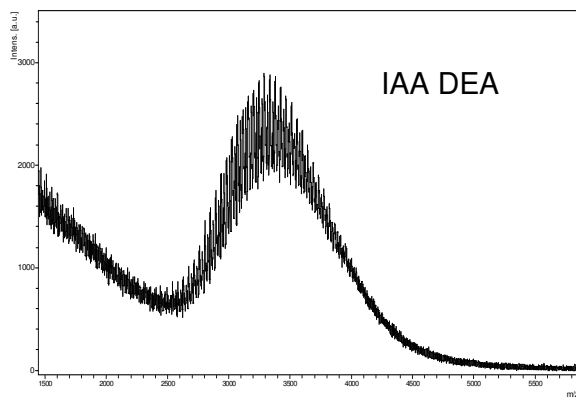
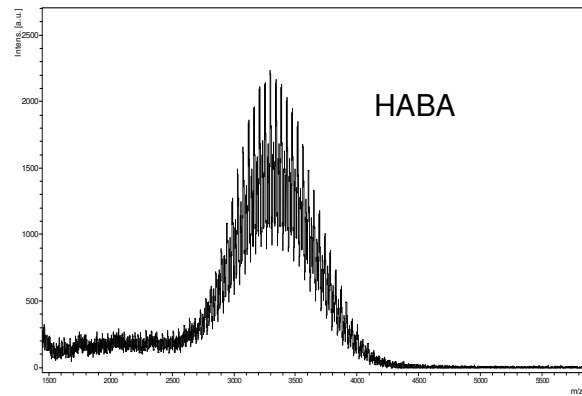
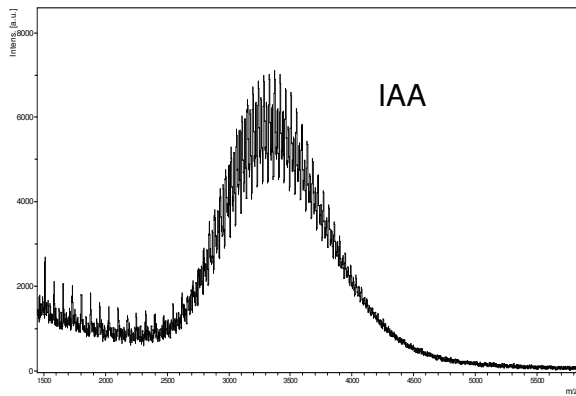
## Polymer 12



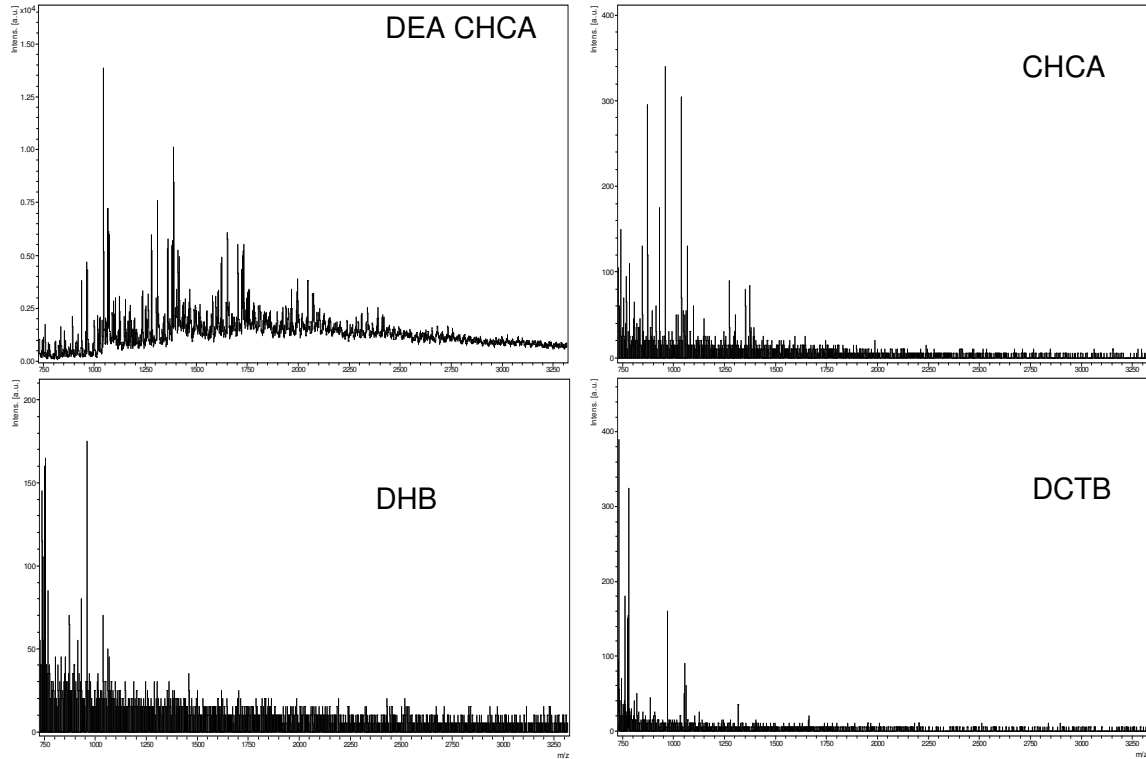
## Polymer 13



## Polymer 13

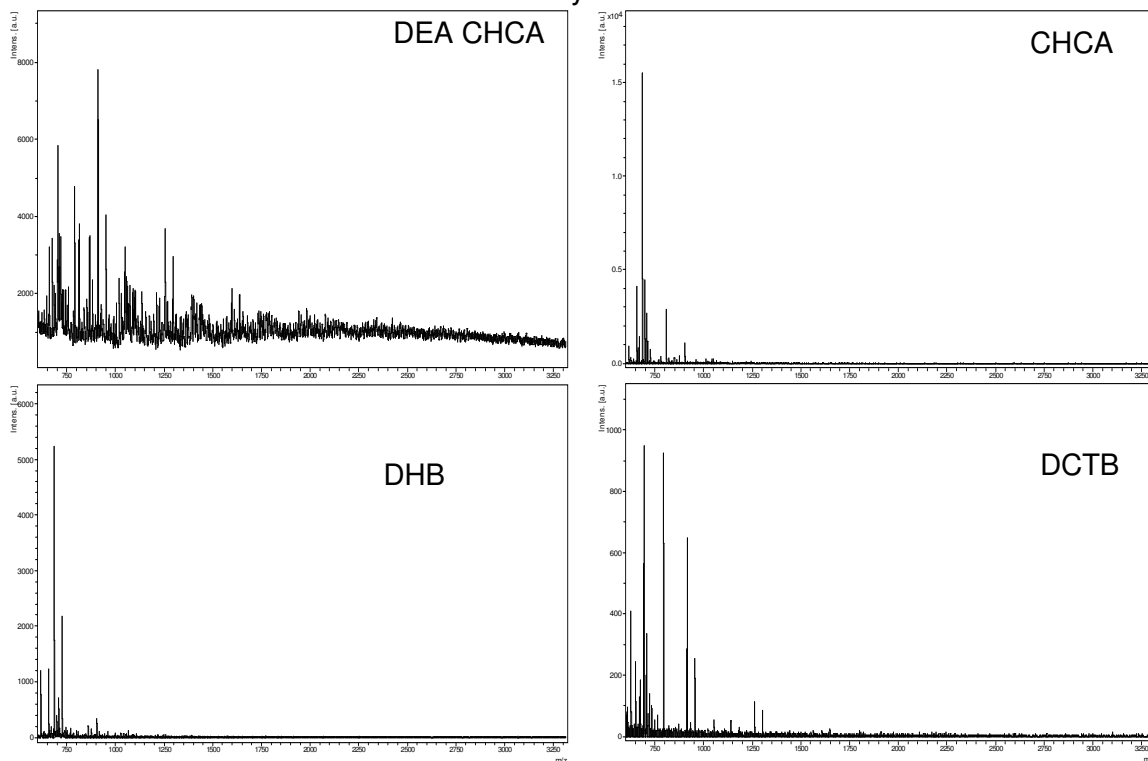


## Polymer 14



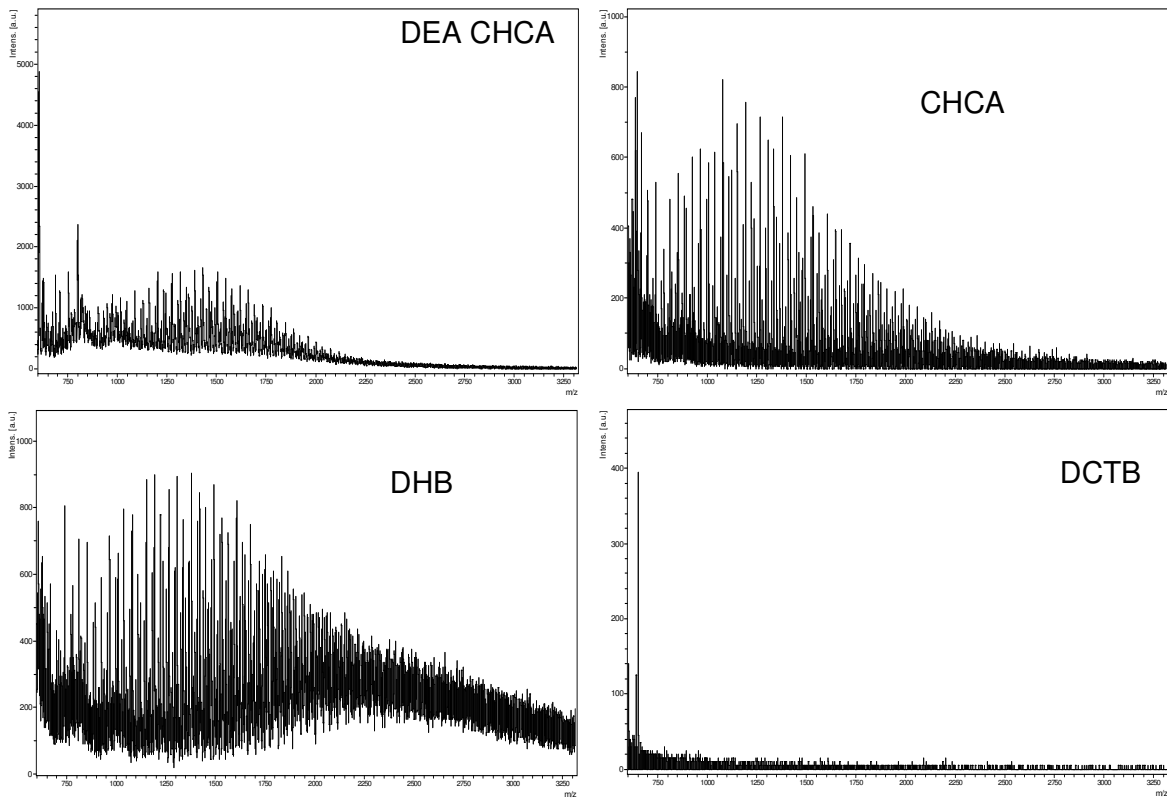
No analyte signal seen for IAA, HABA, and DEA IAA

## Polymer 15



No analyte signal seen for IAA, HABA, and DEA IAA

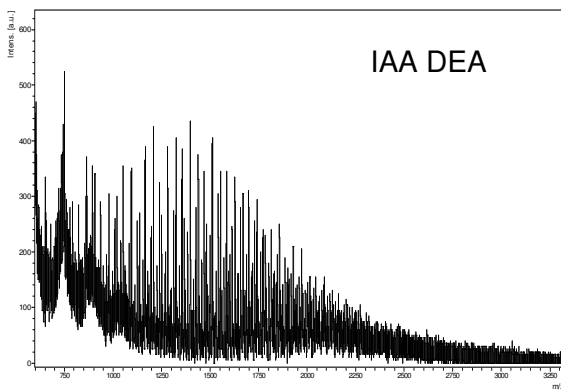
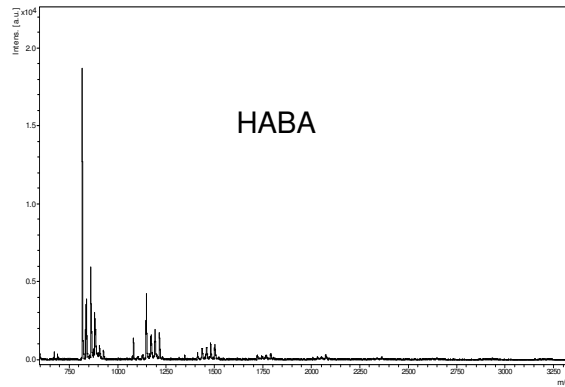
## Polymer 16





## Polymer 16

IAA no signal



**CHAPTER 4****RAPID DETERMINATION OF COMPLEX MIXTURES BY DUAL-COLUMN GAS CHROMATOGRAPHY WITH A NOVEL STATIONARY PHASE COMBINATION AND SPECTROMETRIC DETECTION**

Gordon R. Lambertus<sup>a</sup>, Jeffrey A. Crank<sup>b</sup>, Megan E. McGuigan<sup>c</sup>, Shai Kendler<sup>a,d</sup>, Daniel W. Armstrong<sup>b</sup>, Richard D. Sacks<sup>a</sup>

a Department of Chemistry, University of Michigan, Ann Arbor, MI 48109, USA

b Department of Chemistry, University of Texas at Arlington, Arlington, TX 76019, USA

c Department of Atmospheric, Oceanic, and Space Science, University of Michigan, Ann Arbor, MI 48109, USA

d Israel Institute of Biological Research, Department of Physical Chemistry, Ness-Ziona 74100, Israel

**Abstract**

Fast GC separations of a broad range of analytes are demonstrated using a capillary column coated with a novel immobilized ionic liquid (IIL) stationary phase. Both completely cross-linked and partially cross-linked columns were evaluated, yielding ~1600 and ~2000 theoretical plates per meter, respectively. Enhanced separation is demonstrated using a dual-column ensemble comprised of an IIL column, a commercially coated Rtx-1 column, and a pneumatic valve connecting the inlet to the junction point between the two columns. Enhanced separation of 20 components, with two sets of co-eluting peaks is shown in ~150 s, while sacrificing only a length of time equivalent to the sum of the stop flow pulses, or about 15.5 s. A novel application of a band trajectory model that shows band position as a function of analysis time as analytes move through the column ensemble is employed to determine pulse application times. The model predicts component retention times within a few seconds. Another method of selectivity enhancement of the IIL stationary phase-coated columns is

demonstrated using a differential mobility spectrometer (DMS) that provides a second dimension separation based on ion mobility in a high-frequency electrical field. The DMS is able to separate all but one set of co-eluting components from the IIL column. The separation of 13 components found in the headspace above U.S. currency is demonstrated using the IIL column in a dual-column ensemble as well as with the DMS.

### **Introduction**

Gas chromatography (GC) is the most widely used method for the analysis of mixtures of volatile and semi-volatile organic compounds. Positive attributes of GC include high selectivity, low detection limits with low cost ionization detectors, and high accuracy and precision. In recent years, decreasing analysis time has become a primary focus in GC research [1-3]. Decreasing column length is a straightforward method for increasing analysis speed. However, this results in a decrease in column resolving power, and consequently an increase in the probability of having co-eluting components [4,5].

In order to resolve chromatographic co-elutions from relatively short columns of modest resolving power, increased column or detector selectivity is required [6-10]. New stationary phases with enhanced selectivity for specified mixtures are useful but limited in application [11-17]. If the target mixture varies, the new stationary phases may no longer be useful. Column ensembles with tunable pressure selectivity have been described which can have increased application [18-23].

Ionic liquids (IL) are non-molecular ionic solvents with low melting points. Most consisting of asymmetrically substituted nitrogen containing cations (e.g., imidazolium, pyrrolidinium,

and pyridinium) with inorganic ions (e.g.,  $\text{Cl}^-$ ,  $\text{PF}_6^-$ , and  $\text{BF}_4^-$ ) [24-26]. Their wetting ability and high viscosity allow for deposition on fused silica capillary columns, and thus can be used as stationary phases for gas chromatography [24-27]. The cation/anion combination can easily be tuned prior to coating a column to provide the desired stationary phase properties [24]. Ionic liquids exhibit dual nature retention in that they are able to separate non-polar molecules similarly to a non-polar stationary phase and polar molecules similarly to a polar stationary phase [27]. This is possible because ionic liquids are capable of all types of intermolecular interactions, including dipolar, hydrogen bonding,  $n-\pi/\pi-\pi$  and charge interactions [28]. These stationary phases have been shown to provide high-efficiency separations of isomeric sulfoxides and PAHs [26] as well as fatty acid methyl esters and chlorinated pesticides [24]. The columns have been shown to be thermally stable to 350 °C [26]. Retention factors for a wide range of components on IIL columns have been compared to several conventional stationary phases [27]. Cross-linked versions of geminal dicationic ionic liquids are particularly stable and apropos as GC stationary phases [24,29].

A useful column configuration is the series combination of two columns having different stationary phases and a low-dead-volume valve connecting the column junction point to an auxiliary source of carrier gas maintained at the head pressure of the first column [19-21,30]. When the valve is closed, the ensemble can be viewed as a single column with selectivity determined by the selectivities of the individual columns in the ensemble. When the valve is opened, flow stops in the first column and increases in the second column. To simplify the instrumentation, a bypass connecting the inlet of the first column to the junction point between the two columns through a pneumatic valve can be used [31].

When a multi-functional vapor mixture is separated by a series-coupled ensemble of two columns with different selectivities, some compounds are separated by the first column and remain separated after eluting from the second column. Other compounds that are not separated by the first column are separated by the second column. Finally, some component pairs are separated by the first column but co-elute from the ensemble due to the different selectivities of the two columns. For these component pairs, the valve (stop-flow valve, SFV) can be opened for a few seconds after the first of each component pair elutes from the first column and enters the second column. This inserts a time window between each component pair in the ensemble chromatogram, thus decreasing the number of co-elutions. A limitation of this method is the availability of columns with large differences in selectivity.

Selective detectors such as an electron capture detector, which is selective toward electronegative heteroatoms, and the flame photometric detector, which is selective toward phosphorus- and sulfur-containing compounds, are limited in application to compounds containing these elements. Thermal conductivity detectors (TCD) scale well, and due to their simplicity and ease of fabrication, microfabricated TCDs have been developed. Temperature constraints and poor minimum detectable limits have proven to be problematic for some applications [32-34]. Detection that can provide complementary chemical information about a sample, and in some cases, provide for deconvolution of overlapping peaks in targeted analysis applications has received considerable attention. Notably, microfabricated arrays of polymer-coated surface acoustic wave (SAW) devices [30,35-37] and chemiresistor devices [8,38,39] have been used as detectors for GC with microfabricated columns. Analyte

characterization is based on the relative sensitivities of each sensor in the array to each component and chromatographic retention times [30].

Conventional ion mobility spectrometers (IMS) have been used for selective detection of volatile organic compounds [40-42]. Typically, these devices are operated in the time-of-flight (TOF) mode. Atmospheric-pressure chemical ionization (APCI) produces packets of ions, usually by means of  $\beta$  radiation from  $^{63}\text{Ni}$  [40,43]. These ion packets are electronically gated into a region containing a linear electric field and their TOF to an ion collector is measured. Ions are identified according to their specific mobility ( $K_0 - \text{cm}^2 \text{V}^{-1} \text{s}^{-1}$ ) which is calculated from the TOF in the following way [40]:

$$K_0 = \left( \frac{L}{(TOF \times E)} \right) \left( \frac{P}{760} \right) \left( \frac{273.16}{T} \right) \quad (1)$$

where  $L$  is the drift tube length (cm),  $E$  is the electric field ( $\text{V cm}^{-1}$ ),  $P$  is the pressure (Torr) and  $T$  is the temperature (K) in the drift tube. It has been previously reported that APCI may be accompanied by several processes such as ion-molecule clustering and ion dissociation [44]. Eiceman et al. studied butyl acetate isomer fragmentation upon APCI in low humidity [45]. Lawrence and Neudorfl showed that dichloromethane readily gives chloride ions upon APCI. The obtained chloride ions were later used for the detection of ethylene glycol dinitrate via ion-molecule clustering [46].

Recently, a novel microfabricated mobility-based detector, a differential mobility spectrometer (DMS) with high selectivity and excellent detection limits for many volatile organic compounds has been described [47-51]. With DMS, an asymmetric radio-frequency

(RF) electric field is applied between a pair of metallic electrodes. At low electric field strength, ion mobility is relatively field-independent. For high field strength (greater than about  $10 \text{ kV cm}^{-1}$ ) ion mobility may show a strong field dependence. For DMS, the field oscillates between a high and a low field value, and the difference in mobility determines the ion trajectory through the detector cell. Ions with an appropriate differential mobility pass through the cell, and a pair of biased collector electrodes collect both positive and negative ions from the same experiment. A DC compensation voltage applied to one of the RF plates is scanned to allow ions with a variety of differential mobilities to pass through the cell without being neutralized at the plates. Data are displayed as ion current versus compensation voltage and analysis time. Separate readout channels are provided for positive and negative ions.

Recent work has shown the separation of 45 compounds within 400 s using a single 3-m long dimethyl polysiloxane stationary phase-coated microfabricated column coupled to the microfabricated DMS [10]. In this article, demonstration of fast GC separations of a test group of 20 components with differing functionalities and polarities, and of 13 markers found in the headspace of U.S. currency are presented. A dual-column ensemble comprised of a novel IIL stationary phase-coated column and a commercially-coated Rtx-1 column is utilized. A band trajectory model is used to predict appropriate pulse application times to enhance the separation of co-eluting peaks. The integration of a novel IIL stationary phase-coated column with a microfabricated DMS that resolves co-eluting components along a second-dimension separation is also presented.

## Experimental

### *Apparatus*

Fig. 1 shows the experimental system used for implementing stop-flow programmable selectivity with conventional fused silica capillary columns. The two columns used in the ensemble are a 2.8-m long Rtx-1 column, 250  $\mu\text{m}$  i.d. with a film thickness of 0.25  $\mu\text{m}$  (Restek Corp, Bellefonte, PA) and a 2.8-m long, 250  $\mu\text{m}$  i.d. immobilized ionic liquid (IIL) stationary phase column, coated in-house at the University of Texas, Arlington [24] with a 250  $\mu\text{m}$  i.d. and a 0.15  $\mu\text{m}$  film thickness. The flame ionization detector (FID) from a Varian 3500 GC (Varian, Walnut Creek, CA) was used with a high-speed electrometer, built in-house [52].

A commercial split/splitless inlet for an HP 6890 GC (Agilent Technologies, Palo Alto, CA) was used for all experiments. The two columns,  $C_1$  and  $C_2$ , were mounted on a platform inside the Varian GC. A low-dead-volume pneumatically-actuated valve,  $V_1$  (stop-flow valve) (P/N 1236091, SGE International Pty. Ltd., Ringwood, Australia), was connected from the column junction point to the inlet of the first column. The valve is operated by a 50–55 psig compressed air source connected through an electronically-actuated solenoid valve (model 74313-0115, Schrader Bellows, Pittsburgh, PA). Connections were made by use of low-dead-volume Y connectors (MXT “Y” Connectors for 0.28-mm i.d. tubing, Restek Corp., Bellefonte, PA).

For comparison of the IIL stationary phase column, a system using a split/splitless injector and a DMS (Sionex Corporation, Bedford, MA) connected to the outlet of the separation column was used. For DMS detection, a 30-cm long, 0.1-mm i.d. segment of deactivated



fused silica tubing passed from the downstream end of the column through the GC wall and was plumbed into the high-velocity flow ( $300 \text{ mL min}^{-1}$ ) of dry nitrogen entering the ionization region of the DMS. The connection line was wrapped with heating wire and heated to  $150 \text{ }^\circ\text{C}$  in order to reduce band broadening contributions. The sample residence time in the microfabricated detector cell is about 1 ms, and the device appears to contribute no significant instrumental dead time to the system.

For DMS transport gas, house nitrogen was purified using hydrocarbon and moisture traps and passed through a coil of copper tubing immersed in a Dewar of liquid nitrogen. The nitrogen flow rate was set at  $300 \text{ cm}^3 \text{ min}^{-1}$  by means of a flow controller in the DMS unit.

### *Column Design*

The ionic liquid stationary phase was prepared as previously reported [24]. In short, 1,9-di(3-vinylimidazolium)nonane bromide was synthesized by reacting 2 M equivalents of 1-vinylimidazole (Aldrich, St. Louis, MO) and 1 M equivalent of 1,9-dibromononane (Aldrich, St. Louis, MO). The mixture was heated to  $45 \text{ }^\circ\text{C}$  and stirred for 4 h. The bromide salt was then dissolved in water. Eight extractions were performed with ethyl acetate to remove impurities. Anion exchange of 1,9-di(3-vinylimidazolium)nonane bromide to 1,9-di(3-vinylimidazolium)nonane bis[(trifluoromethyl)sulfonyl]imide ( $\text{NTf}_2$ ) was achieved by first dissolving the bromide salt in water. Next, an equimolar amount of lithium bis[(trifluoromethyl)sulfonyl]imide was dissolved in water and added to the bromide salt solution and stirred until the aqueous layer became clear. The  $\text{NTf}_2$  salt was then dissolved in methylene chloride and extracted with water eight times. A rotary evaporator was used to remove the excess methylene chloride. The  $\text{NTf}_2$  salt was then placed under vacuum

overnight to achieve complete dryness. The monomer, 1-vinyl-3-nonylimidazolium NTf<sub>2</sub>, for the partially cross-linked IIL was made in an analogous manner.

IIL columns were coated using the static method at 40 °C. The coating solution for the completely cross-linked IL stationary phase was comprised of 0.02 g dicationic ionic liquid, 0.0007 g of AIBN (2,2'-azobisisobutyronitrile), and 10 mL of methylene chloride. The partially cross-linked IL stationary phase coating solution was made in an analogous manner with 0.01 g of dicationic ionic liquid and 0.01 g of monocationic ionic liquid to control the amount of cross-linking. After successful coating, the capillary ends were flame sealed and the ionic liquid was polymerized at 80 °C for 5 h in a GC oven. The ends of the capillary were then opened and the column was conditioned to 250 °C and 350 °C for the partially cross-linked and completely cross-linked columns, respectively.

### *DSMS Design*

The differential mobility spectrometer is composed of an ionization region, which houses a 5 mCi <sup>63</sup>Ni ionization source, a tunable ion filter region, and two collector electrodes [6]. Ions formed in the ionization region due to APCI are passed by a transport gas through the ion filter region composed of two planar electrodes separated by an analytical gap. The electrode dimensions are 15 mm × 1.5 mm and the gap is 0.5 mm. Filtered ions are detected downstream from the filter by two electrodes connected to detection circuits that measure the induced ion current. As ions move with the transport gas flow, both positive and negative ions can be filtered simultaneously and detected by corresponding detector electrodes. Ion filtering is produced by the superposition of two electric fields, a high frequency ~1.2 MHz RF field with an associated voltage variable from 800 to 1500 V, and a compensation

voltage. The compensation voltage can be ramped from approximately  $-43$  to  $+15$  V and is synchronized with the data collection system to generate a plot of ion current intensity versus compensation voltage [49]. Depending on the analytes of interest, the scan range and the voltage step size can be tailored to allow for faster scan rates or to provide longer collection times during each step of a scan.

### *Materials*

Compounds used in test mixtures were all reagent grade or better (Aldrich, Milwaukee, WI). Injection size was typically  $0.2 \mu\text{L}$  with a split ratio of about 50:1. Pre-purified hydrogen was used as carrier gas. Gases were purified with filters for water vapor and hydrocarbons. Isothermal studies at  $50 \text{ }^\circ\text{C}$  were performed in the oven of a Varian 3500 GC. The Varian FID was interfaced to a PC by means of a 16-bit A/D board (CIODAS 1602, Computer Boards, Inc., Marshfield, MA). The board was controlled by LabTech Notebook software (Laboratory Technologies Inc., Wilmington, VA). Chromatograms were processed by GRAMS/32 software (Galactic Industries, Salem, NH).

The DMS has an on-board heater, and the detector temperature was varied as needed. The RF voltage is user adjustable and programmable. The scanning range of the compensation voltage is programmable, and scanning parameters were adjusted as needed. Data from the DMS as ion current versus compensation voltage and analysis time are logged directly into Excel spreadsheets with independent data sets logged simultaneously from the positive and negative-ion channels.

## Results and discussion

### *Column Efficiency*

To evaluate column efficiency for the IIL stationary phase coated columns, plots of height equivalent to a theoretical plate ( $H$ ) versus average linear carrier gas velocity (Golay plots) were generated using hydrogen as the carrier gas. Headspace vapor containing  $n$ -decane was injected using an inlet split ratio of 50:1 and an FID detector. The temperature of the GC oven was set to 50 °C to obtain a retention factor of  $\sim 2$  for decane. Fig. 2 shows Golay plots for two IIL coated fused silica capillary columns with (a) partially cross-linked and (b) completely cross-linked stationary phases

The trend lines shown in Fig. 2 are regression fits to the Golay–Guiochon kinetic model for band dispersion in capillary columns given in Eq. (2),

$$H = \frac{B}{u} + Cu + Du^2 \quad (2)$$

where  $B$  is the coefficient of longitudinal diffusion,  $C$  is the sum of the terms associated with resistance to mass transport in the gas and stationary phases, and  $D$  accounts for extra-column sources of band broadening including the inlet, the connection lines, and electronic dead times. Note that the minimum plate height ( $H_{\min}$ ) value and the optimum carrier gas velocity ( $u_{\text{opt}}$ ) are  $\sim 22\%$  and  $25\%$  better for the partially cross-linked column, respectively. The values of  $H_{\min}$  and  $u_{\text{opt}}$  for the partially cross-linked columns were 0.050 cm and 24 cm s<sup>-1</sup>, while the values for the completely cross-linked column were 0.064 and 18 cm s<sup>-1</sup>, respectively. The number of theoretical plates generated by the partially cross-linked and

completely cross-linked columns after conditioning is about 2000 and 1600 plates per meter at 50 °C. The effect of conditioning temperature on efficiency of the IIL columns has been discussed previously [52].

The lower resolving power of the completely cross-linked column is indicative of a greater contribution to band dispersion from resistance to mass transport in the stationary phase. The completely polymerized stationary phase increases the average amount of time that a component molecule takes to diffuse through the stationary phase. This, in turn, allows for molecules remaining in the mobile phase to move further down the column before the retained molecules diffuse back into the carrier gas flow, broadening analyte bands relative to the partially cross-linked column. The benefit, however, of a completely cross-linked stationary phase is that the cross linking helps to immobilize the coating on the column wall. The more highly-networked stationary phase provides greater thermal stability and should help to prevent stationary phase bleed at elevated temperatures. Generally, the completely polymerized column (designed for high temperatures) is not used at low temperatures where the efficiencies are lower. The maximum operating temperature before column degradation of the partially cross-linked column is 250 °C, while the completely cross-linked stationary phase column can operate up to 350 °C using hydrogen as carrier gas [45].

#### *Isothermal separations*

The higher resolution, partially cross-linked IIL column will be discussed in the remainder of the article. Fig. 3 shows chromatograms for the separation of a 20-component test mixture achieved using: (a) the commercially-coated dimethyl polysiloxane capillary columns; (b) the IIL-coated column; and (c) the dual-column ensemble using hydrogen carrier gas at

50 °C. Table 1 lists the 20 components and their retention factors on each of the two columns. Chromatograms (a) and (b) in Fig. 3 were collected at linear carrier gas velocities of 54 and 53 cm s<sup>-1</sup>, respectively, while the ensemble chromatogram had a linear velocity of ~53 cm s<sup>-1</sup>. Operating velocities were chosen in an effort to help minimize analysis time without sacrificing column resolution. At 53 cm s<sup>-1</sup> the IIL stationary phase-coated column has ~3500 theoretical plates. The peak shapes for the IIL column are relatively symmetric with minimal artifacts. The analyses were complete in less than 120 s for the individual columns and in ~150 s for the column ensemble. It is important to point out that in no case was a complete separation of all 20 components obtained. For the commercially-coated Rtx-1 column, component pair 15/16 co-elutes from the column. For the IIL stationary phase-coated column, there are several sets of co-eluting peaks (1/2, 3/7, 5/6, 9/10/11, 14/15, 16/17, 12/18). Note that peaks 15/16 that co-elute from the non-polar column are separated by the immobilized ionic liquid stationary phase column. The two sets of co-eluting peaks in the ensemble chromatogram (c), peaks 11/12 and 19/20 are separated by both of the individual columns, but as a result of the differing selectivities of the two columns, co-elute from the column ensemble.

### *Stop-flow Operation*

Because component pairs 11/12 and 19/20, which co-elute in the ensemble chromatogram, are completely separated by both the Rtx-1 column and the IIL column, enhanced separation of these components in the ensemble chromatogram is possible using stop-flow tunable selectivity. The fact that both columns can separate the co-eluting components suggests that either column can be used as the first column of the ensemble. The broad, overlapping peaks

generated from the IIL column lend themselves to being split during application of a stop-flow pulse while a component is crossing the junction point. Therefore, the commercial column was used as the first column in the ensemble to reduce the probability of splitting peaks. The use of stop-flow tunable selectivity to more efficiently utilize the available peak capacity of a column ensemble is illustrated in Fig. 4 for the 20-component mixture with no stop-flow pulses (a) and with two separate stop-flow pulses (b) applied at 22 and 95 s for durations of 12 and 3.5 s, respectively. The separations were performed isothermally at 50 °C. This mixture contains a variety of volatile organic compounds with a variety of functional groups. The boiling point range of the mixture is 20 °C (acetaldehyde) to 183 °C (butyl benzene), shown in Table 1.

The plots accompanying the two chromatograms are band trajectory plots that show band position as a function of time as components move through the column ensemble. Injection occurs at the lower left corner of the plots at position 0, and elution occurs at position 560, indicating that the band has traveled through both 280-cm long columns. The horizontal line at position 280 is the junction point between the two columns. The model calculates carrier gas velocity and retention time at 1 cm intervals over the length of the ensemble. Carrier gas velocity is assumed to be constant over the length of each interval. Model inputs include column dimensions, system pressures, experimental temperatures, retention factors, and the temperature-dependent carrier gas viscosity. The slopes of the band trajectory plots at any point indicate a local band migration velocity. The sharp changes in band migration velocity observed at the junction point are the result of differences in retention factors on the two

columns and carrier gas velocity changes. The development of this band trajectory model has been described [53].

The band trajectory plots accurately predict the observed co-elutions, and the correlation between the predicted and experimentally observed retention times is very good. Using the model, it was determined that the mixture could be completely separated by adding two appropriately timed stop-flow pulses. The stop-flow pulses are indicated with vertical dashed lines in Fig. 4 (b). Pulses are timed such that the first component of the co-eluting pair has crossed the junction and the second component remains on the first column for the duration of the pulse. This provides a retention time shift of the two components relative to one another nearly equal to the length of the pulse. The increase in the slope of the band trajectory plots of components on the second column during a pulse indicates an increase in linear velocity generated from the higher pressure drop across the second column. The horizontal lines shown for components on the first column during a pulse indicate that these bands are frozen in position as a result of no pressure drop along the first column. The increased linear velocity of components in the second column, coupled with no flow on the first column, act to enhance the separation of the co-eluting pair on the column ensemble. This is demonstrated in Fig. 4 (b) where two stop-flow pulses are used to enhance the separation of the 20-component mixture. Stop-flow pulses are applied at 22 s for a duration of 12 s to enhance the separation of component pair 11/12 and at 95 s for a duration of 3.5 s to enhance the separation of component pair 19/20.

The change in elution order of component 12 with respect to components 9/10/11 is important. The elution order shift arises due to the length of the pulse applied at 22 s. If a



pulse duration less than 12 s was used, peak 12 would have been pushed into either peak 9 or 10 and the separation would remain incomplete. At the pulse application time (22 s), component 12 has crossed the junction point, while components 9, 10, 11 remain on the first column. The duration of the pulse not only enhances the separation of peak pair 11/12, but also pushes component 12 to an open part of the chromatogram (earlier elution time with respect to peaks 9/10/11). The separation enhancement gained comparing Fig. 4 (a) to (b) is remarkable considering that the only sacrifice is a loss in analysis time equal to the sum of the length of the stop-flow pulses. Enhancing this 20-component separation extends the analysis time by about 15.5 s.

#### *Application*

Table 2 lists 13 components found as markers in the headspace above U.S. currency [54] and lists their retention factors on each independent column. These compounds have been associated with U.S. currency, U.S. currency inks, and Canadian currency, and are attributed to the ink curing processes. Fig. 5 (a) and (b) show separations of the 13-component mixture using the IIL and Rtx-1 stationary phase-coated columns, respectively. The separations in Fig. 5 (a) and (b) were done isothermally at 50 °C using flow rates producing average linear carrier gas velocities of ~50 and 52 cm s<sup>-1</sup>, respectively. Notice that neither column is capable of separating all components in the mixture. There are three sets of co-elutions on the IIL stationary phase-coated column, peak pairs 2/4, 3/7, and 8/12, and three sets of co-eluting peaks on the Rtx-1 stationary phase-coated column, peak pairs 2/1, 6/8 and 9/11.

Fig. 5 (c) shows the ensemble chromatogram for the 13-component mixture. This separation was done isothermally at 50 °C, with a carrier gas flow of  $\sim 50 \text{ cm s}^{-1}$ , and was complete in just over 250 s. The ensemble chromatogram shows two sets of co-eluting peaks 1/2 and 6/7. Peaks 6 and 7 are separated by both of the individual columns in the ensemble, but as a result of the different stationary phase interactions, co-elute from the column ensemble. Peak pair 1/2, however, is separated by the IIL column, and not by the Rtx-1 column. In order for stop-flow tunable selectivity to work, the components that co-elute from the column ensemble have to be separated by the first column in the ensemble. The necessary separation for peaks 1 and 2 is provided by the IIL column, so it must be the first column in the ensemble. The targeted peaks lose their separation in the ensemble chromatogram due to additional band-broadening from the inclusion of the second column. For this set of studies the column order is reversed compared to the 20-component test mixture analysis, and the IIL column is first. Fig. 6 (a) shows the 13-component separation on the dual-column ensemble accompanied by the corresponding band trajectory plots showing co-elutions for peak pairs 1/2 and 6/7. The plots predict a narrow window of time where a stop-flow pulse can be applied to enhance the ensemble separation of components 1 and 2. The timing of this pulse is important so that the pulse is not applied as one of the components is crossing the junction point. An improperly timed stop-flow pulse, applied while a component is crossing the junction point, will result in deformation of the peak shape [31].

Fig. 6 (b) shows how two appropriately timed stop-flow pulses enhance the ensemble chromatogram. The pulse used to separate peaks 1 and 2 was applied at 7 s for a duration of 2 s, and the pulse used to separate peaks 6 and 7 was applied at 14.5 s for a duration of 3 s.

The sacrifice to achieve baseline separation of all 13 components is about 5 s in total analysis time.

### *Spectrometric detection*

An important advantage of differential mobility spectrometry devices is that they offer an adjustable second-dimension separation along a compensation voltage axis. The information content gained from the two-dimensional data relative to the one-dimensional FID data is remarkable. The second dimension compensation voltage axis increases the effective peak capacity of the overall system by resolving co-elutions from the separation column. For these studies, the IIL column was interfaced to the DMS by means of a heated connection line. The two-dimensional DMS contour plot of electrometer output for the positive-ion channel is shown in Fig. 7 (a) and a portion of the negative-ion channel (25 s) is shown in Fig. 7 (b) using only the IIL column and the same temperature and flow rates as Fig. 3 (b). Only components that co-eluted from the column were included in the mixture. The vertical axis is the time after sample injection, and the horizontal axis is the DMS compensation voltage. The display color indicates peak amplitude. The RF voltage for the DMS was 1500 V, and the detector temperature was 120 °C. The compensation voltage was scanned from +10 V to -35 V at 1 Hz. Note that there is a substantial portion of the compensation voltage scan for which both positive (right panel) and negative ions (left panel) are collected. The one-dimensional FID chromatogram is placed between the DMS signals to show the co-elutions. Under these operating conditions the DMS is able to resolve three sets of co-eluting pairs (1/2, 5/6, 12/20) and a three-component co-elution (9/10/11). Peaks 9/10 are separated on the compensation voltage axis of the positive channel, while peak 11 (iodopentane) appears on

the negative channel due to detection of the fragmented halide ion. The pentane solvent peak is labeled "A".

The DMS was also able to resolve a co-elution between peaks 14/15 and the peak labeled 21, which was not detected in previous studies using the FID. This contaminant originated from the acetaldehyde sample in the lab. Mass spectral analysis identified the contaminant peak as acetic acid. This was confirmed by spiking the mixture before subsequent analyses. In the case of acetic acid, the sensitivity and selectivity of the DMS allowed for the enhanced separation of a co-elution the FID was unable to detect.

It should be pointed out that the operating parameters utilized for the chromatographic column and the DMS did not resolve peak pairs 14/15 and 16/17. Fig. 7 (c) shows the separation of peak pair 16/17 along the compensation voltage axis of the positive channel at an RF voltage of 1200 V and a detector temperature of 60 °C. Components 14/15 were not separated under any conditions.

Fig. 8 shows spectra for three sets of co-elutions from the IIL column using the 13-component mixture that contains markers for the headspace above U.S. currency. The DMS was able to resolve all three sets of co-elutions (peak pairs 2/4, 3/7, and 8/12) along the compensation voltage axis. The parameters for separation of the co-elutions between peaks 2/4 and 3/7, parts (a) and (b), respectively, included a detector temperature of 120 °C and an RF voltage of 1300 V, while peaks 8/12, part (c), were separated using a detector temperature of 120 °C and an RF voltage of 1500 V.

It is important to notice that all three sets of co-eluting peaks include straight-chain saturated hydrocarbons. Typically, saturated hydrocarbon compounds have high minimum detectable limits in APCI techniques [40]. Thus, for detection in DMS, these components are required to be present at high concentrations. Fig. 8 (b) and (c) of Fig. 8 show the effects of the high concentrations of the saturated hydrocarbons on the chromatographic separation. For isothermal analysis, the higher retention factors for the heavier hydrocarbons cause them to saturate the stationary phase of the column. Saturation of the stationary phase by these components generates retention time shifts to earlier elution for other components during an analysis. The inlet to the column acts as a cold spot to the heavier compounds, saturating the stationary phase and causing other components to move further down the column before interacting with the stationary phase. These effects are illustrated in shifts to earlier retention times for pentanal (3) in Fig. 8 (b) and most noticeably for heptanal (8) in Fig. 8 (c).

### Conclusions

High-speed GC separations of complex mixtures with components spanning a wide range of boiling points and polarities pose a great analytical challenge. This work has attempted to bridge this gap by demonstrating fast GC separations of a broad range of analytes using a novel IIL chromatographic stationary phase in a dual-column ensemble and in conjunction with a microfabricated DMS. Columns generated 2000 and 1600 theoretical plates per meter for the partially cross-linked and the completely cross-linked IIL columns, respectively. A dual-column ensemble integrating an IIL stationary phase-coated column and a dimethyl

polysiloxane stationary phase column in series was utilized to enhance the separation of co-eluting components. A band trajectory model was used to predict the pulse application times necessary to resolve specific peak pairs. The separation of a test group of 20 components with two sets of co-eluting peaks from the column ensemble was enhanced using two stop-flow pulses that added ~15.5 s to the total analysis time. Enhanced separation of 13 components found in the headspace above U.S. currency with two sets of co-eluting peaks was achieved while sacrificing only ~5 s in total analysis time.

Further improvements in selectivity were gained by integrating an IIL column with a microfabricated DMS. The DMS provides a second-dimension separation based on ion chemistry and an ionized species' mobility in a high-frequency electric field. The DMS contribution to the analysis time is negligible; furthermore, it enhances the sensitivity of certain components by 2–3 orders of magnitude relative to FID. The DMS, in most cases, was able to resolve co-eluting peak pairs from the chromatographic column.

Ongoing development of the IIL stationary phase, coating techniques, and the implementation of these phases in microfabricated GC columns are in progress. The success of this work will contribute to the development of a field-portable instrument integrating microfabricated GC columns and a microfabricated DMS for on-site analysis of complex mixtures.

### Acknowledgements

Funding for this work was provided by the University of Michigan Center for Wireless Integrated Microsystems (WIMS) through the Engineering Research Centers Program of the National Science Foundation under Award Number ERC-9986866, the Idaho National Environmental Laboratory, and Sionex Corporation for support on this work. The authors acknowledge Dr. Raanan Miller (Sionex Corporation), Dr. Ekinjon Nazarov (Sionex Corporation), and Professor Edward Zellers (University of Michigan, Department of Environmental Health Sciences/Department of Chemistry) for helpful discussions and critical review of the manuscript. The remaining authors dedicate this article to the memory of Professor Richard D. Sacks.

### References

- [1] S. Dagan, A. Amirav, *J. Am. Soc. Mass Spectrom.* 7 (1996) 737.
- [2] P. Kroyt'ar, H.-G Janssen, E. Matisov'a, U.A.Th. Brinkman, *Trends Anal. Chem.* 21 (2002) 558.
- [3] E. Matisova, M. Domotorova, *J. Chromatogr. A* 1000 (2003) 199.
- [4] R.D. Sacks, H. Smith, M. Nowak, *Anal. Chem. News and Features A-37* (1998) 29.
- [5] N.H. Snow, *J. Liq. Chromatogr. Related Technol.* 27 (2004) 1317.
- [6] S.S. Brody, J.E. Chaney, *J. Gas Chromatogr. A* 4 (1966) 42.
- [7] D.G. Westmoreland, G.R. Rhodes, *Pure Appl. Chem.* 61 (1989) 1147.
- [8] C.-J. Lu, W.H. Steinecker, W.-C. Tian, M. Agah, J.A. Potkay, M.C. Oborny, J. Nichols, H. Chan, J. Driscoll, R.D. Sacks, S.W. Pang, K.D. Wise, E.T.

Zellers, Lab on a Chip 5 (2005) 1123.

[9] C.A. Veasey, C.L.P. Thomas, Analyst 129 (2004) 198.

[10] G.R. Lambertus, C.S. Fix, S.M. Reidy, R.A. Miller, D. Wheeler, E. Nazarov, R. Sacks, Anal. Chem. 77 (2005) 7563.

[11] B. Larsen, M. Cont, L. Montanarella, N. Platzner, J. Chromatog. A 708 (1995) 115.

[12] G.L. Reid III, C.A. Monge, W.T. Wall, D.W. Armstrong, J. Chromatog. 633 (1993) 135.

[13] G.L. Reid III, W.T. Wall, D.W. Armstrong, J. Chromatog. 633 (1993) 143.

[14] Y. Tang, Y. Zhou, D.W. Armstrong, J. Chromatog. A. 666 (1994) 147.

[15] D.W. Armstrong, K. Le, G.L. Reid III, S.C. Lee, K.K. Beutelmann, M. Horak, P. Tran, J. Chromatog. A. 688 (1994) 201.

[16] G.L. Reid III, D.W. Armstrong, J. Microcolumn Sep. 6 (1994) 151.

[17] D.W. Armstrong, G.L. Reid III, M.P. Gasper, J. Microcolumn Sep. 8 (1996) 83.

[18] H. Smith, E.T. Zellers, R.D. Sacks, Anal. Chem. 71 (1999) 1610.

[19] T. Veriotti, R. Sacks, Anal. Chem. 73 (2001) 3045.

[20] T. Veriotti, R. Sacks, Anal. Chem. 73 (2001) 4395.

[21] T. Veriotti, M. McGuigan, R. Sacks, Anal. Chem. 73 (2001) 279.

[22] J. Krupcik, I. Spanik, E. Benicka, M. Zabka, T. Welsch, D.W. Armstrong, J. Chromatogr. Sci. 40 (2002) 483.

[23] E. Benicka, J. Krupcik, J. Lehotay, P. Sandra, P.D. Armstrong, J. Liq. Chromatogr. Related Technol. 28 (2005) 1453.



- [24] J.L. Anderson, D.W. Armstrong, *Anal. Chem.* 77 (2005) 6453.
- [25] J.L. Anderson, D.W. Armstrong, G.-T. Wei, *Anal. Chem.* 78 (2006) 2893.
- [26] J.L. Anderson, D.W. Armstrong, *Anal. Chem.* 75 (2003) 4851.
- [27] D.W. Armstrong, L. He, Y.-S. Liu, *Anal. Chem.* 71 (1999) 3873.
- [28] J.L. Anderson, D.W. Armstrong, R. Ding, T. Welton, *JACS* 124 (2002) 14247.
- [29] J.L. Anderson, R. Ding, A. Ellern, D.W. Armstrong, *JACS* 127 (2005) 593.
- [30] C.-J. Lu, J.J. Whiting, R.D. Sacks, E.T. Zellers, *Anal. Chem.* 75 (2003) 1400.
- [31] G.R. Lambertus, R.D. Sacks, *Anal. Chem.* 77 (2005) 2078.
- [32] E.D. Kolesar, R.R. Reston, *IEEE Trans. Compon. Packag. Manuf. Technol.* 21 (1998) 324.
- [33] K. Chen, Y.E. Wu, *Sens. Actuators A* 79 (2000) 211.
- [34] Y.E. Wu, K. Chen, C.W. Chen, K.H. Hsu, *Sens. Actuators A* 100 (2002) 37.
- [35] R. Kottenstette, R.P. Lewis, D. Adkins, G. Dulleck, *Proceedings of the 2nd Joint Conference on Point Detection for Chemical and Biological Defense*, Williamsburg, VA, March 1–5, 2004.
- [36] R.P. Manginell, M. Okandan, J.M. Bauer, R. Manley, D. Trudell, R.J. Kottenstette, P.R. Lewis, D.R. Adkins, E.J. Heller, H. Stewart, R.J. Shul, *Proceedings of the micro-TAS 2004 Workshop*, Malmo, Sweden, September 26–30, 2004, p. 61.

- [37] F. Bender, N. Barie, G. Romoudis, A. Voigt, M. Rapp, *Sens. Actuators B* 93 (2003) 135.
- [38] W.H. Steinecker, M.P. Rowe, A.J. Matzger, E.T. Zellers, *Proceedings of the 12th International Conference on Solid-State Sensors, Actuators and Microsystems, Transducers'03*, Boston, MA, June 8–12, 2003, p. 1343.
- [39] Q.-Y. Cai, E.T. Zellers, *Anal. Chem.* 74 (2002) 3533.
- [40] G.A. Eiceman, Z. Karpas, *Ion Mobility Spectrometry*, CRC Press, Boca Raton, FL, 1994.
- [41] R.G. Ewing, D.A. Atkinson, G.A. Eiceman, G.J. Ewing, *Talanta* 54 (2001) 515.
- [42] D.C. Collins, M.L. Lee, *Anal. Bioanal. Chem.* 372 (2002) 66.
- [43] T.W. Carr (Ed.), *Plasma Chromatography*, Plenum Press, New York, 1984.
- [44] G.A. Eiceman, Z. Karpas, *Ion Mobility Spectrometry*, CRC Press, Boca Raton, FL, 1994.
- [45] G.A. Eiceman, D.B. Shoff, C.S. Harden, A.P. Snyder, *Int. J. Mass Spectrom. Ion Proc.* 85 (1988) 265.
- [46] A.H. Lawrence, P. Neudorfl, *Anal. Chem.* 60 (1988) 104.
- [47] R.A. Miller, G.A. Eiceman, E.G. Nazarov, T.A. King, *Solid-State Sensor and Actuator Workshop*, Hilton Head Island, SC, June 4–8, 2000.
- [48] G.A. Eiceman, B. Tadjikov, E. Krylov, E.G. Nazarov, R. Miller, J. Westbrook, P. Funk, *J. Chromatogr. A.* 917 (2001) 205.
- [49] R.A. Miller, E.G. Nazarov, N.S. Krylova, A.T. King, *Anal. Chem.* 91 (2001) 301.

- [50] G.A. Eiceman, E.V. Krylov, N.S. Krylova, *Anal. Chem.* 76 (2004) 4937.
- [51] G.A. Eiceman, E.V. Krylov, B. Tadjikov, R.G. Ewing, E.G. Nazarov, R.A. Miller, *Analyst* 129 (2004) 297.
- [52] A. Peters, M. Klemp, L. Puig, C. Rankin, R. Sacks, *Analyst* 116 (1991) 1313.
- [53] M.E. McGuigan, R.D. Sacks, *Anal. Chem.* 73 (2001) 3112.
- [54] D.-T. Vu, *J. Forensic Sci.* 48 (2003) 754.

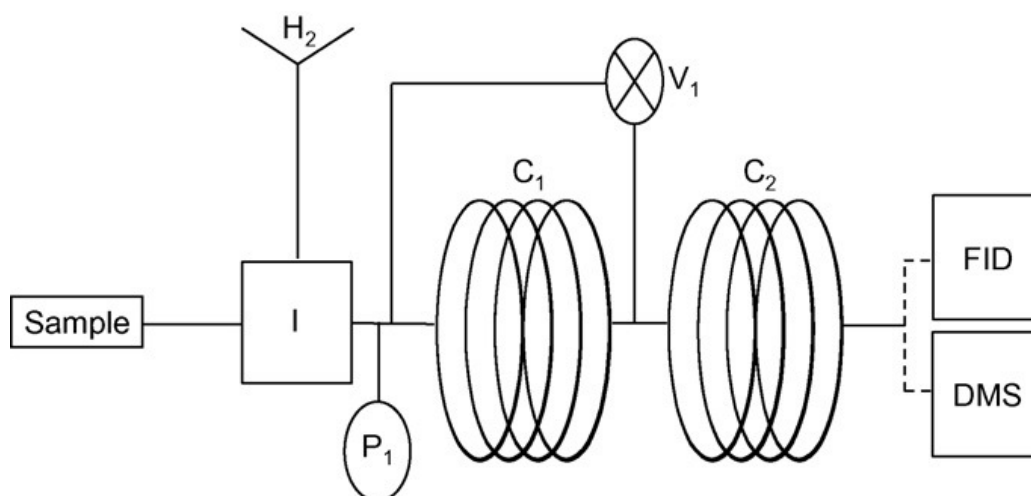


Fig. 1. Apparatus for stop-flow selectivity enhancement with a dual-column ensemble using an IIL stationary phase-coated column and a Rtx-1 column.  $C_1$  and  $C_2$  are the columns;  $V_1$ , stop-flow valve; I, split inlet;  $P_1$ , pressure gauge; FID, flame ionization detector; DMS, differential mobility spectrometer.

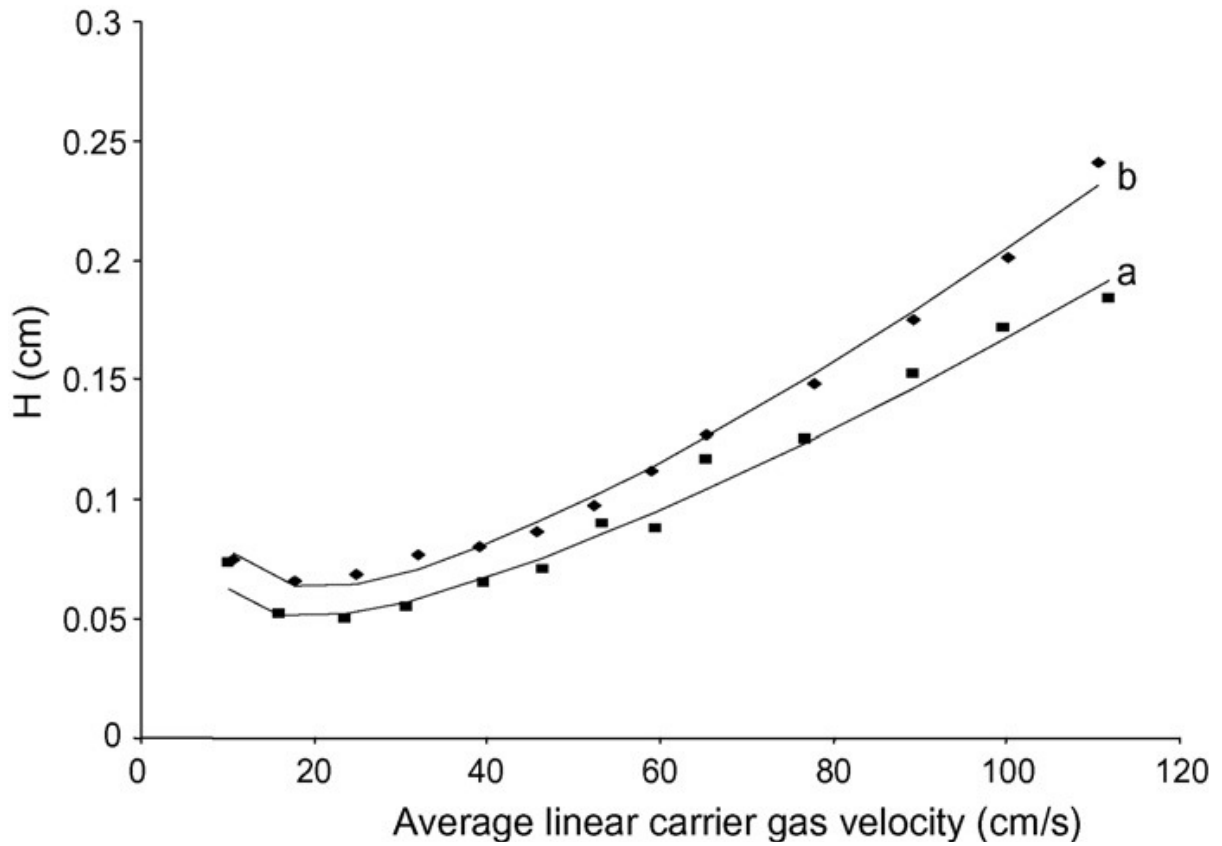


Fig. 2. Height equivalent to a theoretical plate vs. average linear carrier gas ( $H_2$ ) velocity for (a) 2.8-m long partially cross-linked IIL stationary phase-coated column and (b) a 2.8-m long completely cross-linked IIL stationary phase-coated column for experimental data using *n*-decane at 50 °C.

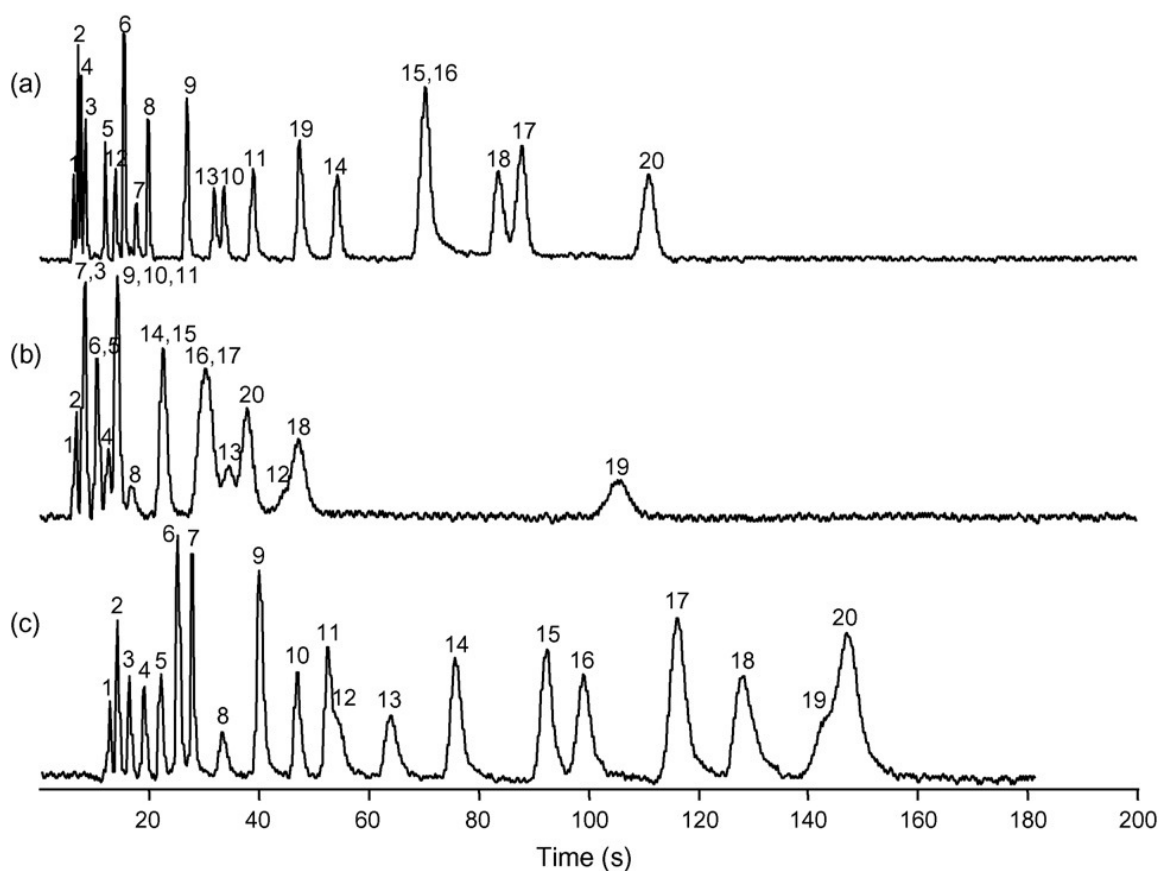


Fig. 3. Chromatograms of the 20-component test mixture using H<sub>2</sub> carrier gas at 50 °C: (a) commercially-coated Rtx-1 column; (b) IIL stationary phase-coated column; (c) column ensemble. Peak numbers correspond to compound numbers in Table 1. Chromatograms were obtained at carrier gas velocities of ~54, 53, and 54 cm s<sup>-1</sup>, respectively.

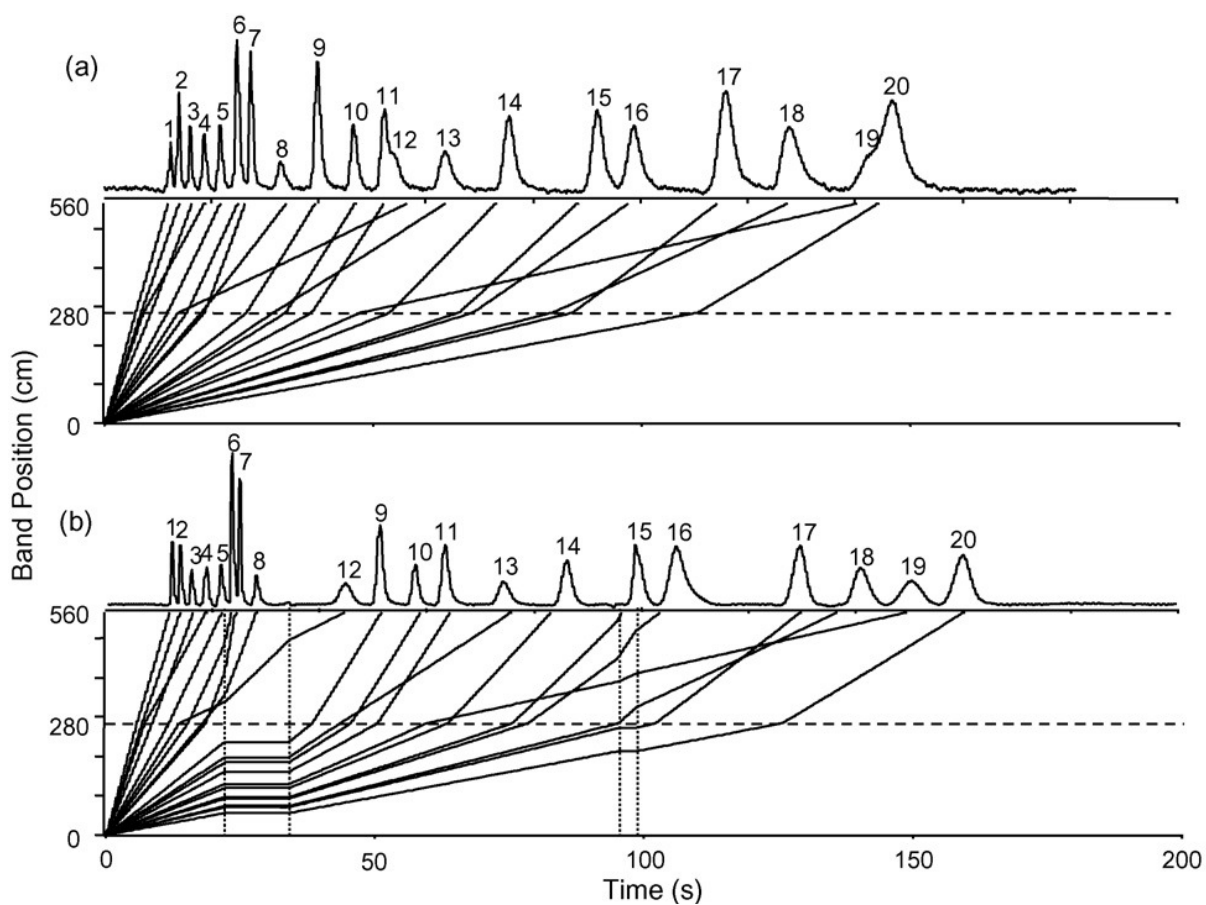


Fig. 4. Band trajectory plots indicating band position vs. time and the corresponding chromatograms for the 20-component test mixture with no stop-flow pulses (a) and two stop-flow pulses as indicated by the vertical broken lines (b). See text for details. Peak numbers correspond to compound numbers in Table 1.

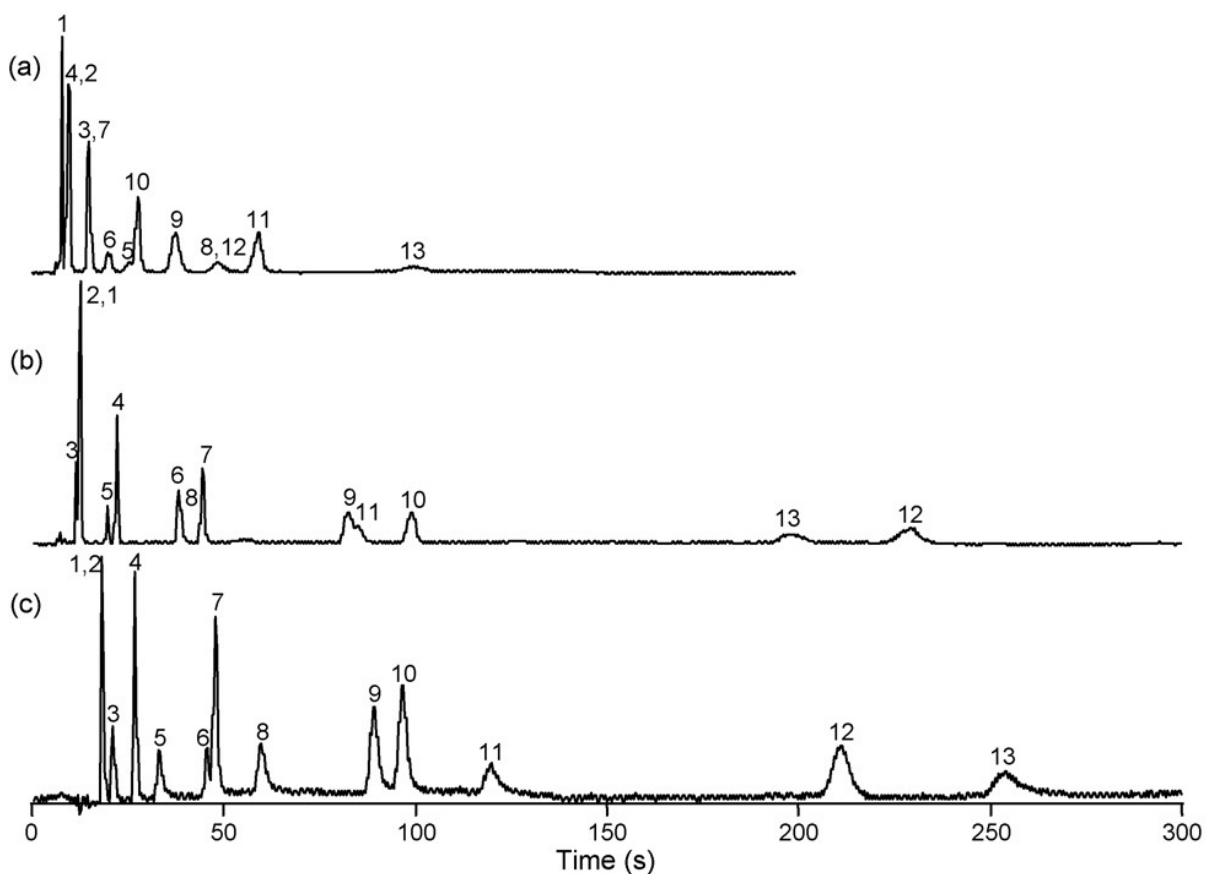


Fig. 5. Chromatograms of the 13-component test mixture of the markers found in the headspace of U.S. currency using  $H_2$  carrier gas at  $50\text{ }^\circ\text{C}$ : (a) IIL stationary phase-coated column; (b) commercially-coated Rtx-1 column; (c) column ensemble. Peak numbers correspond to compound numbers in Table 2. Chromatograms were obtained at carrier gas velocities of 50, 52, and  $50\text{ cm s}^{-1}$ , respectively.



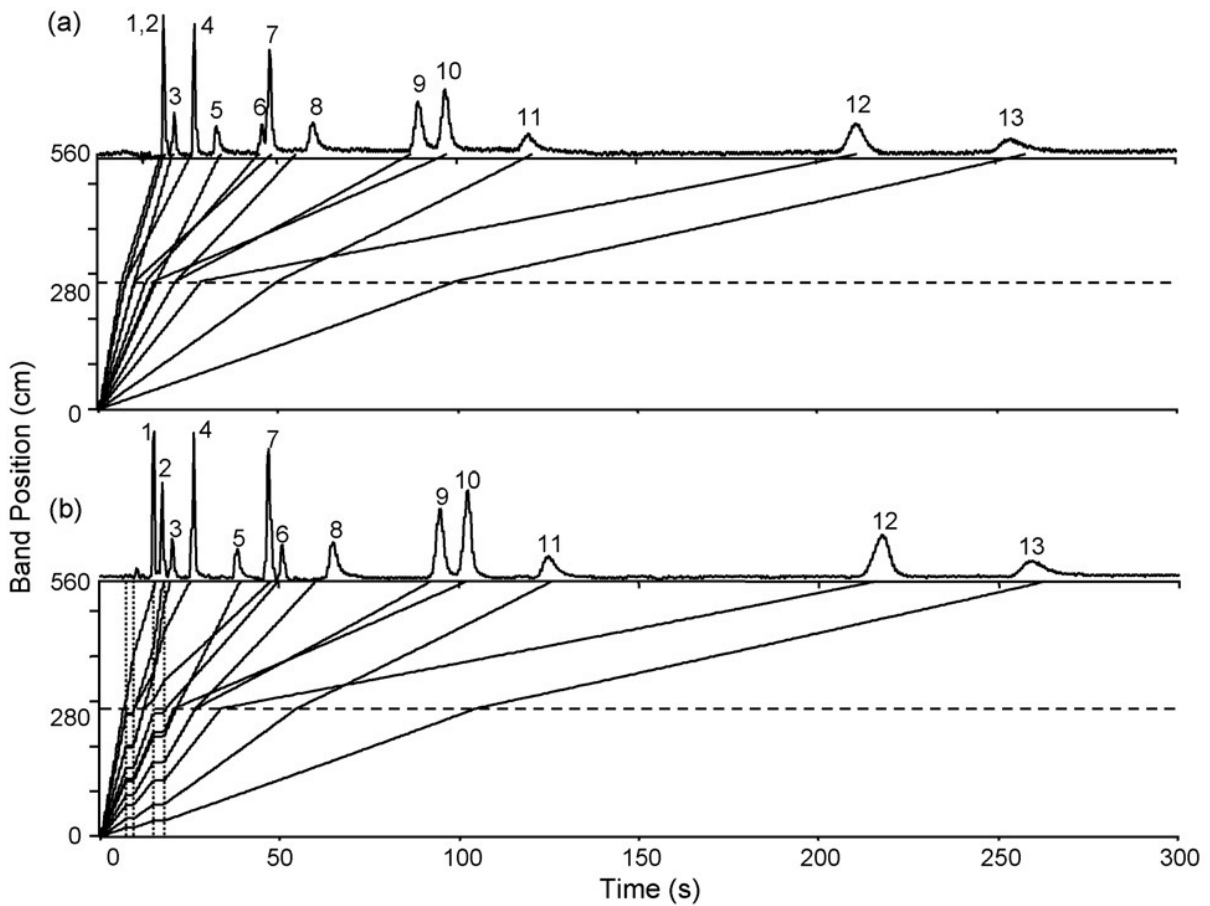


Fig. 6. Band trajectory plots indicating band position vs. time and the corresponding chromatograms for the 13-component test mixture of the markers found in the headspace of U.S. currency with no stop-flow pulses (a) and two stop-flow pulses as indicated by the vertical broken lines (b). See text for details. Peak numbers correspond to compound numbers in Table 2.

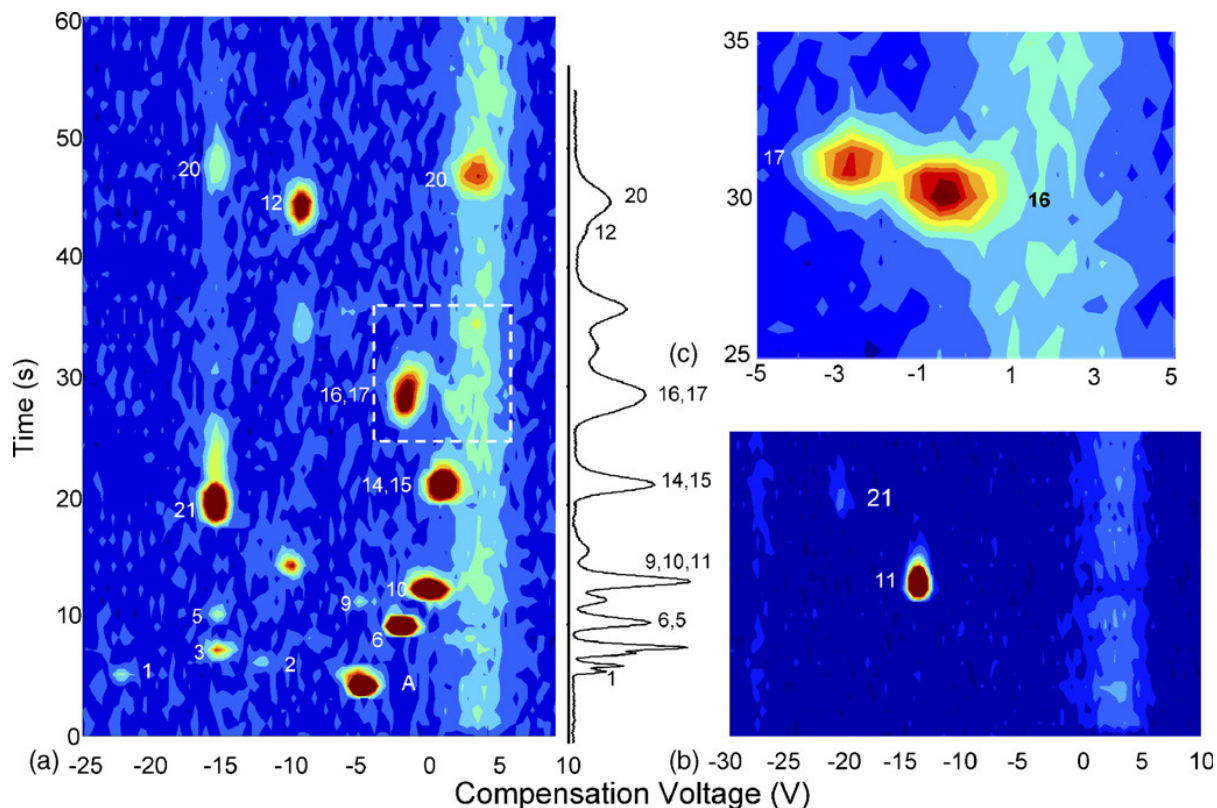


Fig. 7. Contour plots for the co-eluting components of the 20-component text mixture from the IIL column—DMS system accompanied by a vertically-oriented FID trace showing the one-dimensional separation. The contours show ion current (color) as a function of retention time (vertical axis) and compensation voltage (horizontal axis) for the positive ion channel (a) and a portion of the negative ion channel (b) with a detector RF voltage of 1500 V and an operating temperature of 120 °C. Contour (c) shows the separation of peak pair 16 and 17 with a detector Rf voltage of 1200 V and an operating temperature of 60 °C.

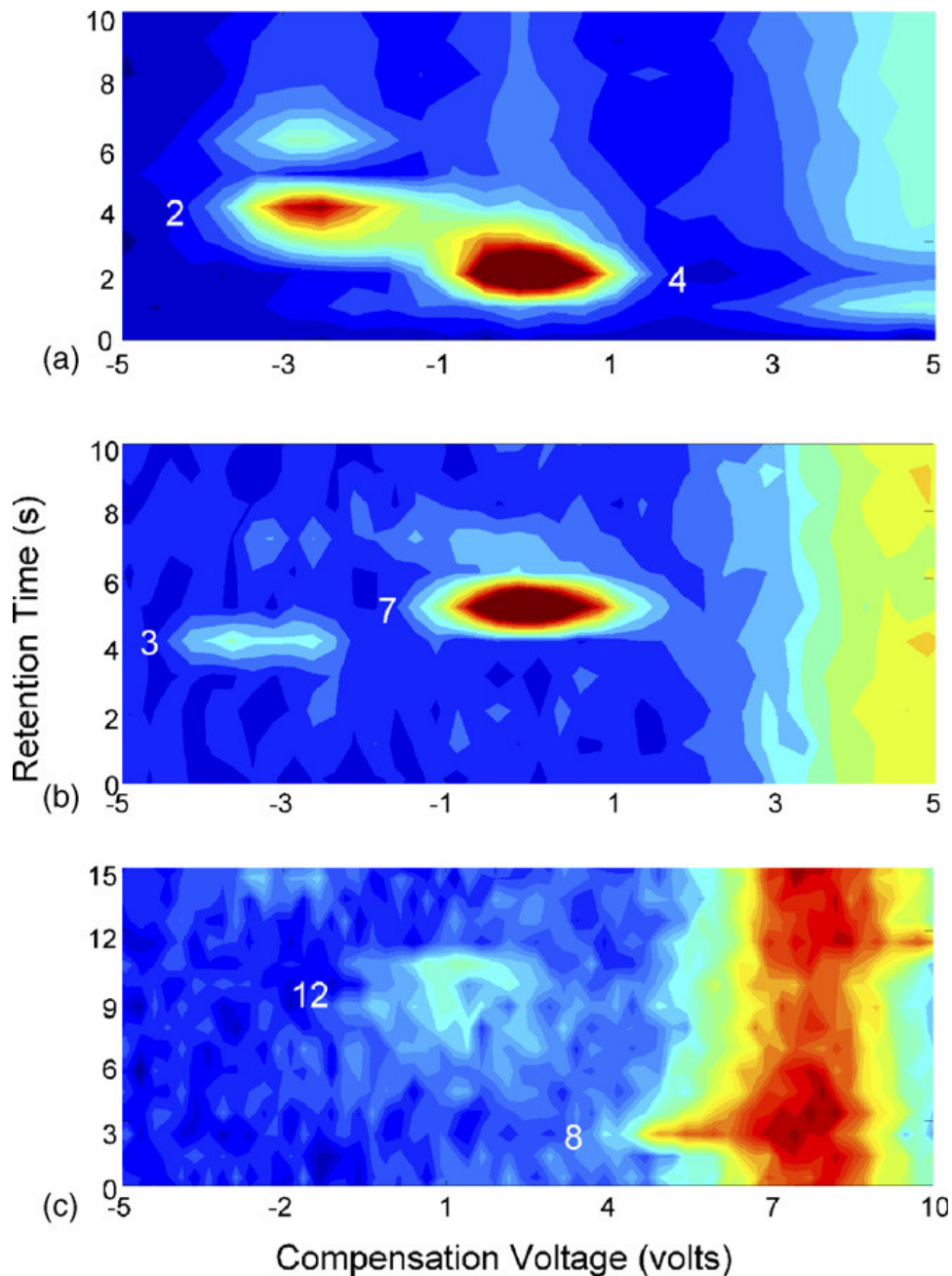


Fig. 8. Contour plots showing the separation of the co-eluting components from the 13-component mixture of the markers found in the headspace of U.S. currency. Component peak pairs 2/4 (a) and 3/7 (b) were separated using a detector Rf voltage of 1300 V and an operating temperature of 120 °C, while component pair 8/12 was separated using a detector Rf voltage of 1500 V and an operating temperature of 120 °C.

Table 1. Components and retention factors for the 20-component test mixture

	Compound	Retention factors		
		Rtx-1™	IIL stationary phase	Boiling point (°C)
1	Acetaldehyde	0.07	0.05	20.1
2	Isopropyl alcohol	0.26	0.18	82.4
3	Ethyl acetate	0.51	0.36	77.1
4	Propionitrile	0.26	1.02	97.2
5	Propyl acetate	1.1	0.75	102
6	Toluene	1.7	0.68	111
7	Octane	2.3	0.35	126
8	Hexanal	2.2	1.8	131
9	Ethylbenzene	3.7	1.3	136
10	2-n-Butylfuran	4.9	1.3	153
11	Iodopentane	5.8	1.4	157
12	Pyrolle	1.4	6.6	130
13	2-Heptanone	4.5	4.7	150
14	3-Ethyltoluene	8.1	2.4	161
15	2-n-Pentylfuran	10.2	2.8	175
16	1,3-Dichlorobenzene	10.8	4	173
17	P-cymene	14.4	3.8	177
18	Hexyl acetate	13.7	6.8	171
19	Benzaldehyde	7.4	15.5	179
20	Butyl benzene	18.5	5	183

Table 2. Components and retention factors for mixture that are used as a fingerprint for the headspace vapor above U.S. currency.

	Compound	Retention factors		
		Rtx-1™	IIL stationary phase	Boiling point (°C)
1	Heptane	0.1	0.94	98.4
2	2-Ethylfuran	0.3	0.9	92.5
3	Pentanal	0.74	0.87	103
4	Octane	0.29	2.3	126
5	Hexanal	1.8	2.2	131
6	2-n-Butylfuran	1.3	4.6	153
7	Nonane	0.76	5.8	151
8	Heptanal	3.8	5	153
9	2-n-Pentylfuran	2.8	10.6	175
10	Decane	1.7	13.5	174
11	Octanal	7.8	11.6	171
12	Undecane	4	31.5	196
13	Nonanal	16.6	27.2	191

**CHAPTER 5****CHARACTERIZATION AND UTILIZATION OF A NOVEL TRIFLATE IONIC LIQUID STATIONARY PHASE FOR USE IN COMPREHENSIVE TWO-DIMENSIONAL GAS CHROMATOGRAPHY**

Vanessa R. Reid<sup>1</sup>, Jeffery A. Crank<sup>2</sup>, Daniel W. Armstrong<sup>2</sup>, Robert E. Synovec<sup>1</sup>

<sup>1</sup>Department of Chemistry, University of Washington, Seattle, WA, USA

<sup>2</sup>Department of Chemistry and Biochemistry, The University of Texas at Arlington, Arlington, TX, USA

**Abstract**

A novel triflate (trifluoromethylsulfonate) ionic liquid (IL) thin film (0.08  $\mu\text{m}$ ) stationary phase was implemented for use within the second column of a comprehensive GC $\times$ GC configuration. The first column in the configuration had a 5% phenyl/95% dimethyl polysiloxane (DMPS) stationary phase with a 0.4  $\mu\text{m}$  film. The DMPS $\times$ IL column configuration was used to separate a mixture of 32 compounds of various chemical functional classes. The GC $\times$ GC results for the IL column were compared with a commercially available polar column (with a 0.1  $\mu\text{m}$  PEG stationary phase film) used as the second column instead. Additional studies focused on the rapid and selective separation of four phosphorous–oxygen (P–O) containing compounds from the 32-compound matrix: dimethyl methylphosphonate (DMMP), diethyl methylphosphonate (DEMP), diisopropyl methylphosphonate (DIMP), and triethyl phosphate (TEP). van't Hoff plots (plots of  $\ln k$  vs.  $1/T$ ) demonstrated the difference in retention between the P–O containing compounds (with

DMMP reported in detail) and other classes of compounds (*i.e.*, 2-pentanol and *n*-dodecane as representative) using either the IL column or the commercial PEG column. The selectivity ( $\alpha$ ) of the triflate IL column and the commercially available PEG column were also compared. The IL column provided significantly larger selectivities between DMMP and the other two compounds (2-pentanol and *n*-dodecane) than the commercial PEG column. The  $\alpha$  for DMMP relative to *n*-dodecane was 3.0-fold greater for the triflate IL column, and the  $\alpha$  for DMMP relative to 2-pentanol was 1.7-fold greater for the triflate IL column than for the PEG column.

### Introduction

Comprehensive GC×GC is a powerful analytical tool used for the separation of complex mixtures [1–6]. GC is a very important chemical analysis technique and multidimensional separation techniques, GC×GC in particular, are evolving into essential analysis tools [7]. The key to successful GC×GC separations is to select two columns with stationary phases that provide complementary selectivity, or sometimes referred to as “orthogonal” separation dimensions, thus allowing for both separation dimensions to separate specific compounds within a matrix [1, 8]. While retention indices [9, 10] and selectivity can both be used to determine the relative selectivity of the two stationary phases, herein we use the traditional selectivity definition, *i.e.*, the ratio of the retention factors for two compounds of interest. In many cases, a column with a nonpolar stationary phase is chosen for the first dimension and a polar stationary phase is employed in the second column [1]. Using this column

arrangement the first column separates the compounds primarily by boiling point, while the second column separates the compounds primarily by polarity (which is usually correlated to the class of compounds). This “traditional” column combination has been a workhorse for separating complex mixtures such as petroleum samples [11, 12] and pesticides in food extracts [13, 14].

Ideally, the GC×GC separation will widely distribute the chemical compounds in a given complex mixture across the 2-D separation space [15]. However, in the case of targeted analysis, where only a subset of compounds (*i.e.*, a class of compounds or selected classes of compounds) needs to be separated from the bulk sample matrix, the second dimension separation column should be tailored to that specific application. The smaller the number of compound classes, the more specific the selectivity of the second separation column must be. For some targeted separations, the use of a highly selective novel stationary phase may be necessary. Indeed, the fabrication of novel stationary phases should address this challenge, providing highly selective retention properties.

Numerous novel materials such as, but not limited to, monolayer protected nanoparticles (MPNs) [16, 17], carbon nanotubes [18], and room temperature ionic liquids (ILs) [19–24] have recently been utilized as stationary phases in GC. Developments in the area of ILs have proven them to be robust stationary phases for GC [22, 23]. More specifically, previous temperature limitations have been overcome through the crosslinking of dicationic monomers resulting in stationary phases that are stable at temperatures above 350°C. ILs allow for



tunable selectivity of the stationary phase through the alteration of the functionality of the cation or anion.

In this report, a novel triflate IL stationary phase is characterized and utilized in the second dimension column of a GC×GC system, serving as the “polar” stationary phase. The novel triflate IL column is compared to another polar stationary phase, a commercially available PEG column. In order to characterize the novel triflate IL stationary phase, van't Hoff ( $\ln k$  vs.  $1/T$ ) and selectivity plots ( $\alpha$  vs.  $1/T$ ) were created, using single-column GC data, to compare the difference in compound retention and selectivity between the two polar columns. Lastly, the triflate IL column was implemented as the second column in a rapid GC×GC separation of phosphorous–oxygen (P–O) containing compounds from a complex sample matrix, containing compounds representing several functional groups, using a dimethyl polysiloxane (DMPS) stationary phase with the first dimension column. For comparison, rapid separations of the P–O compounds from the same complex sample were also collected with GC×GC using the same DMPS first column, but with the commercially available PEG column in the second dimension. In this comparison, the advantage of using the triflate IL column relative to the PEG column for separating the P–O containing compounds by GC×GC from a relatively complex sample is demonstrated.

## Experimental

### *Column fabrication*

The dication, 1,9-di(3-vinylimidazolium)nonane bromide, was synthesized by reacting 2.2 molar equivalents of 1-vinylimidazole and 1 molar equivalent of 1,9-dibromononane. The

reaction mixture was stirred at room temperature until the IL solidified (~6 h). The bromide salt was then dissolved in water and eight extractions were performed with ethyl acetate to remove impurities. The bromide IL was then placed under vacuum overnight to ensure complete dryness. Anion exchange of the dication salt from the dibromo salt to the triflate (trifluoromethylsulfonate) form of the salt was achieved as follows. First, the bromide salt was dissolved in acetonitrile (ACN). Then, exactly 2 molar equivalents of silver triflate were dissolved in ACN and added to the dication solution. The flask was covered in aluminum foil and stirred overnight. The solution was then filtered and the ACN was removed by a rotary evaporator. The triflate IL was then placed under vacuum overnight to ensure complete dryness. Note, if there is any excess silver present the product turns black, then the IL must be resynthesized. The triflate IL columns have been coated using the static coating method at 40°C as previously reported [22, 25] resulting in a 4 m×100 µm×0.08 µm film thickness column. The dication stationary phase 1,9-di(3-vinylimidazolium) nonane triflate will be referred to as the triflate IL column. Thermal stability of the triflate IL column was tested by two methods. The first method was thermogravimetric analysis (TGA). TGA results showed that the triflate IL was stable to a temperature of 358°C, with only a 5% weight loss. The second method used to test the thermal stability of the triflate IL column used GC-FID data. A column was coated, placed in a GC oven, and heated at 4°C/min until bleed was observed. The onset of the column bleed occurred at 315°C, with significant column bleed at 331°C.

#### *Chromatographic instrumentation*

The instrument consisted of an Agilent 6890 GC (Agilent Technologies, Santa Clara, CA, USA), fitted with a diaphragm valve (VICI Valco Instruments, Houston, TX, USA) and an

FID with an in-house built high speed electrometer. The GC×GC separations were collected using a diaphragm valve-based 2-D instrument as described previously [5, 11, 26]. Injections onto the first column were made with an auto-injector, and injections from the first column to the second column were made *via* the diaphragm valve utilizing an injection pulse onto the second columns of 25 ms with a 10  $\mu$ L sample loop. Three different modulation periods (3, 5, and 7 s) were used, but only the 3 and 7 s results are presented for brevity.

All single dimension chromatograms were collected using a single diaphragm valve for sample injection as reported previously [5, 11, 26, 27]. The diaphragm valve was used with an injection pulse of 15 ms and a 10  $\mu$ L sample loop. For the single dimension experiments the two “polar” columns were being evaluated alone, in the absence of the first column separation (as in GC×GC).

The timing and actuation of the diaphragm valve (for the GC×GC and single column two systems) was controlled with an in-house written LabVIEW program and utilized a National Instruments data acquisition board (Model PCI-MIO-16XE-10, National Instruments, Austin, TX, USA).

#### *Chromatographic experiments*

All chromatograms were collected with an inlet and FID temperature of 250°C. For the GC×GC experiments, the inlet was run with a split ratio of 1:2 with an absolute head pressure of 18 psi (124000 Pa) of H<sub>2</sub> carrier gas. The first column was a 5 m×100  $\mu$ m id DB-5 column (J&W Scientific/Agilent Technologies) with a 0.4  $\mu$ m film thickness (5%

phenyl/95% DMPS). The second column was either the 4 m×100 µm id triflate IL column described above, or a 4 m×100 µm id DB-Wax column (J&W Scientific/Agilent Technologies) with a film thickness of 0.1 µm (PEG). Temperature programs and oven temperatures are given in the text.

The single dimension data were collected with a split ratio of 1:2 with an absolute head pressure of 65 psi (448000 Pa) of H<sub>2</sub> carrier gas. The data for the van't Hoff plots were collected at four different temperatures: 62, 75, 100, and 125°C. All single dimension data were collected isothermally.

## Results and discussion

### *Comparison of GC×GC separations using triflate IL and DB-WAX columns as the second dimension*

A novel stationary phase, such as a triflate IL, needs to be sufficiently characterized prior to commercialization. A major part of that process is implementing the IL phase within GC instrumentation, and comparing the performance with a commercially available stationary phase (in this case DB-Wax was the commercially available column). A large mixture of compounds of various chemical functionalities was used as the test mixture to determine how compound retention on the novel and commercial columns differed. This mixture was also designed to help fine tune the possible applications for which the triflate IL column could be

used. The identities of the 32 compounds in the test mixture are listed in Table 1 (in their order of retention on DB-5). The separation of the 32-compound mixture utilizing a 7 s modulation period is shown as a contour plot in Fig. 1A. Nearly all 32 compounds are visible above the baseline in this contour plot and are distributed across the first dimension. The second dimension separation, however, is not using the separation space optimally. By reducing the modulation period, and allowing the peaks to “wrap around” in the second dimension (*i.e.*, elute later than the modulation period on the second column so appearing to elute before the dead time) the use of the separation space is optimized as shown in Fig. 1B. The shorter modulation period also increased the S/N of some of the compounds because less sample is vented when the frequency of the injections is increased. Another way to evaluate the triflate IL stationary phase is to compare the retention selectivity properties relative to a commercially available DB-Wax column. The GC×GC separation of the 32-compound mixture using DB-Wax as the second column is shown in Fig. 1C. This separation utilized the 3 s modulation period in order to allow the compounds to wrap around the column.

#### *Comparison of single dimension data*

In the initial GC×GC separations, shown in Fig. 1, diethyl methylphosphonate (DEMP) was not evident in the separation since the conditions (flow rate and temperature program) were not optimized in order to observe DEMP with high enough S/N. This experimental observation prompted an in-depth study of the single dimension retention of compounds of various functionalities, *e.g.*, to see if compounds such as DEMP exhibited interesting retention properties on the triflate IL column, as compared to the DB-Wax column. Four different compounds (methane, *n*-dodecane, 2-pentanol, and dimethyl methylphosphonate

(DMMP)) were selected for individual study, and ultimately followed by comparison to each other *via* van't Hoff and selectivity plots, with methane used as the dead time marker.

The overlay plot for the triflate IL column is shown in Fig. 2A. The overlay plot for the DB-Wax column is shown in Fig. 2B. Each overlay plot contains five replicated injections for each of the four compounds to demonstrate the high injection-to-injection reproducibility (the reproducibility will be discussed more in the following section). The isothermal efficiencies,  $N$ , calculated for compounds shown in Fig. 2A, are reasonable for the novel IL column, considering some of the band broadening comes from the injection pulse width for such a short separation time. At 125°C,  $N$  of 35000, 42000, 35000, and 10000 were obtained for methane ( $k = 0$ ), *n*-dodecane ( $k = 0.019$ ), 2-pentanol ( $k = 0.069$ ), and DMMP ( $k = 2.6$ ), respectively, for the 4 m column length.

It is important to note that the retention order of the compounds is different for each of the columns. The retention order of *n*-dodecane and 2-pentanol has been reversed for the two columns. This suggests that *n*-alkanes are not significantly retained using the triflate IL column (this is also supported by the GC×GC chromatograms in Fig. 1). The difference in the retention times, on the triflate IL column, for the first three compounds is minimal (less than 200 ms). In fact, the retention times of methane and *n*-dodecane differ by only 60 ms. In comparison, DMMP is highly retained on the triflate IL column. Indeed, the retention time of DMMP on the triflate IL column is two-fold greater than the retention time on the DB-Wax column. However, since DMMP is significantly more retained on the triflate IL column as

compared to the DB-Wax column, this results in a more asymmetric peak. Foremost, the triflate IL column appears to exhibit an interesting selectivity for DMMP.

*van't Hoff plots for triflate IL and DB-WAX columns*

The interesting selectivity of the triflate IL column for DMMP was further explored. Single dimension data were collected for both separation columns at four different isothermal temperatures (62, 75, 100, and 125°C). The retention times for each of the analytes were measured to the nearest millisecond. The largest SD (2.1 s) in the retention time (133 s), with the triflate IL column, was for DMMP at 62°C, which corresponds to a %RSD of 1.6%. A compound less retained on the triflate IL column (such as methane with a retention time less than 3 s) had a maximum retention time SD of 0.3 ms (at 62°C), which corresponds to a %RSD of 0.01%. There is very little variation in the retention time, which can be attributed to the repeatability using single diaphragm valve injection. The low %RSD values for the retention times also suggest that neither of the columns degraded over time or the range of temperatures used within the scope of the characterization and evaluation of the columns. The triflate IL and DB-Wax stationary phases both exhibited robust behavior. Methane was used as a dead time marker for each of the temperatures so the retention factor,  $k$ , of each compound could be calculated. The retention factors for each of the three compounds (*n*-dodecane, 2-pentanol, and DMMP) at all four temperatures for both separation columns are listed in Table 2. Five replicates were collected for each compound and temperature. The absolute SD is also reported in Table 2 for each retention factor. The SD of each retention factor is reported with one significant digit and the average retention factor is reported to the

number of digits warranted by the SD. The high level of precision in the retention factor data is directly related to the high precision in the retention time data for both columns. The single dimension data were used to create van't Hoff plots for both the triflate IL and DB-Wax columns. A van't Hoff plot provides thermodynamic information for the compounds under study, and information about compound specific retention with a particular stationary phase [28–31]. The slope of the line created in a van't Hoff plot is related to the enthalpy of the compound under investigation. The y-intercept provides information about compound specific retention of the stationary phase under investigation. A large distance between the lines for two compounds (*i.e.*, offset) is indicative of chemical selectivity differences in retention (analyte–stationary phase interactions via the entropy term), albeit not corrected for the phase volume ratio at this stage. The van't Hoff plot for the triflate IL column is shown in Fig. 3A. The line approximated by the data for DMMP is significantly offset, vertically, from the other two compounds (*n*-dodecane and 2-pentanol). Meanwhile, the van't Hoff plot for the DB-Wax column is shown in Fig. 3B. Note that the offset between DMMP and the other compounds is not as large for the DB-Wax column as it was for the triflate IL column. The reversed retention order of *n*-dodecane and 2-pentanol for the two columns can also be seen in these two plots. The van't Hoff plots, however, may not be the most appropriate way to directly compare two different columns because of their dependence on the phase to volume ratio of the separation column. This parameter is different for the two columns because the film thickness of both columns is not equal.



### *Selectivity differences*

The best way to directly compare both the triflate IL and DB-Wax columns is to plot the selectivity,  $\alpha$ , for each compound as a function of  $1/T$ , to further see if there is a temperature dependence on selectivity. The selectivity,  $\alpha$ , of a particular separation column, for one compound relative to another compound, is the ratio of the retention factors of both compounds [30]. Selectivity plots (plots of  $\alpha$  vs.  $1/T$ ) allow for a direct comparison of two separation columns by removing the dependence of the compound retention on the phase to volume ratio. The selectivity plot for DMMP relative to 2-pentanol for both separation columns is shown in Fig. 4A. The selectivity plot in Fig. 4A suggests that the triflate IL column is more selective for DMMP (when compared to 2-pentanol) than the commercially available DB-Wax column. The selectivity plot for DMMP relative to *n*-dodecane for both columns is shown in Fig. 4B. The same trend (with an even larger offset between the two separation columns) is observed in this selectivity plot. These results led to the conclusion that the triflate IL column is more selective for DMMP (when compared to both polar and nonpolar compounds) than the DB-Wax column. Additionally, the lines that can be approximated by the data in both selectivity plots in Fig. 4 are essentially constant because plotting  $\alpha$  eliminates the dependence of the compound retention on temperature, *i.e.*, the thermodynamic quantities are almost constant, hence essentially independent of temperature over the temperature range studied. Quantitatively, for the data in Fig. 4A,  $\alpha$  for DMMP relative to *n*-dodecane is  $5.1 (\pm 0.1)$  for the triflate IL column, and  $1.7 (\pm 0.1)$  for the DB-Wax column, hence  $3.0 (\pm 0.2)$ -fold more selectivity for the IL column relative to the DB-Wax column (ignoring the slight temperature dependence). Note that  $\alpha$  was calculated at each temperature and then averaged across all temperatures with the SD also provided. Likewise,

for the data in Fig. 4B,  $\alpha$  for DMMP relative to 2-pentanol is 4.0 ( $\pm 0.3$ ) for the triflate IL column, and 2.3 ( $\pm 0.2$ ) for the DB-Wax column, resulting in 1.7 ( $\pm 0.1$ )-fold more selectivity for the triflate IL column relative to the DB-Wax column.

#### *Rapid and selective GC×GC separations for P–O containing compounds*

The high selectivity of the triflate IL column for DMMP has multiple useful applications. Many P–O containing compounds (such as DMMP) are used as chemical warfare agent (CWA) simulants due to their chemical similarity [32]. Rapid separations that target the separation of the CWA simulants from a sample matrix are highly useful for government applications. Hence, we investigated using the triflate IL column in a high speed GC×GC separation of P–O containing compounds, added to the relatively complex 32-compound mixture. Three other P–O containing compounds, DEMP, diisopropyl ethylphosphonate (DIMP), and triethyl phosphate (TEP) have been identified as CWA simulants. The stimulant DEMP was in the 32-compound mixture that was originally used to test the triflate IL column by GC×GC. This compound was not identified in the separations shown in Fig. 1. This was most likely due to it being highly retained on the second column, and the separation conditions not initially optimized as previously mentioned. The high selectivity for P–O containing compounds leads to significant broadening of the observed peaks, which results in poor S/N, unless the separation conditions are carefully chosen. Such highly retained compounds can be targeted by optimizing the temperature program to tune the retention and thus limit the amount of peak broadening. The GC×GC separation shown in Fig. 5A is a separation of the original 32-compound mixture (which already contained DEMP) spiked

with the three additional P–O containing compounds (DMMP, DIMP, and TEP). By using a fast temperature program at high temperatures (150–200°C at 7°C/min) the four P–O containing compounds are separated from the large matrix in less than 7 min. With the DB-Wax column in the second dimension of GC×GC, the same mixture of compounds was separated as shown in Fig. 5B. Using the DB-Wax column to target the P–O compounds resulted in a separation where the P–O compounds elute in the midst of the sample matrix (with TEP being buried in the middle of the matrix).

### Conclusions

A triflate IL stationary phase was examined in the second column for GC×GC separations. The triflate IL phase was found to have substantially higher selectivity than PEG (DB-Wax) for P–O containing compounds. It is intriguing to consider studying other IL materials as stationary phases in order to exploit the unique and potentially useful chemical selectivity properties. While not explored in this current study, the high temperature operating range for the IL materials make them ideally suited for high temperature GC×GC. This warrants future exploration since PEG phases have shortcomings in high temperature application.

Additionally, since the IL phases provide unique selectivity relative to many commercial phases, the IL phases should be explored in higher dimensional separation approaches such as GC×GC×GC [33].

### Acknowledgements

We thank Matthew VanWingerden for assistance with preliminary experiments.

### References

- [1] Gorecki, T., Harynuk, J., Panic, O., *J. Sep. Sci.* 2004, 27, 359 – 379.
- [2] Liu, Z., Phillips, J. B., *J. Chromatogr. Sci.* 1991, 29, 227.
- [3] Phillips, J. B., Beens, J., *J. Chromatogr. A* 1999, 856, 331 – 347.
- [4] van Deursen, M., Beens, J., Reijenga, J., Lipman, P., Cramers, C., Blomberg, J., *J. High Resolut. Chromatogr.* 2000, 23, 507 – 510.
- [5] Fraga, C. G., Prazen, B. J., Synovec, R. E., *Anal. Chem.* 2000, 72, 4154 – 4162.
- [6] Mayadunne, R., Nguyen, T., Marriott, P. J., *Anal. Bioanal. Chem.* 2005, 382, 836 – 847.
- [7] Janssen, H., Marriott, P., Vreuls, R., *J. Chromatogr. A* 2008, 1186, 1.
- [8] Venkatramani, C. J., Xu, J., Phillips, J. B., *Anal. Chem.* 1996, 68, 1486 – 1492.
- [9] Evans, M. B., Haken, J. K., *J. Chromatogr.* 1987, 406, 105 – 115.
- [10] West, S. D., *J. Chromatogr. Sci.* 1989, 27, 2 – 12.
- [11] Bruckner, C. A., Prazen, B. J., Synovec, R. E., *Anal. Chem.* 1998, 70, 2796 – 2804.
- [12] Beens, J., Blomberg, J., Schoenmakers, P. J., *J. High Resolut. Chromatogr.* 2000, 23, 182 – 188.
- [13] Dalluge, J., van Rijn, M., Beens, J., Vreuls, R. J. J., Brinkman, U. A. T., *J. Chromatogr.* 2002, 965, 207 – 217.
- [14] Mondello, L., Casilli, A., Tranchida, P. Q., Presti, M. L., Dugo, P., Dugo, G., *Anal. Bioanal. Chem.* 2007, 389, 1755 – 1763.
- [15] Watson, N. E., Davis, J. M., Synovec, R. E., *Anal. Chem.* 2007, 79, 7924 – 7927.
- [16] Gross, G. M., Nelson, D. A., Grate, J. W., Synovec, R. E., *Anal. Chem.* 2003, 75, 4558 – 4564.
- [17] Gross, G. M., Grate, J. W., Synovec, R. E., *J. Chromatogr. A* 2004, 1060, 225 – 236.
- [18] Stadermann, M., McBrady, A. D., Dick, B., Reid, V. R., Noy, A., Synovec, R. E., Bakajin, O., *Anal. Chem.* 2006, 78, 5639 – 5644.
- [19] Armstrong, D. W., He, L., Liu, Y., *Anal. Chem.* 1999, 71, 3873 – 3876.
- [20] Berthod, A., He, L., Armstrong, D. W., *Chromatographia* 2001, 53, 63 – 68.
- [21] Pacholec, F., Butler, H. T., Poole, C. F., *Anal. Chem.* 1982, 54, 1938 – 1941.
- [22] Anderson, J. L., Armstrong, D. W., *Anal. Chem.* 2005, 77, 6453 – 6462.

- [23] Anderson, J. L., Armstrong, D. W., *Anal. Chem.* 2003, 75, 4851 – 4858.
- [24] Shamsi, S., Danielson, N. D., *J. Sep. Sci.* 2007, 30, 1729 – 1750.
- [25] Lambertus, G. R., Crank, J. A., McGuigan, M. E., Kandler, S., Armstrong, D. W., Sacks, R. D., *J. Chromatogr. A* 2006, 1135, 230 – 240.
- [26] Sinha, A. E., Johnson, K. J., Prazen, B. J., Lucas, S. B., Fraga, C. G., Synovec, R. E., *J. Chromatogr. A* 2003, 983, 195.
- [27] Hope, J. L., Johnson, K. J., Cavelti, M. A., Prazen, B. J., Grate, J. W., Synovec, R. E., *Anal. Chim. Acta* 2003, 490, 223 – 230.
- [28] Purnell, H., *Gas Chromatography*, Wiley, New York 1962.
- [29] Conder, J. R., Young, C. L., *Physicochemical Measurement by Gas Chromatography*, John Wiley & Sons, New York 1979.
- [30] Karger, B. L., Snyder, L. R., Horvath, C., *An Introduction to Separation Science*, John Wiley & Sons, New York 1973.
- [31] Giddings, J. C., *Unified Separation Science*, Unified Separation Science, Wiley, New York 1991.
- [32] Gross, G. M., Grate, J. W., Synovec, R. E., *J. Chromatogr. A* 2004, 1029, 185 – 192.
- [33] Watson, N. E., Siegler, W. C., Hoggard, J. C., Synovec, R. E., *Anal. Chem.* 2007, 79, 8270 – 8280.

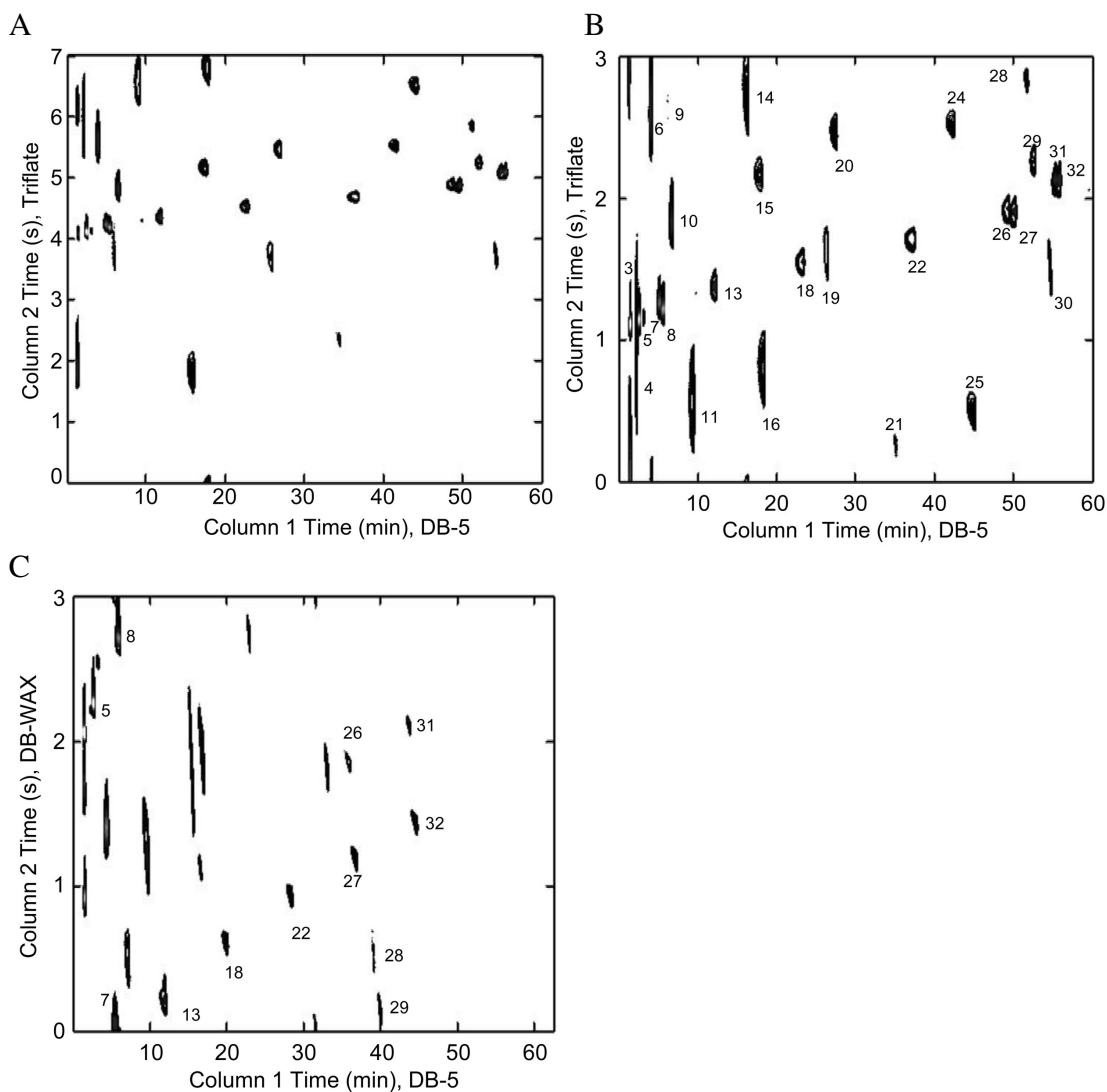


Figure 1. GCxGC separations of a 32-compound mixture for two different second columns. The compounds are listed in Table 1. For all separations the first column is 5 m $\times$ 100  $\mu$ m $\times$ 0.4  $\mu$ m DB-5 and H<sub>2</sub> carrier gas at an absolute head pressure of 18 psi (124000 Pa). The second column was operated with H<sub>2</sub> carrier gas at an absolute head pressure of 40 psi (276000 Pa). (A) Column 2 is the triflate IL column (4 m $\times$ 100  $\mu$ m $\times$ 0.08  $\mu$ m film) utilizing a 7 s modulation period and the following temperature program: hold at 35°C for 5 min, 35–75°C at 1°C/min, 75–150°C at 5°C/min. (B) Column 2 is the triflate IL column (4 m $\times$ 100  $\mu$ m $\times$ 0.08  $\mu$ m film) utilizing a 3 s modulation period and the same temperature program as (A). (C) Column 2 is a DB-Wax column (4 m $\times$ 100  $\mu$ m $\times$ 0.1  $\mu$ m PEG) utilizing a 3 s modulation period and the following temperature program: hold at 35°C for 5 min, 35–150°C at 2°C/min.

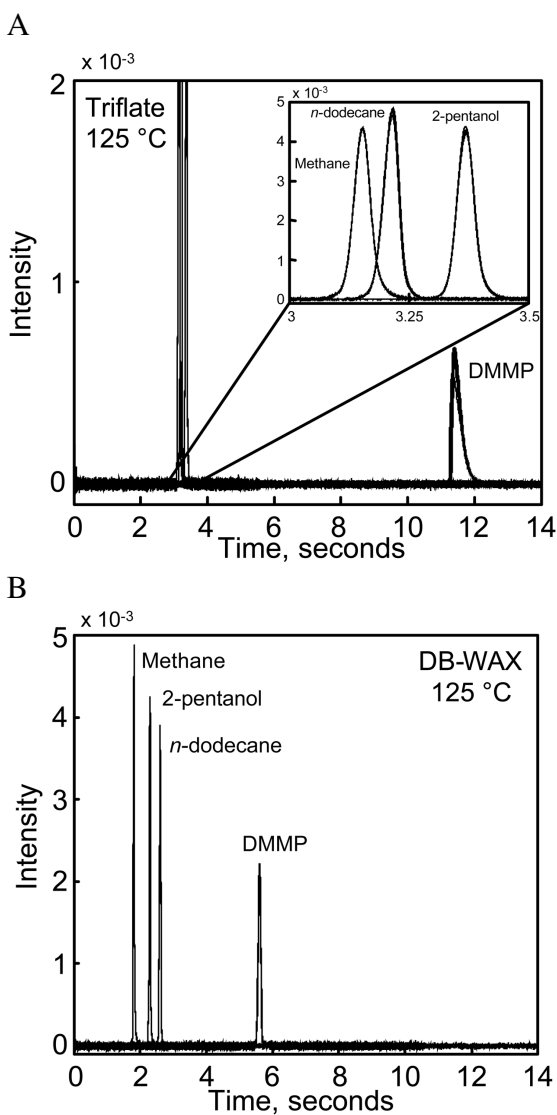


Figure 2. Overlay plot of single dimension chromatograms of 4 different compounds. All compounds normalized to peak area. All chromatograms collected at 125°C and H<sub>2</sub> carrier gas at an absolute head pressure of 65 psi (448000 Pa). (A) triflate IL column (4 m×100 μm×0.08 μm film). The y-axis was cropped for clarity. (B) DB-Wax column (4 m×100 μm×0.1 μm).

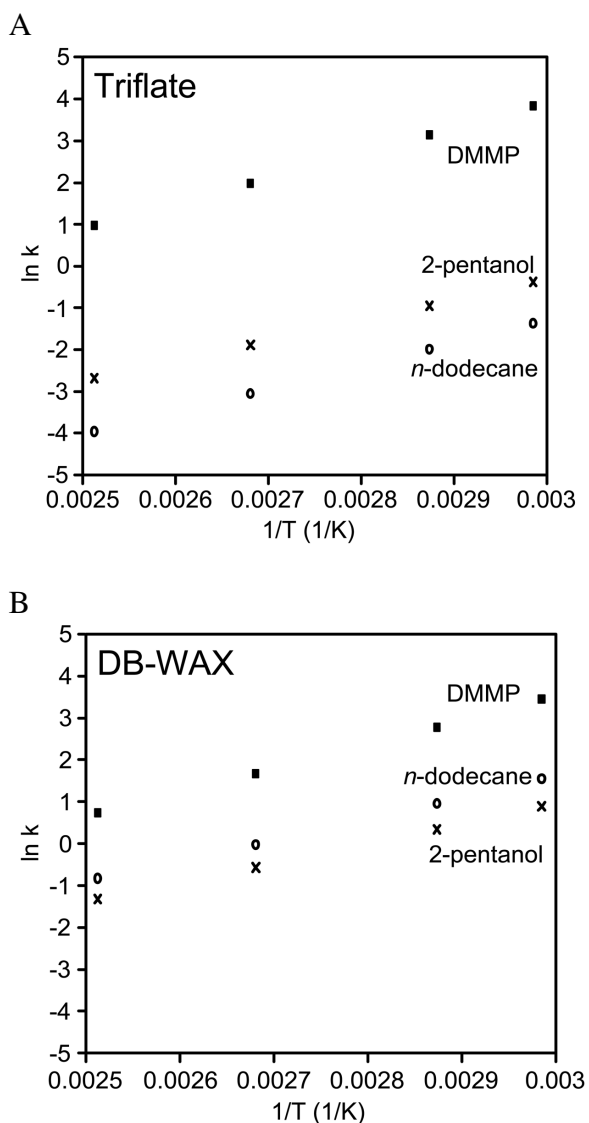


Figure 3. van't Hoff plots ( $\ln k$  vs.  $1/T$ ) for the triflate IL and DB-Wax columns for *n*-dodecane, 2-pentanol, and DMMP. All data collected using  $H_2$  carrier gas at an absolute head pressure of 65 psi (448000 Pa). (A) Triflate IL column ( $4 \text{ m} \times 100 \text{ } \mu\text{m} \times 0.08 \text{ } \mu\text{m}$ ). (B) DB-Wax column ( $4 \text{ m} \times 100 \text{ } \mu\text{m} \times 0.1 \text{ } \mu\text{m}$ ). Error bars are smaller than the symbols, per SDs are listed in Table 2, so they have been omitted.



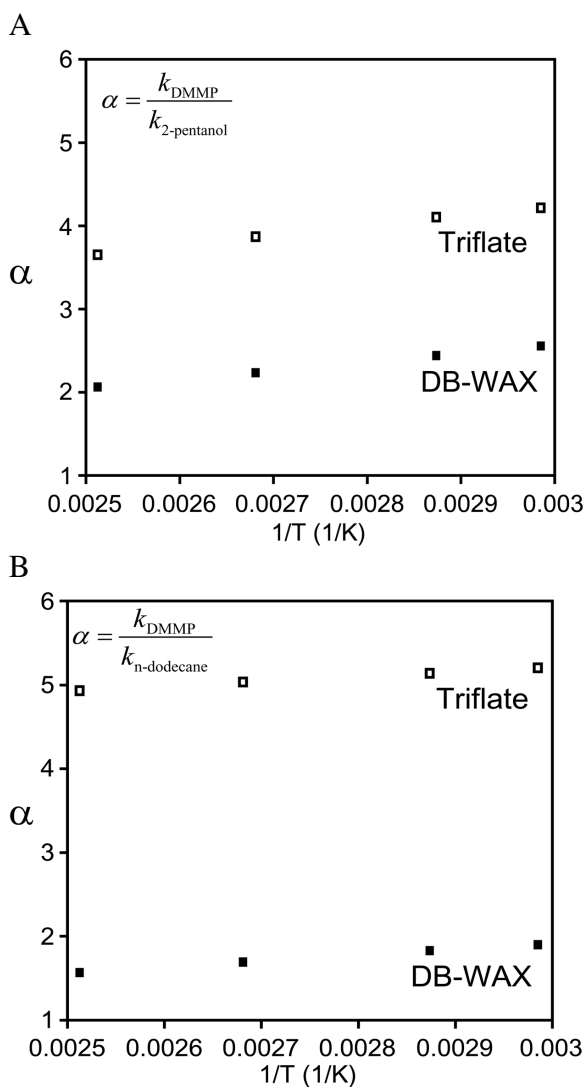


Figure 4. Selectivity plots ( $\alpha$  vs.  $1/T$ ) for triflate IL and DBWax columns, using data from Fig. 3. All data collected using  $\text{H}_2$  carrier gas at an absolute head pressure of 65 psi (448 000 Pa). (A)  $k_{\text{DMMP}}/k_{2\text{-pentanol}}$  for both separation columns as labeled. (B)  $k_{\text{DMMP}}/k_{\text{n-dodecane}}$  for both separation columns as labeled.

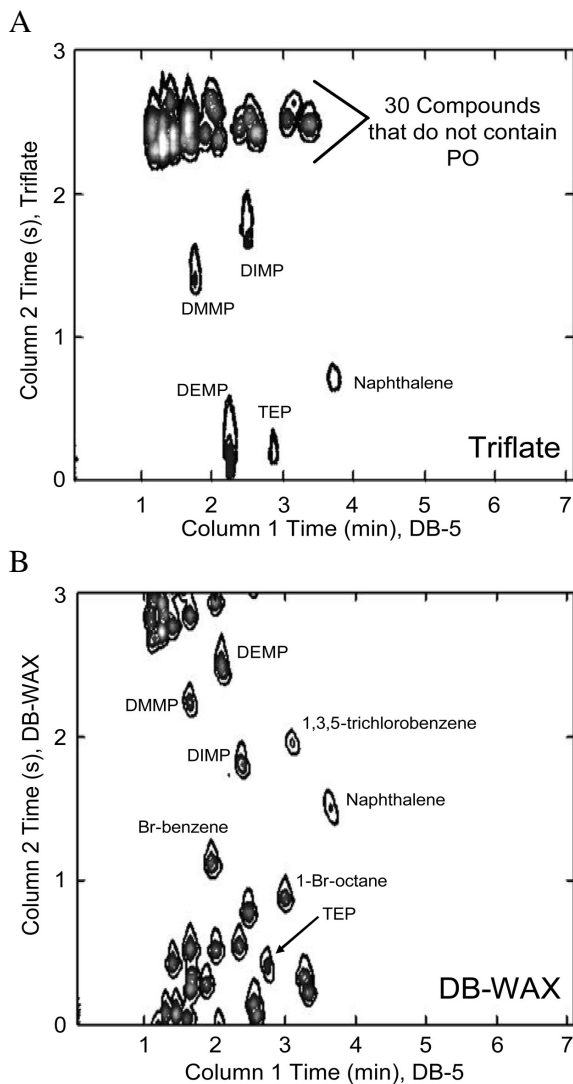


Figure 5. Rapid GCxGC separations of a 32-compound mixture spiked (in Table 1) with three additional P–O containing compounds (DMMP, DIMP, and TEP). For all separations the first column is 5 m×100  $\mu$ m×0.4  $\mu$ m DB-5 and H<sub>2</sub> carrier gas at an absolute head pressure of 18 psi (124000 Pa). The second column was operated with H<sub>2</sub> carrier gas at an absolute head pressure of 40 psi (276000 Pa) and a modulation period of 3 s. The following temperature program was applied: 150–200°C at 7°C/min. (A) Column 2 is the triflate IL column (4 m×100  $\mu$ m×0.08  $\mu$ m). (B) Column 2 is the DB-Wax column (4 m×100  $\mu$ m×0.4  $\mu$ m).

Table 1. Contents of 32-compound mixture listed in order of retention on DB-5

(1) Ethanol	(17) 2-Heptanone
(2) Acetone	(18) <i>n</i> -Nonane
(3) <i>n</i> -Pentane	(19) Br-Benzene
(4) 1-Propanol	(20) 1-Br-hexane
(5) <i>n</i> -Hexane	(21) 3-Octanone
(6) Benzene	(22) <i>n</i> -Decane
(7) 1-Heptene	(23) DEMP
(8) <i>n</i> -Heptane	(24) 1-Br-heptane
(9) 2-Pentanol	(25) Butylbenzene
(10) 1-Heptyne	(26) 1-Undecene
(11) Toluene	(27) <i>n</i> -Undecane
(12) 1-Pentanol	(28) 1,3,5-Trichlorobenzene
(13) <i>n</i> -Octane	(29) 1-Br-octane
(14) Cl-benzene	(30) Naphthalene
(15) 1-Cl-hexane	(31) 1-Dodecene
(16) Ethylbenzene	(32) <i>n</i> -Dodecane

Table 2. Repeatability of  $k$  for the triflate and DB-Wax columns for four different temperatures (see fig. 2 for experimental conditions)

Compound	Triflate 62°C $k$	Triflate 75°C $k$	Triflate 100°C $k$	Triflate 125°C $k$	Wax 62°C $k$	Wax 75°C $k$	Wax 100°C $k$	Wax 125°C $k$
n-Dodecane	0.2538 (0.0002)	0.1367 (0.0003)	0.0473 (0.0002)	0.0191 (0.0002)	4.693 (0.002)	2.597 (0.001)	0.9768 (0.0003)	0.4359 (0.0005)
2-Pentanol	0.685 (0.001)	0.3849 (0.0001)	0.1514 (0.0001)	0.0686 (0.0002)	2.4348 (0.001)	1.4055 (0.001)	0.5672 (0.0002)	0.2652 (0.0002)
DMMP	46.2 (0.7)	23.28 (0.08)	7.25 (0.03)	2.643 (0.008)	31.36 (0.01)	16.17 (0.01)	5.305 (0.002)	2.091 (0.001)

Values in parentheses are the absolute SD. Methane was used as a dead time marker.

## CHAPTER 6

### General conclusions

The research presented in chapter 2 of this thesis showed that of the 114 ILMs tested, three have been found to be the best ILMs for the detection of proteins, peptides and carbohydrates. These ILMs are *N,N*-diisopropylethylammonium  $\alpha$ -cyano-4-hydroxycinnamate, *N*-isopropyl-*N*-methyl-*t*-butylamine  $\alpha$ -cyano-4-hydroxycinnamate, and *N,N*-diisopropylethylammonium ferulate. *N,N*-Diisopropylethylammonium  $\alpha$ -cyano-4-hydroxycinnamate and *N*-isopropyl-*N*-methyl-*t*-butylamine  $\alpha$ -cyano-4-hydroxycinnamate were the best matrices for proteins and peptides and that *N,N*-diisopropylethylammonium  $\alpha$ -cyano-4-hydroxycinnamate and *N,N*-diisopropylethylammonium ferulate were the best matrices for carbohydrates. Furthermore, these ILMs have a wider mass detection range than solid matrices. This expanded mass range is from less than 1,000 Da to greater than 270,000 Da. ILMs were also shown to detect many different classes of analytes. It was also demonstrated that ILMs cations should have a proton affinity greater than or equal to 930 kJ/mole and a  $pK_a$  greater than or equal to 11. Dextran and mannan were also successfully characterized using ionic liquid matrices with no degradation.

The research presented in chapter 3 demonstrates the characterization of 16 biodegradable polymers with the ionic liquid matrix DEA CHCA. This matrix is compared to five solid matrices and one other ionic liquid matrix. Furthermore, it was shown that DEA CHCA typically produces almost Gaussian peak distributions with larger values for both the number average molecular weight and weight average molecular weight. It was also shown that when

DEA CHCA is used as a matrix and multiple measurements of a polymer sample are taken, precise  $M_n$  values are obtained. It was also demonstrated that when a well characterized polymer such as poly(ethylene glycol) is examined, the  $M_n$  calculated from a spectrum using DEA CHCA as a matrix is accurate.

Chapter 4 demonstrates the use of ionic liquids as gas chromatography stationary phases. Specifically, ionic liquids stationary phases used as the secondary column in two dimensional stop-flow gas chromatography separations. A 20 compound test mixture and 13 markers found in the headspace of US currency are separated. It is shown that individually the columns have many co-eluting peaks. When the columns are connected in series the separation is improved, but some co-elutions are still present. These co-eluting peaks were separated in the one dimensional separation by each column. Furthermore, when the stop-flow operation is used all peaks are separated with only a small increase in total analysis time.

Chapter 5 demonstrated that the triflate ionic liquid stationary phase has a unique selectivity for phosphorous-oxygen (P-O) containing compounds. These P-O containing compounds are used as chemical warfare simulants. It is shown by one dimensional separations, van't Hoff plots, and by plotting selectivity vs. the inverse of temperature that the selectivity of the triflate for the P-O containing compounds is much larger than the selectivity for the same compounds on a DB-WAX column (PEG). It is also shown that when DB-5 (5% diphenyl 95% dimethyl polysiloxane) and the triflate IL column are connected in series all P-O

containing compounds are baseline separated from each other and the complex mixture of 30 compounds that do not contain P-O.